Aus der Medizinischen Universitätsklinik und Poliklinik Tübingen

Abteilung VIII, Medizinische Onkologie und Pneumologie

Inhibition of measles virus replication by proteasome inhibitor Argyrin F constituting a novel virostatic compound

Inaugural-Dissertation
zur Erlangung des Doktorgrades
der Medizin

der Medizinischen Fakultät
der Eberhard Karls Universität
zu Tübingen

vorgelegt von

Warth, Paul-Philipp Armin

2021

Dekan: Professor Dr. B. Pichler

1. Berichterstatter: Professor Dr. U. Lauer
2. Berichterstatter: Professor Dr. F. Stubenrauch

Tag der Disputation: 21.12.2021

Content

List of figures

List of tables

Index of abbreviations

ADEM	Acute disseminated encephalomyelitis
AF	Argyrin F
CD	Cluster of Differentiation
CMC	Carboxymethylcellulose
CNS	Central nervous system
DMEM	Dulbecco's Modified Eagle's Medium
DMSO	Dimethylsulfoxide
EBNA1	Epstein-Barr virus nuclear antigen 1
EBV	Epstein-Barr virus
ECACC	European collection of authenticated cell cultures
EDTA	Ethylenediaminetetraacetic acid
EF	Elongation factor
ELISA	Enzyme linked immunosorbent assay
EMA	European Medicines Agency
FACS	Fluorescence activated cell sorting
FCS	Fetal calf serum
FDA	Food and Drug Administration
Fig.	Figure
GFP	Green fluorescent protein
HBV	Hepatitis B virus
hbi	Hours before infection
hpi	Hours post infection
hpt	Hours post treatment
JRF	Joint Reporting Form
MeOH	Methanol
MeV	Measles virus
MIBE	Measles inclusion body encephalomyelitis
MOI	Multiplicity of infection
nM	Nanomole
OD	Optical density
Opti-MEM	Modification of Eagle's Minimum Essential Media

PBS	Phosphate buffered saline
PE	Phycoerythrin
PEP	Post exposure prophylaxis
PFA	Paraformaldehyde
pfu	Plaque forming units
R_0	Basic reproduction number
RNA	Ribonucleic acid
rpm	revolutions per minute
RT	Room temperature
SD	Standard deviation
SLAMF1	Signaling lymphocytic activation molecule family member 1
SRB	Sulforhodamine B
SSPE	Subacute sclerosing panencephalitis
STIKO	Ständige Impfkommission
TBS	Tris buffered saline
TCA	Trichloroacetic acid
$TCID_{50}$	Tissue culture infective dose 50
TRIS	2-Amino-2-(hydroxymethyl)propane-1,3-diol
UV	Ultraviolet
WHO	World Health Organization

1. Introduction

1.1. Measles impact on public health

According to the World Health Organization (WHO) *"measles remain an important cause of death among young children globally, despite the availability of safe and effective vaccines"* [1]. Most of the more than 140,000 deaths worldwide in 2018 were children under the age of five [2]. While the global Measles and Rubella Initiative starting in 2001 was successful in reducing the number of measles deaths in the first years after launch, it remained at a constant level since 2007 [3]. The development of measles cases reported to the WHO is worrying (Fig.1). After the number of cases reported worldwide fell substantially in the last decades, there has been a clear reversal of this trend since 2017, reaching its peak with more than 850,000 reported cases in 2019 [4].

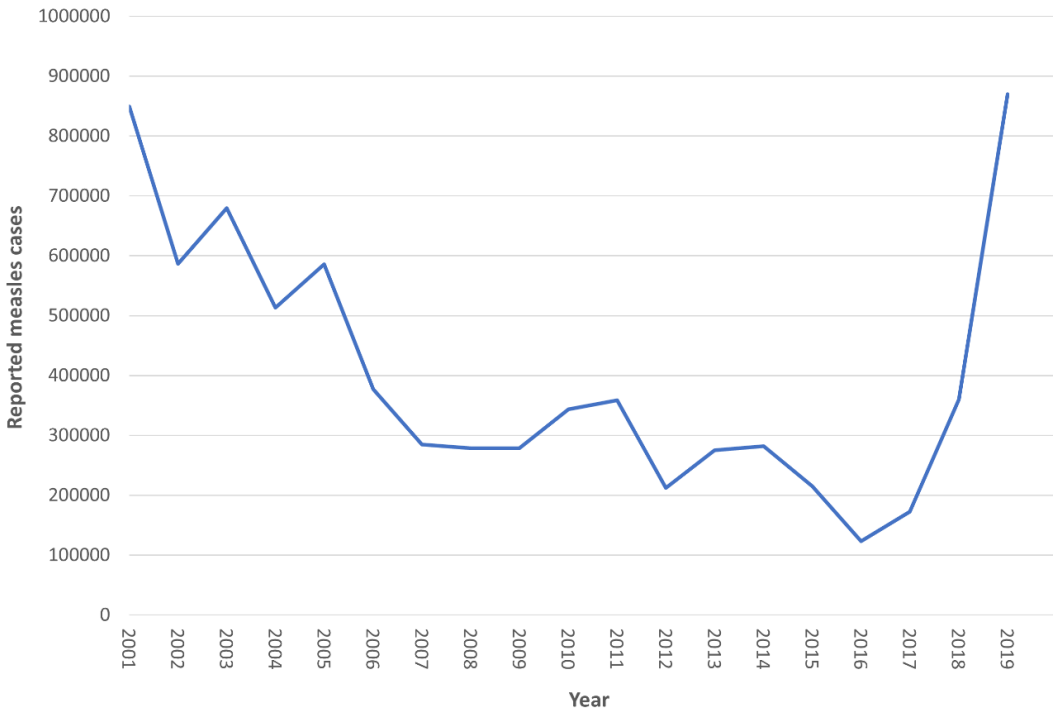

Figure 1: Annual reported cases of global measles infections from 2001 to 2019. Data were extracted from the WHO database (Update of 2020-7-10) [4] and depicted as a line diagram. According to their specifications *"data is based on reported cases data as reported in the Joint Reporting Form (JRF). For 2019, if a country did not submit a joint reporting form, measles cases were sourced from data reported through the monthly surveillance data."*

This is due in particular to severe measles outbreaks in the African countries of the Democratic Republic of the Congo (333,000 reported cases in 2019) and Madagascar (213,000 reported cases in 2019), but there is currently a high incidence of infections in the Ukraine (57,000 reported cases in 2019) and thus in Europe as well [4].

In addition to measles outbreaks the weak health systems in Africa now also have to cope with corona virus. This has already led to a temporal suspension of measles vaccination campaigns in more than 20 countries [5]. Furthermore, vaccine hesitancy is still a major problem even in high income countries [6, 7] and was called out by the WHO as one of the 10 threats to global health in 2019 [8]. With global immunization rates for the second dose of the measles vaccine of 69 % in 2018 [9], while the vaccination coverage should reach and remain at or exceed 95 % [10], the goal of eradicating measles is still a long way off.

1.2. Clinical presentation of measles virus infection

Measles virus is a highly contagious virus with a basic reproduction number R_0 of 12-18 [11] which can only be maintained in human populations and is transmitted via droplet infection [12]. After an average incubation period of 12.5 days [13] clinical signs such as increasing fever, cough, coryza, conjunctivitis or Koplik's spots appear in the prodromal phase. About three days later most of the time a rash appears, which typically begins behind the ears and then spreads to trunk and extremities and persists for three to four days. In case of uncomplicated measles, recovery typically occurs one week after the appearance of the rash [12]. While the measles case-fatality rate is ranging from 0.01 % to 0.1 % in high income countries, 3 % to 30 % die in low income countries [14]. Risk factors for complications are young age, pregnancy, immunodeficiency and malnutrition (in particular vitamin A deficiency) [12]. Pneumonia is the most common complication accounting for 56 % - 86 % of measles associated mortality. [14]. Rare but serious are the complications of the central nervous system (CNS): the acute disseminated encephalomyelitis (ADEM), measles inclusion body encephalitis (MIBE) and subacute sclerosing panencephalitis (SSPE) [15]. The

immunosuppression that can follow the infection for years, also appears to increase the overall mortality of the disease [16-18].

1.3. Current treatment options

So far there is no clinically approved specific antiviral therapy against measles [19].

In addition to supportive therapy (prevention or correction of nutritional deficiencies and dehydration, treatment of secondary bacterial infections [12]), especially vitamin A substitution is recommended by the WHO in all acute cases [20], because a deficiency is associated with a delayed recovery and an increased rate of post-measles complications and mortality [21].

The main focus lies on the prevention of the disease. The most important factor here is the primary prevention through active immunization. In Germany, the STIKO recommends the first dose of the vaccine at the age of 11-14 months and the second dose between 15 and 23 months [19]. In the context of a measles outbreak, the first vaccination can be justified in exceptional cases from the age of 6 months on after carefully weighing the risks [19]. Illness can also be prevented, or the severity of the disease can be reduced through a timely post exposure prophylaxis (PEP) [19]. The STIKO and the WHO recommend that people who are not or only insufficiently immunized receive a one-time vaccination as soon as possible within 3 days of exposure after contact with measles [19, 20]. If there are contraindications to this active immunization, a passive immunization using measles immunoglobulins is recommended by the STIKO and the WHO under certain circumstances as soon as possible within 6 days of exposure for i) infants under the age of 6 months, ii) pregnant women or iii) immunodeficient patients [20, 22]. A review of the Cochrane collaboration published in 2014 found that immunoglobulins were effective at preventing measles within seven days of exposure [23].

1.4. Important properties and possible indications for a new drug to be developed

As can be deduced from the still inadequately high numbers of infections (1.1.) combined with the dangerous complications caused by measles infection (1.2), further steps are needed in dealing with the disease. In this context Richard K. Plemper described [3], which properties a new drug must have in order to help together with the vaccination to eradicate measles [3]. He formulates four fundamental requirements for the drug [3]:

I) Cost effective manufacture
II) Shelf stable at ambient temperature
III) Orally bioavailable
IV) Safe for prophylactic use in children

These would be necessary for an effective application, especially in low-income countries [3]. The use as a post exposure prophylaxis (PEP) seemed to him to be most effective due to the virus titers that already drop quickly after the rash [24] and the immunosuppressive character of the disease [16-18], which probably results in a short treatment window [3]. Plemper wants to base the therapy on the already existing PEP treatment with measles immunoglobulins (passive immunization) [22], without having their disadvantages (IgG batches are not standardized, cost intensive, a cold chain and intravenous treatment are both required) [3]. Rapid treatment could possibly also prevent or treat the immunosuppression, which can occur for months after the measles virus infection [3]. Finally, in addition to the use as a PEP, Plemper sees a specific measles drug as a chance to treat MIBE and SSPE, which are both characterized by a prolonged viral replication in the brain [3, 15].

1.5. Structure and replication cycle of the measles virus

The structure (Fig. 2) and replication cycle of the measles virus is important, as starting points for antiviral therapy can be derived from them. The entry of the virus into the cell is mediated by the two surface proteins: hemagglutinin and fusion protein. First hemagglutinin mediates attachment to the cell. Possible receptors differ between vaccine and wild-type measles strains. Both can bind via CD150 (SLAMF1), which is found on activated B and T cells, dendritic cells, monocytes and macrophages as well as Nectin 4, which is expressed on many polarized epithelial cells e.g. airway epithelium. In addition, the measles vaccine virus can bind via the complement regulatory protein CD46, which is expressed on all human cells except erythrocytes [25-29]. The binding of hemagglutinin triggers a conformational change of the fusion protein, driving membrane fusion of virus and cell and thus virus entry [30, 31]. Subsequently, the ribonucleoprotein complex (single stranded negative polarized RNA encapsidated by nucleocapsid proteins) is used as a template for the RNA-dependent RNA-polymerase complex for transcription and by synthesizing a positive polarized antigenome in an intermediate step, also for replication. The RNA-dependent RNA-polymerase complex consists of the large protein, having the catalytic centers, the phospho protein, working as an essential cofactor, and additional host factors [32, 33]. Finally, in a complex process, virus components are assembled at the plasma membrane of the infected cell to egress as virions by budding. The matrix protein appears to play a critical role in both assembly and budding [32, 34, 35].

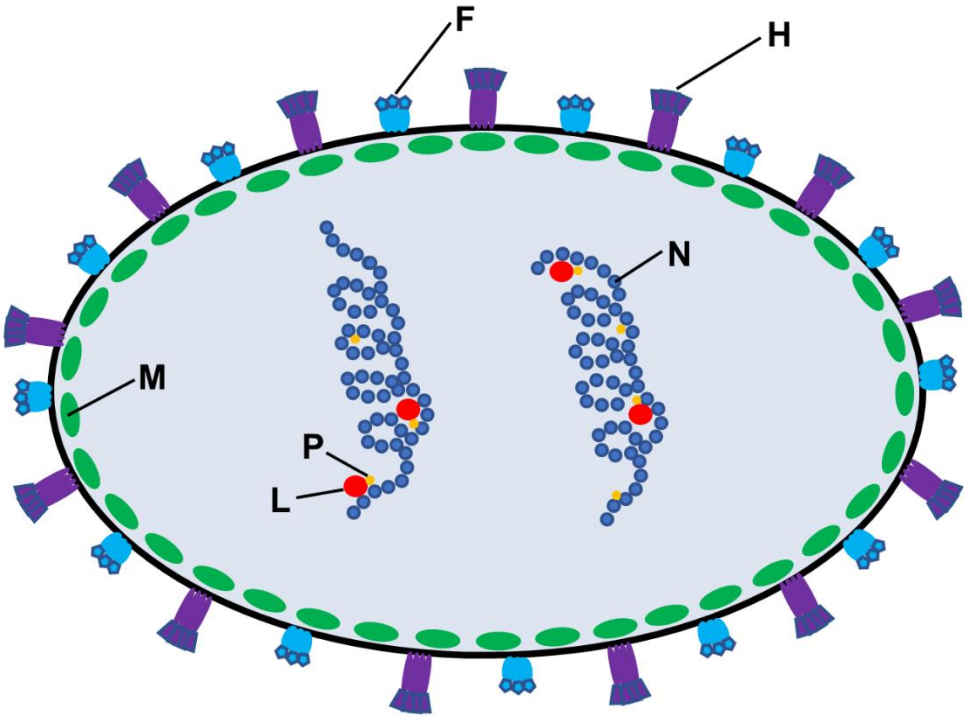

Figure 2: Structure of the measles virion. Created with reference to Springfeld et al. 2004 [36]. The single stranded, non-segmented, negative polarized viral RNA (not shown) encodes 6 structural (and 2 nonstructural) proteins: The surface proteins hemagglutinin (H) and fusion protein (F), which are integrated in the lipid envelope (black) and are responsible for receptor fusion and cell entry, the nucleocapsid (N) protein which surrounds the RNA forming the ribonucleoprotein (RNP) complex, the phospho protein (P) and large protein (L) building the RNA-dependent RNA-polymerase complex, as well as the matrix protein (M) which organizes the assembly of the virion by interacting with the other proteins [25, 36].

1.6. Current status of measles drug development

While broad-spectrum antiviral agents such as ribavirin [37-40] or interferon alpha [41-43] have been used in experimental settings to treat severe measles diseases and showed partly also clinical improvements, so far no specific antiviral drugs against measles are in clinical use.

However, there is a diverse array of experimental antiviral compounds (small molecules, natural extracts, semisynthetic compounds, therapeutic peptides, antisense molecules, peptide-conjugated morpholino oligomers) in the preclinical

context of in vitro and animal experiments [44]. Of these, peptide entry inhibitors, small-molecule inhibitors of the viral RNA-dependent RNA-polymerase complex and morpholino oligomers are best characterized [44]. In 2020 Plemper [3] rated the entry inhibitor AS-48 [45, 46], which prevents refolding of the fusion (F) protein into a post fusion conformation, and the inhibitor of the viral RNA-dependent RNA polymerase ERDRP-0519 [47-49] as the most advanced candidates to date.

1.7. The argyrins, their derivative Argyrin F and further proteasome inhibitors

To further complement this diverse array, we investigated whether Argyrin F (AF) could also be considered as a possible new drug against measles. AF belongs to the argyrins, a family of cyclic octapeptides, which were found when screening for antiproliferative compounds in myxobacteria [50]. 8 derivatives, Argyrin A-H (Fig. 3), could be isolated first from the myxobacterium Archangium gephyra and were later also found in different strains of genera Archangium and Cystobacter [50]. Various medically useful properties have already been demonstrated for this group of natural compounds. First it was observed by Sasse et al. in 2002, that argyrins can slightly inhibit mammalian cell growth [50]. Argyrin B in particular was proven to be an effective immunosuppressant [50]. Furthermore, an antibacterial activity, including against Pseudomonas sp., was detected [51]. It could be shown that Argyrin B inhibits protein synthesis by targeting the elongation factor G in bacteria and its homologue in mammalian cells, the mitochondrial elongation factor EF-G1 thus inhibiting mitochondrial translation [52]. Finally, argyrins were found to be anti-tumorigenic as well. Nickeleit et al. proved in 2008, that Argyrin A exerts this effect by inhibition of the proteasome and the resulting stabilization of one of the most common dysregulated tumor suppressor proteins in human cancers, the cyclin kinase inhibitor p27. This inhibits the tumor cell directly by inducing apoptosis and indirectly through affecting the tumor angiogenesis [53].

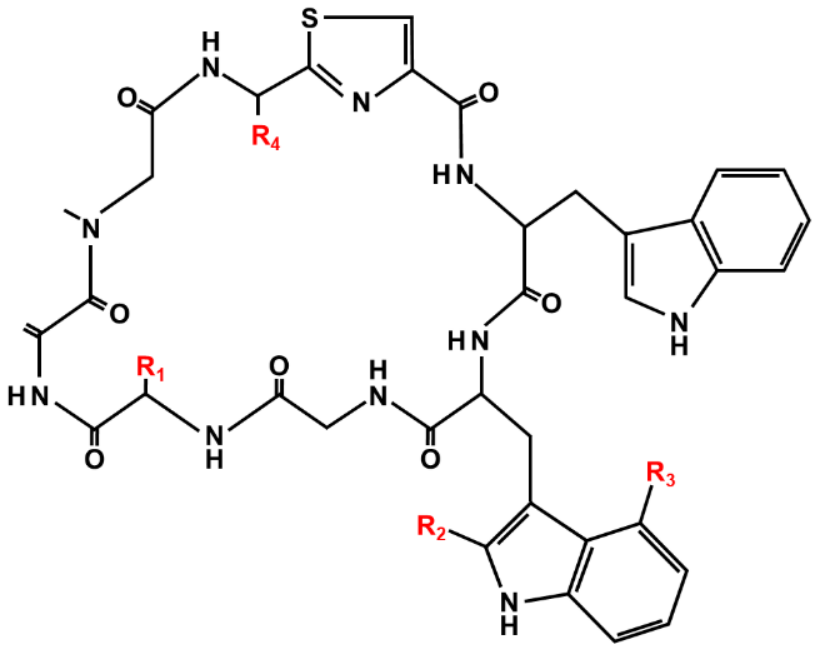

Argyrin A	R_1: CH_3	R_2: H	R_3: OCH_3	R_4: CH_3
Argyrin B	R_1: C_2H_5	R_2: H	R_3: OCH_3	R_4: CH_3
Argyrin C	R_1: CH_3	R_2: CH_3	R_3: OCH_3	R_4: CH_3
Argyrin D	R_1: C_2H_5	R_2: CH_3	R_3: OCH_3	R_4: CH_3
Argyrin E	R_1: CH_3	R_2: H	R_3: H	R_4: CH_3
Argyrin F	R_1: CH_3	R_2: H	R_3: OCH_3	R_4: CH_2OH
Argyrin G	R_1: C_2H_5	R_2: H	R_3: OCH_3	R_4: CH_2OH
Argyrin H	R_1: CH_3	R_2: H	R_3: OCH_3	R_4: H

Figure 3: The chemical structure of the argyrins. Created with reference to Sasse et al. 2002 [50]. Highlighted in red Argyrin F.

Compared to Argyrin A, AF has an additional hydroxy group, which results in an increased water solubility and thereby in improved pharmacokinetic parameters of the compound [54]. With equally strong inhibitory effects on the proteasome and resulting p27 stabilization as argyrin A, Bülow et al. rated AF in 2010 as the most promising antitumor compound of the argyrin family [54]. While both argyrins are acting as competitive reversible inhibitors of the catalytic β-subunits of the 20S proteasome (Fig. 4), they exhibit different subunit selectivity [55]. In particular, AF shows the highest selectivity for the β5-site and is to a lesser degree also more selective for the β2-site, whereas Argyrin A shows a higher

selectivity for the β1-site [54, 55]. In 2017 Chen et al. demonstrated in mice that AF can prevent pancreatic adenocarcinoma progression [56]. In addition to the p27 stabilization, an upregulated cyclin dependent kinase inhibitor 1 and a downregulated mitochondrial-encoded cytochrome c oxidase subunit 2 were measured under AF treatment, too [56].

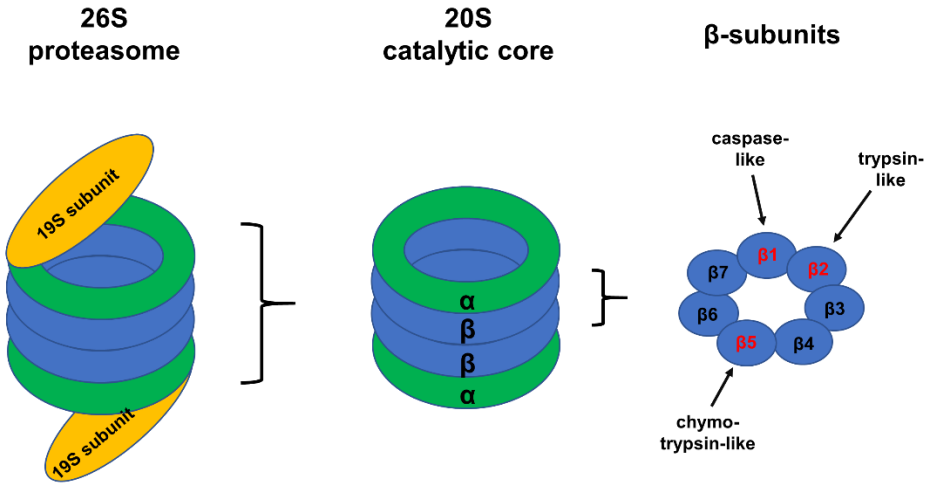

Figure 4: Structure and function of the proteasome. Created with reference to Yong et al. 2018 [57]. The 26S proteasome consists of a central 20S catalytic core and two regulatory 19S subunits. The 20S catalytic core in turn consists of two outer α-rings and two inner β-rings. Each ring consists of 7 subunits (α1-α7 and β1-β7). The proteolytic sites are in the inner β-rings: the caspase-like β1-subunit, the trypsin-like β2-subunit and the chymotrypsin-like β5-subunit. The proteasome is responsible for the degradation of intracellular proteins (regulatory proteins, misfolded proteins, damaged proteins). Those proteins are "marked" by polyubiquitination. Polyubiquitinated proteins are recognized and bound by the regulatory 19S subunit. Subsequently proteins are unfolded, deubiquitinated and transported into the central 20S catalytic core to be proteolytically degraded [57, 58].

The clinical use of proteasome inhibitors is not new. There are already some clinically approved therapeutics in this class of substances which are compared with AF in Tbl. 1. It is noticeable here that AF does not have any of the common active moieties (boronic acid, epoxyketone) for inhibiting the proteasome.

Table 1: Comparison of AF with other proteasome inhibitors

	Argyrin F	Bortezomib	Carfilzomib	Ixazomib
Active moiety	multiple interactions; pivotal structural requirements: methoxy group of Trp2, exo-methylene group [54, 59]	boronic acid [57]	epoxyketone [57]	boronic acid [57]
Binding	reversible [54]	reversible [60]	irreversible [61]	reversible [62]
Binding sites	primary β5, secondary β1 and β2 subunit [54]	primary β5, secondary β1 and β2 subunit [63]	primary β5, secondary β1 and β2 subunit [64]	primary β5, secondary β1 and β2 subunit [65]
Clinical approval (FDA)	not yet approved	multiple myeloma, mantle cell lymphoma [66]	multiple myeloma [67]	multiple myeloma [68]
Application route	-	intravenous, subcutaneous [66]	intravenous [67]	oral [68]
Trade name	-	Velcade® [66]	Kyprolis® [67]	Ninlaro® [68]

1.8. Objectives

As described before, despite the availability of safe and effective vaccines, measles still has a tremendous impact on public health and further steps are needed in dealing with the disease.

By searching for anti-tumorigenic synergisms between small molecule agents and the recombinant measles vaccine virus virotherapeutic MeV-GFP, our working group surprisingly found, contrary to the assumed increased anti-tumor effect, a reduced oncolysis when using Argyrin F (AF) in combination with MeV-GFP. Preliminary tests showed a clear reduction of MeV-GFP titers in this combined therapy, which is why AF could represent a completely unknown potent novel antiviral drug against measles.

Against this background, the aim of this dissertation was to work out this virostatic effect in detail in order to be able to better evaluate, whether AF can be used as a lead compound for a new effective virostatic agent.

In particular, the following questions had to be investigated *in vitro*:

I) Which dosage is necessary to achieve a significant antiviral effect when using Argyrin F (AF) in combination with MeV-GFP?

II) To which extent can titers of MeV-GFP be reduced when using AF in combination with MeV-GFP?

III) In which time period before and after infection with MeV-GFP inhibition of measles virus replication was achieved by application of AF?

IV) Does the virostatic effect of AF also depend on the used cell lines?

V) Does AF also inhibit measles vaccine virus strains other than MeV-GFP?

VI) Does AF also inhibit measles wild-type virus strains?

VII) What is the molecular mechanism of the virostatic effect of AF?

2. Material and Methods

2.1. Material

2.1.1. Antibodies

Anti-human-CD46 PE: *BioLegend*

Anti-human-CD150 PE: e*Bioscience*

Anti-MeV N-Protein NP clone 120 Mouse IgG2: *ECACC*

Alexa Fluor® 546 Goat Anti Mouse IgG (H+L), A11003: *Invitrogen*

Gamunex: *Talecris*

PE conjugated anti-mouse IgG1, κ-isotype: *Biolegend*

2.1.2. Consumables

Cell scrapers: *Corning Inc*

Cell strainer 40 µm: *Greiner Bio-One*

Combitips 12.5 ml: *Eppendorf*

Cryotubes 1 ml: *Corning Inc*

Microplate 96 well: *Greiner Bio-One*

96 well electronic microtiter plate: *ACEA*

Pasteur pipettes 230 mm long size: *WU Mainz*

Pipettes 50 ml, 25 ml, 10 ml, 5ml: *Corning Inc*

Filter tips 1000 µl: *Peqlab*

Filter tips 200 µl, 100 µl: *Starlab*

Filter tips 10 µl: *Peqlab/ Eppendorf*

Reaction tubes 2 ml, 1.5 ml, 0.5 ml: *Eppendorf*

Tissue culture flasks 175 cm^2: *Greiner Bio-One*

Tissue culture flasks 75 cm^2: *TPP*

Tissue culture plates 96 well, 6 well: *Falcon*

Tissue culture plates 48 well, 12 well: *Corning Inc*

Tissue culture plates 24 well: *Falcon/ TPP*

Tube (conical bottom) 50 ml: *Falcon*

Tube (conical bottom) 15 ml: *Greiner Bio-One*

Tube (conical bottom) 5 ml: *Sarstedt*

2.1.3. Chemicals

Acetic acid: *VWR Chemicals*
Carboxymethylcellulose: *Sigma*
Descosept: *Dr. Schumacher GMBH*
Dimethylsulfoxide: *AppliChem*
Isopropanol 100%: *VWR Chemicals*
Paraformaldehyde 4%: *Otto Fischar GMBH*
Secusept: *ECOLAB*
Sulforhodamine B: *Sigma Aldrich*
Trichloroacetic acid: *Carl Roth*
Triton X-100: *Carl Roth*
Trypan blue: *Sigma*

2.1.4. Laboratory equipment

Autoclave: *Systec (VX-150)*, *HP Medizintechnik GMBH (Varioklav)*
Centrifuge: *Heraeus (Megafuge 2.0R), Eppendorf (miniSpin)*
Digital shaker: *Heidolph (PROMAX 1020)*
FACS Attune NxT: *Thermo Fisher Scientific*
Fluorescence microscope: *Olympus (IX50-S8F2)*
Haemocytometer: *Hecht Assistent (Neubauer improved)*
Heating cabinet: *Binder*
Incubator: *Heraeus (HERAcell), Memmert*, *Sanyo (MCO-18M)*
Laminar flow work bench: *Heraeus (HERAsafe)*
Light microscope: *Olympus (CK40-F200)*
Magnetic stirrer: *IKA (RCT basic)*
Microplate reader: *Tecan (GENios Plus)*, *BioTek (Synergy HT)*
Multichannel pipette 1200 µl (electronic): *Eppendorf*
Multichannel pipette 100 µl (mechanical): *Eppendorf*
Pipette Boy: *Integra*
Pipettes 1000 µl, 200 µl, 100 µl, 10 µl, 2.5 µl: *Eppendorf*
Freezer (-18 °C, -80 °C, -150 °C): *Liebherr*

Repeating pipette: *Brand (Handy Step)*

Sonifier: *Branson*

Vortexer: *neoLab (VM 300), Scientific Industries (G-560E)*

Water bath (37 °C): *Köttermann*

xCELLigence™ RTCA SP: *ACEA Bioscience, Inc*

2.1.5. Media and solutions

Accutase: *Sigma-Aldrich*

Antibiotic antimycotic solution: *Mediatech*

Dulbecco's Modified Eagle's Medium: *Sigma-Aldrich*

Fetal calf serum: *Biochrom GmbH*

Opti-MEM: *Life technologies*

Phosphate buffered saline: *Sigma-Aldrich*

Tris buffered saline and Tween 20: *Carl Roth GmbH*

Tris(hydroxymethyl)aminomethan: *Carl Roth GmbH*

Trypsin: *Sigma Aldrich*

2.1.6. Proteasome inhibitors

Argyrin F: *Prof. Dr. med. Nisar Peter Malek (University Tübingen)*

Argyrin derivatives: *Prof. Dr. Markus Kalesse (University Hannover)*

Bortezomib: *Santa Cruz Biotechnology*

Carfilzomib: *PD Dr. med. M. Schittenhelm (University Tübingen)*

Ixazomib: *Selleckchem*

2.1.7. Viruses

GLV-1h68: *Genelux Corp. (San Diego, USA)*

MeV-AIK-C: *Hokken (Kitasato, Japan)*

MeV-L16: *Robert Koch-Institut (Berlin)*

MeV-Mérieux: *Sanofi Pasteur MSD GmbH*

MeV-GFP: *Prof. U.M. Lauer (University Tübingen)*

MeV-Nse-GFP: *Prof. S. Russell (Mayo Clinic, Rochester, USA)*

Wild-type MeV-B3*: Robert Koch-Institut (Berlin)*

Wild-type MeV-D4: *Robert Koch-Institut (Berlin)*

Wild-type MeV-D8: *Robert Koch-Institut (Berlin)*

2.1.8. Cell lines

Table 2: Used cell lines and their properties

Cell line	Species	Tissue	Source
B95a	Monkey	B-cells (derivative of cell line B95-8)	*European Collection of Authenticated Cell Cultures*
CV-1	Monkey	Kidney	*Genelux Corp., San Diego*
HCT 116	Human	Colorectal adenocarcinoma	*U.S. National Cancer Institute's NCI-60 tumor cell panel (Charles River Laboratories Inc., New York, NY, USA)*
Hep3B	Human	Hepatocellular carcinoma	*European Collection of Authenticated Cell Cultures*
MIA PaCa-2	Human	Pancreatic carcinoma	*European Collection of Authenticated Cell Cultures*
Vero	Monkey	Kidney	*Deutsche Sammlung von Mikroorganismen und Zellkulturen*
Vero/hSLAM	Monkey	Kidney (hSLAM transfected Vero cells)	*Robert Koch-Institut, Berlin*

2.2. Methods

2.2.1. Cell culture

2.2.1.1. General cell culture

The cell lines described in 2.1.8 were cultivated as adherent monolayer in Dulbecco's Modified Eagle's Medium (DMEM) containing 10 % fetal calf serum (FCS). Only Vero/hSLAM cells were cultivated in DMEM supplemented with 5 % FCS and additionally geneticin to select CD150 expressing cells. Cells were stored in tissue culture flasks at 37 °C, 5 % CO_2 and 95 % humidity in the incubator. Cell confluence was assessed under the light microscope daily. When reaching confluence, cells were passaged to avoid a lack of nutrients. Therefore, medium was aspirated and adherent cells were carefully rinsed with prewarmed (37 °C) phosphate buffered saline (PBS) to dislodge cell debris and FCS which inactivates trypsin. To detach the adherent cells trypsin/EDTA (0.05 %) was added and cell culture flasks were stored in the incubator to reach the thermal optimum for 2 to 5 minutes. Thereon cells were suspended with 10 ml fresh medium to inactivate trypsin, transferred into a falcon tube and centrifuged at 1200 rpm for 4 minutes. After aspirating the supernatant and resuspending the pellet with fresh medium 1/3 to 1/10 of the cells was further cultivated.

Table 3: Growth area and volumes used for cell culture

Culture flask	Growth area [cm^2]	Volume of medium [ml]	Trypsin/EDTA [ml]
Small	75	15	2.5
Large	175	25	4

2.2.1.2. Determination of the cell density

Cell density was determined using the improved Neubauer chamber, a hemocytometer with a central counting grid of nine 1×1 mm large squares. To prepare the chamber a cover glass was placed on the hemocytometer covering the counting grid. When Newton´s rings appeared the distance between the

chamber and the cover was 0.1 mm. Thus, each square could be loaded with a defined volume of 100 nl of diluted cell suspension and the concentration of cells in the fluid could be calculated.

For counting the cell suspension was mixed in a ratio of 1:2 to 1:10 with trypan blue (0.4% w/v), which only dyes cells with a damaged cell membrane and therefore allows to differentiate between vital and dead cells. Subsequently the hemocytometer was loaded with 10 µl of the diluted sample and cells were counted in the four squares in the corners under the light microscope. The cell density of the sample was determined applying the following formula:

$$\text{Cell density}\left[\frac{\text{cells}}{\text{ml}}\right] = \frac{\text{vital cells counted}}{\text{squares}} \times 10^4 \times \text{dilution factor}$$

2.2.1.3. Seeding of cells

For experiments cells were seeded in well plates. Initially cells were detached and counted as described in 2.2.1.1 and 2.2.1.2. Knowing the needed volume and cell number per well, the cell suspension was diluted in DMEM containing 10 % FCS (Vero cells and Vero/hSLAM in DMEM + 5 % FCS) and spread with a repeating pipette. To avoid an unequal distribution the cell suspension was vortexed and in case of agglutinated cells passed through a cell strainer before seeding.

Table 4: Growth areas and volumes used per well for seeding cells

Well plate	Growth area [cm^2]	Volume of medium [ml]
6 Well	9.5	2
24 Well	2	0.5
96 Well	0.32	0.2

The cell number seeded in each well was chosen dependent on the well plate and cell line (Tbl. 5). Unless otherwise stated, cells were treated 24 hours after seeding.

Table 5: Seeded cells per well depending on cell line and well plate. Exceptions: * 4 x 10^5 cells per well: virus titration of AIK-C, L-16, Mérieux, Nse-GFP, GLV-1h68 + AF; virus titration of MeV-GFP + further proteasome inhibitors; SRB assay of AIK-C + AF. ** 4 x 10^4 cells per well: SRB assay of AIK-C, L-16, Mérieux, Nse-GFP, GLV-1h68 and argyrin derivatives. *** 3 x 10^4 cell per well: SRB assay of MeV-GFP.

Cell line	6 well plate	24 well plate	96 well plate
HCT 116	2 x 10^5 *	2 x 10^4 **	2 x 10^3
MIA PaCa-2	2 x 10^5	2 x 10^4 ***	
Hep3B	4 x 10^5	4 x 10^4	
B95 a	4 x 10^5	4 x 10^4	

2.2.1.4. Cryopreservation of cells

For long time preservation cells were stored in the freezer at -150 °C. Therefore, exponentially growing cells were trypsinized in culture flasks and centrifuged as described in 2.2.1.1. Subsequently cells were resuspended in DMEM containing 20 % FCS and 10 % dimethylsulfoxide (DMSO) to prevent cell damaging crystallization. The suspension was transferred in 1 ml aliquots in cryotubes which were initially stored for 24 h at -80 °C and hereupon at -150 °C to ensure a slow freezing process.

2.2.1.5. Thawing of cells

To minimize cell damage frozen aliquots were thawed in the water bath at 37 °C and subsequently diluted in 10 ml DMEM containing 10 % FCS. After centrifugation the cell pellet was resuspended in DMEM + 10 % FCS and cells were cultivated in culture flasks as described in 2.2.1.1.

2.2.2. Virological methods

Before describing virological methods, some special terms must be defined:

The **multiplicity of infection** (MOI) describes the ratio of infectious agents (here virus) to targets (here cells) during infection. The MOI was chosen experiment and cell line dependent.

Plaque forming units (pfu) describes the quantity of infectious virus particles per volume.

The **tissue culture infective dose 50** ($TCID_{50}$) [69] describes the amount of virus necessary to show infection signs in 50 % of inoculated cells. The relationship between $TCID_{50}$ and pfu is described as follows:

$$\frac{\text{pfu}}{\text{ml}} = \frac{\text{TCID}_{50}}{\text{ml}} \times 0.7$$

2.2.2.1. Virus infection

a) Measles virus

Cells seeded in well plates as described in 2.2.1.3 were stored one day in the incubator to adhere. Frozen virus aliquots (-80 °C) were thawed at room temperature (RT) and vortexed. The amount of virus suspension needed for the experiment to infect at a respective MOI, was calculated applying the following formula:

$$\text{Virus suspension [ml]} = \frac{\text{cell number} \times \text{MOI}}{\text{virus titer} \left[\frac{\text{PFU}}{\text{ml}}\right]}$$

The calculated amount of virus suspension was diluted in the required volume of the infection medium Opti-MEM and vortexed.

Medium was aspirated and cells were rinsed with prewarmed PBS (37 °C) to eliminate complement factors. Subsequently wells were covered with the infection medium and stored in the incubator for 3 hours. To ensure equal infection well plates were carefully slewed and rotated by 90 degrees every 15 minutes. Afterwards the inoculum was aspirated and replaced by standard medium or in case of an additional treatment with a proteasome inhibitor as described in 2.2.3.

b) Vaccinia virus

The infection with vaccinia virus shows some differences towards measles virus infection. First, vaccinia virus samples had to be sonicated to dissolve aggregates. For this, frozen aliquots were thawed and subsequently treated for 30 seconds in the sonifier. To protect the virus from heat exposure the sonication was executed under water cooling (4 °C) and thereupon aliquots were immediately stored on ice. Moreover, cells were infected only for 1h in DMEM containing 2 % FCS.

Table 6: Virus dependent infection conditions

Virus	Infection medium	Infection time [h]	Infection volume (6/24 Well) [ml]
Measles	Opti-MEM	3	1/0.25
Vaccinia	DMEM + 2 % FCS	1	1/0.25

2.2.2.2. Collecting and freezing of samples

For virus titration supernatants were transferred into a reaction tube. Then cells were scraped off in 1 ml of Opti-MEM and transferred in a second reaction tube. If cell lysate and supernatant were titrated together, cells were directly scraped off in the supernatant and transferred into a reaction tube. The samples were immediately stored in the freezer at -80 °C.

2.2.2.3. Virus quantification

The concentration of infectious virus particles in a sample was determined by virus titration. The entire process is summarized in Fig. 5. The individual steps seeding of cells (2.2.1.3), virus infection (2.2.2.1), treatment with proteasome inhibitors (2.2.3) and collecting of samples (2.2.2.2) are described in detail in the respective chapters. This chapter focuses on the virus titration itself.

a) Measles virus

Measles virus was quantified by the endpoint dilution assay of Spearman [70] and Kärber [71]. For this Vero cells (respectively Vero/hSLAM cells in case of measles wild-type virus) were plated as host cells in 96 well plates (1×10^4 cells in 200 µl DMEM + 5 % FCS per well). On the next day seeded cells were controlled under the light microscope.

Frozen samples were thawed in the water bath, vortexed for 10-15 seconds and subsequently centrifugated at 3000 rpm for 2 minutes to separate virus suspension from cell debris. The virus containing supernatant was transferred into a new reaction tube and a dilution series was prepared (Fig. 5). Therefore, in a vertically placed 96-well plate (8 columns, 12 rows) 300 µl of the sample were pipetted in the first column and 270 µl DMEM containing 5 % FCS in the remaining columns. Subsequently 30 µl of the first column were pipetted in the second column and resuspended in the medium. This procedure was continued till in the last column a dilution of 10^{-7} was reached.

Each dilution series was transferred (50 µl) with a mechanic multichannel pipette to 4 rows of a vertically placed 96-well plate (8 columns, 12 rows) containing Vero cells. The inoculated Vero cells were stored for 96 h in the incubator. During this time infectious virus particles could replicate in Vero cells.

Virus replication was quantified under the fluorescence microscope. In case of GFP expressing virus strains (MeV-GFP, Nse-GFP) no further steps were necessary. If a dilution contained infectious virus particles which replicated, the corresponding wells displayed green fluorescence. In case of not GFP expressing virus strains (AIK-C, L-16, Mérieux, B3, D4, D8) a virus-specific immunofluorescence staining was necessary as described in 2.2.2.4.

We differentiated binary between “positive” (infected) and “negative” (not infected) wells. A well was defined “positive” if one fluorescent syncytium was visible. The positive wells were counted and the virus titer calculated applying the following formula:

$$\frac{\mathrm{TCID}_{50}}{\mathrm{ml}} = \frac{10^{\text{dilution step log10} \times \left(\frac{\text{total nubers of positive wells}}{\text{number of wells per dilution factor}} - 0.5\right)}}{0.05\ \mathrm{ml}\ (\text{volume of used virus stock})}$$

Results were converted in the more vivid unit $\frac{\mathrm{pfu}}{\mathrm{ml}}$.

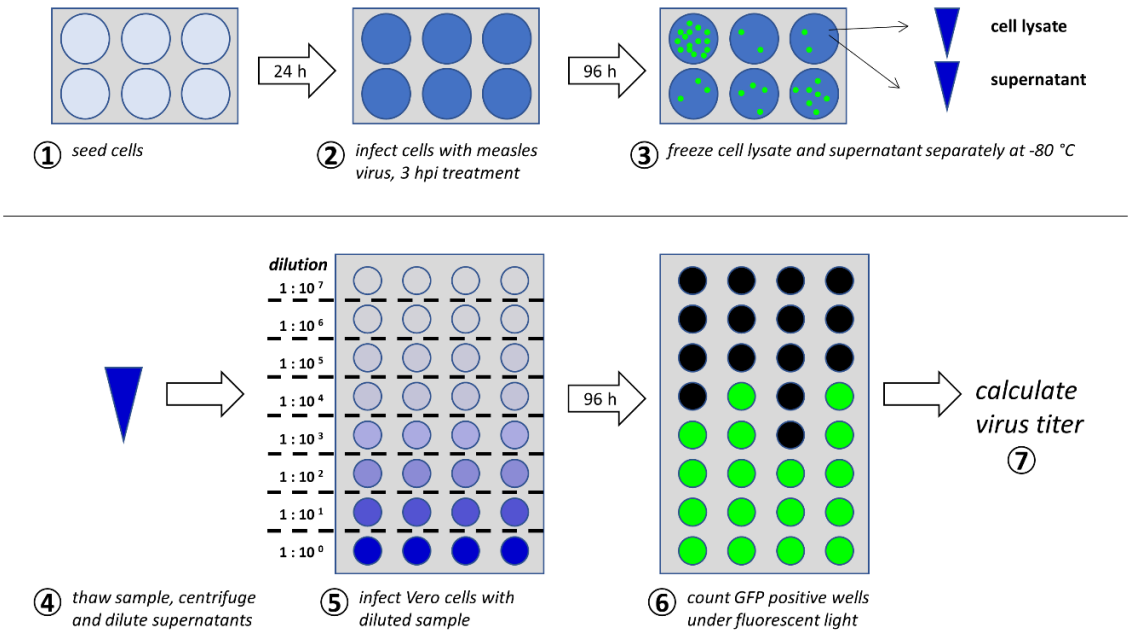

Figure 5: Procedure of determining measles virus titers by virus titration

b) Vaccinia virus

Vaccinia virus was quantified by a plaque assay. For this, CV-1 cells were plated as host cells in 24-well plates (1×10^5 cells in DMEM + 10 % FCS per well). On the next day seeded cells were controlled under the light microscope. Virus titration was performed when CV-1 cells had reached 100 % confluence.

Samples were thawed in the water bath, vortexed for 10-15 seconds and subsequently stored one ice. Before titration samples were sonicated as

described in 2.2.2.1. Thereupon a dilution series was created. In reaction tubes 100 µl of the sample were diluted in 900 µl DMEM containing 2 % FCS. This procedure was repeated up to a dilution of 10^{-8}. Between all steps, dilutions were vortexed.

With each dilution of a sample 2 wells of CV-1 cells were inoculated. For this the medium was removed and CV-1 cells were infected with 250 µl of the dilution. Subsequently the 24-well plates were stored in the incubator for 1 h. To ensure an equal infection, plates were carefully slewed and rotated by 90 degrees every 20 minutes. Afterwards cells were overlaid with 1 ml 1.5 % carboxymethylcellulose (CMC) medium to avoid virus spreading and plates were incubated for 2 days at 37 °C. Finally, 250 µl Cristal violet staining solution (Crystal violet 0.13 %, ethanol 5 %, formaldehyde 11.1 %) were added to each well to visualize virus plaques. After 4 h incubation at RT, medium was removed with a pipette and wells were washed with H_2O twice. Then plates were irradiated for 15 minutes under ultraviolet (UV) light. Subsequently plaques could be counted under a magnifier and the virus titer was calculated applying the following formula:

$$\frac{\text{pfu}}{\text{ml}} = \frac{\text{average number of plaques} \times \text{dilution}}{0.25\ \text{ml (volume of infection medium)}}$$

The CMC medium was produced in advance: 7.5 g CMC (final concentration: 1.5 %) were autoclaved in a bottle with a stir bar inside for 15 min under the conditions for wrapped goods. After the bottle had cooled down 500 ml DMEM and 5 ml antibiotic-antimycotic solution were added. CMC clumped at the bottom was dislodged with a sterile pipette. Afterwards the suspension was placed on a stirrer overnight until CMC was completely dissolved. Subsequently 25 ml FBS were added and the suspension was again carefully mixed. The CMC medium was stored at 4 °C and was warmed at RT before use.

2.2.2.4. Virus specific immunofluorescence staining

To determine titers of measles virus strains not expressing GFP (AIK-C, L-16, Mérieux, B3, D4, D8) a virus specific immunofluorescence staining was necessary. At 96 hpi infected Vero cells were examined under the light microscope. The highest dilution of a sample, in which all 4 wells showed signs of infection, was marked. The 96-well plates were washed with 200 µl PBS per well and subsequently fixed with 4% paraformaldehyde (PFA) for 10 min at RT. To economize staining materials, only the marked dilution and 3 higher dilutions were further treated. Wells were washed twice with 200 µl PBS and blocked with 100 µl tris-buffered saline and Tween 20 (TBS-T: 150 mM NaCl, 50 mM Tris pH 7.4, 0.02 % Tween-20) containing 1 % FCS for 30 min. Subsequently wells were incubated with 50 µl anti-MeV-NP (1:1000 in TBS-T) for 30 min. After washing three times with 200 µl TBS-T wells were incubated with 50 µl of the secondary antibody Alexa Fluor® 546 goat anti-mouse (1:1000 in TBS-T). To protect the light sensitive secondary antibodies plates were stored in the dark. After 30 min wells were washed three times with TBS-T and then covered with 100 µl PBS. Thereupon positive wells could be counted under the fluorescence microscope.

2.2.3. Treatment with proteasome inhibitors

Cells were treated either with the proteasome inhibitor alone or as part of the combined therapy with the virus. In case of a proteasome inhibitor monotherapy the medium (2.2.1.3) was carefully removed and replaced with DMEM + 5 % FCS containing the proteasome inhibitor. If the proteasome inhibitor was applied as part of a combined therapy, it was given immediately (exception kinetics: separately described in 3.2.5) after the infection period (3 hours for measles virus, 1 hour for vaccinia virus). The respective infection medium (Tbl. 6) was removed and replaced by DMEM containing 5 % FCS and the proteasome inhibitor. To reduce the absolute consumption of proteasome inhibitors, the volume per well was reduced (Tbl. 7) compared to the initial seeding of the cells (Tbl. 4). In both settings the added medium was left until the end of the experiment.

Table 7: Growth areas and volumes per well used for treating cells with proteasome inhibitors

Well plate	Growth area [cm^2]	Volume of medium [ml]
6 Well	9.5	1
24 Well	2	0.4

2.2.4. Further readout

2.2.4.1. Cell mass quantification by SRB assay

Remaining cell mass was quantified by SRB assay [72], a colorimetric endpoint assay which provides a sensitive method to determine oncolytic effects of virus strains and cytotoxicity of drugs in a cell culture.

First, treated cells had to be fixed. For this purpose, medium was removed, wells were rinsed with ice cold PBS and covered with 4 °C cold 10 % trichloroacetic acid (TCA). Plates were stored for 30 minutes in the refrigerator. Afterwards TCA was removed, and plates were washed with H_2O. Thereon fixed cells were dried at 40 °C. On the next day wells were stained for 10 minutes with 0.4% sulforhodamine B (SRB) dissolved in 1% acetic acid. Under theses acidic conditions the dye containing a sulfonic group was able to bind electrostatically to basic amino acid residues. Subsequently unbound dye was removed by washing with 1% acetic acid until the washing solution was colorless. Now the quantity of dye was in a linear relationship with the cell mass per well. Well plates were dried again overnight. To extract the protein bound dye, 10 mM TRIS with a basic pH of 10.5 was added and well plates were stored for 10 minutes on a digital shaker. The cell mass dependent dye content of the wells was quantified with a microplate ELISA reader. For this 80 µl of each well were pipetted in duplicates in a 96-well plate. The optical density (OD) was measured at 550 nm and a reference wavelength of 630 nm. To obtain precise results the OD had to be smaller than 1.8. Otherwise all wells were further diluted with TRIS. The OD of the treated wells was compared with MOCK treated wells to determine the oncolytic or cytotoxic effect.

Table 8: Volumes used for SRB assay per well

Well Plate	TCA [ml]	SRB [µl]	TRIS [ml]
6 Well	1	500	5
24 Well	0.5	250	1-2

2.2.4.2. Monitoring of cell proliferation and viability by real time cell analysis system xCELLigence™ RTCA

Besides determining this antiproliferative effect by SRB assay at an endpoint at 96 hpt, real-time monitoring of proliferation was performed for 155 hours using the xCELLigence™ system. It can quantify cell proliferation by non-invasive electrical impedance monitoring [73]: In special electronic microtiter plates, gold microelectrodes are fused to the bottom. Electrons can flow from the negative terminal through the electrically conductive culture medium to the positive terminal. This current is reduced the more cells adhere on the gold microelectrodes and thereby impair the flow through the culture medium, which can be measured by an increasing impedance of the electron flow. The impedance is reported as a cell index:

$$\frac{\text{Impedance at time point n} - \text{impedance in the absence of cells}}{\text{nominal impedance value}}$$

The cell index was normalized right before treatment (48 hours after seeding). Cells were passaged the day before seeding in order to achieve an exponential growth rate. On the next day cells were detached, counted and resuspended in DMEM containing 5% FCS as described in 2.2.1.1 to 2.2.1.3. The xCELLigence™ 96 well electronic microtiter plate, located in a standard CO_2 cell culture incubator and

interfacing with control and analysis units [74], was preincubated with 50 µl DMEM + 5 % FCS per well and 150 µl PBS in every space between the wells for 30 min. Then 100 µl of the cell suspension containing 2 x 10^3 cells were added in each well. At 48 hours after seeding, 40 µl DMEM + 5 % FCS with or without

AF or the vehicle (MeOH) were carefully added in triplicates (MOCK 6 Wells). Four triplicates were covered as controls for complete cell lysis with 20 µl DMEM + 5 % FCS and 20 µl of the detergent Triton X-100 destroying all cells immediately. Data were analyzed using the RTCA software, further calculated with Microsoft Excel and depicted as a cell growth curve.

2.2.4.3. Flow cytometry

To ensure an effective infection of wild-type measles virus, the expression of the virus receptor CD150 was determined by flow cytometry. This was done by staining the receptor with an antibody which is conjugated to a fluorescent dye (PE) getting activated by a laser beam and detected by a photomultiplier.
For analysis cells had to be prepared. Medium was aspirated and cells were rinsed with PBS. Subsequently, cells were detached with accutase (preserves in contrast to trypsin more epitopes for flow cytometry analysis) for 3-5 min in the incubator. Cells were resuspended in DMEM containing 10 % FCS and centrifuged for 4 min at 1200 rpm. Cells were again resuspended in DMEM containing 10 % FCS and counted as described in 2.2.1.2. To determine the background signal due to unspecific binding of the primary antibody, an isotype control was necessary, too. Therefore, 5×10^5 cells were transferred in two 5 ml round bottom tubes. Cells were diluted with 3 ml PBS and subsequently centrifuged for 4 min at 1200 rpm at 4 °C. The cell pellet was resuspended in 50 µl FACS buffer (PBS containing 1 % FCS). 10 µl Fc-block (Gamunex Immune Globulin Intravenous (Human)) were added to each tube to minimize non-specific binding of immunoglobulins to Fc receptors and cells were incubated for 5 min on crushed ice. Thereupon in one tube 5 µl of the primary antibody (PE conjugated anti-human CD150) and in the other tube 5 µl of the isotype control antibody (PE conjugated anti-mouse IgG1, κ-isotype) were added. Tubes were vortexed and subsequently incubated for 30 min in the dark on crushed ice. Then 3 ml PBS were added, and tubes were centrifuged again. Cells were resuspended in 300 µl FACS buffer, fixed by adding 150 µl 4 % PFA and stored on crushed ice until flow cytometry. Readings were analyzed and presented as overlay histograms.

2.2.4.4. Fluorescence microscopy

The spread of infection was controlled under the fluorescence microscope at different points in time after infection. Microscopy was done using the OLYMPUS IX50 microscope. After phase contrast photos were taken with a PhL ocular at 4 lens magnification fluorescence photos were created from the same detail of the sample. Thus, fluorescence signals could be compared with cells displayed in phase contrast.
The emission was visualized with the F-View Soft Imaging System and the corresponding anaLYSIS software.

2.2.4.5. Electron microscopy

To determine changes on cellular and subcellular level as a result of virus infection or proteasome inhibitor treatment, electron microscopy was performed by B. Fehrenbacher, Department of Dermatology, University Hospital Tübingen. For this samples had to be prepared.
After the incubation period (96 hours) medium was aspirated, cells were rinsed with PBS and detached with trypsin/EDTA as described in 2.2.1.1. Subsequently cells were resuspended in DMEM containing 5 % FCS and centrifugated for 3 minutes at 1200 rpm. Supernatant was aspirated and the pellet resuspended in 1 ml Karnovsky fixative. The sample was transferred in a 1.5 ml reaction tube and was stored for 3 h at room temperature and then in the refrigerator at 4 °C.

2.2.5. Software and statistic

Results were calculated with Microsoft Excel and afterwards statistically analyzed and depicted with GraphPad Prism4.

3. Results

3.1. Antiproliferative effects of Argyrin F

Before exploring potential virostatic effects of Argyrin F (AF) it was necessary to determine the already established antiproliferative effect. Therefore, colorectal carcinoma cells were treated with rising concentrations of AF ranging from 0.01 to 1 µg/ml. At 96 hours post treatment (hpt) the remaining cell mass was determined by SRB assay. As a result, a profound dose-dependent effect was observed with relevant anti-proliferative activities of AF starting at a concentration of 0.05 µg/ml (Fig. 6). At a concentration of 0.1 µg/ml a remaining cell mass of about 80 % was detected when compared to untreated control cells, at a concentration of 1 µg/ml it was reduced to about 60 %. Even higher concentrations of up to 5 µg/ml could not increase the antiproliferative effect. Cells treated with the vehicle MeOH were not influenced in their proliferation.

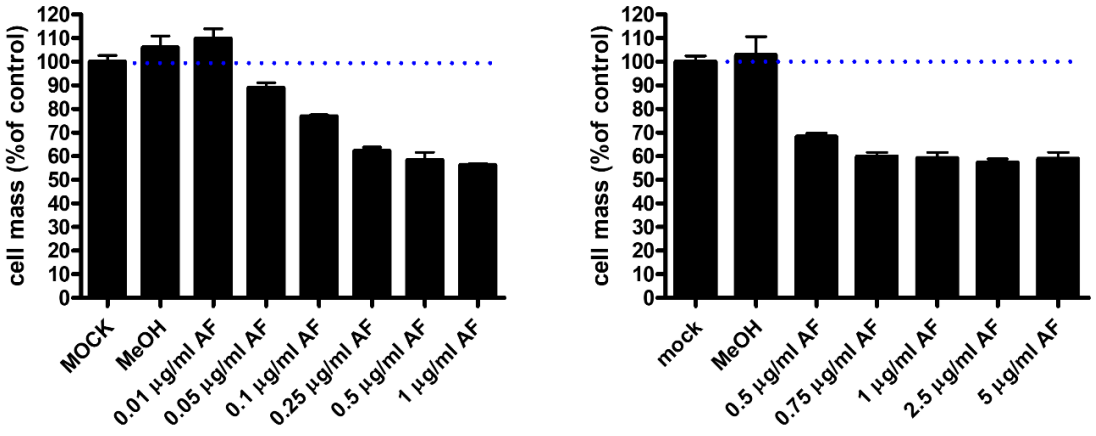

Figure 6: Antiproliferative effects of AF on colorectal carcinoma cells. HCT 116 cells were left untreated (MOCK), treated with vehicle (MeOH) or with rising concentrations of AF. After 96 hours the remaining tumor cell mass was determined by SRB assay. Blue dotted line: mean of untreated cells (100 % cell mass). Values: mean of triplicates. Error bars: SD.

Besides determining this antiproliferative effect by SRB assay at an endpoint at 96 hpt, real-time monitoring of proliferation was performed for 155 hours using the xCELLigence^{TM} RTCA system. Again, a dose dependent antiproliferative effect of AF was observed (Fig. 7). After 24 hours of treatment with AF a dose-

dependent decrease in proliferation started to become visible when compared to untreated cells. After 155 hours (107 hours after treatment) the normalized cell index of untreated cells was about 17.5 while the normalized cell index of cells treated with AF 0.1 µg/ml was about 15.5, with AF 0.5 µg/ml about 12.5 and with AF 2.5 µg/ml about 10. MeOH did not show any effect on proliferation. Treatment with Triton X-100 resulted in complete cell lysis reflected by an immediate decline of the normalized cell index to 0.

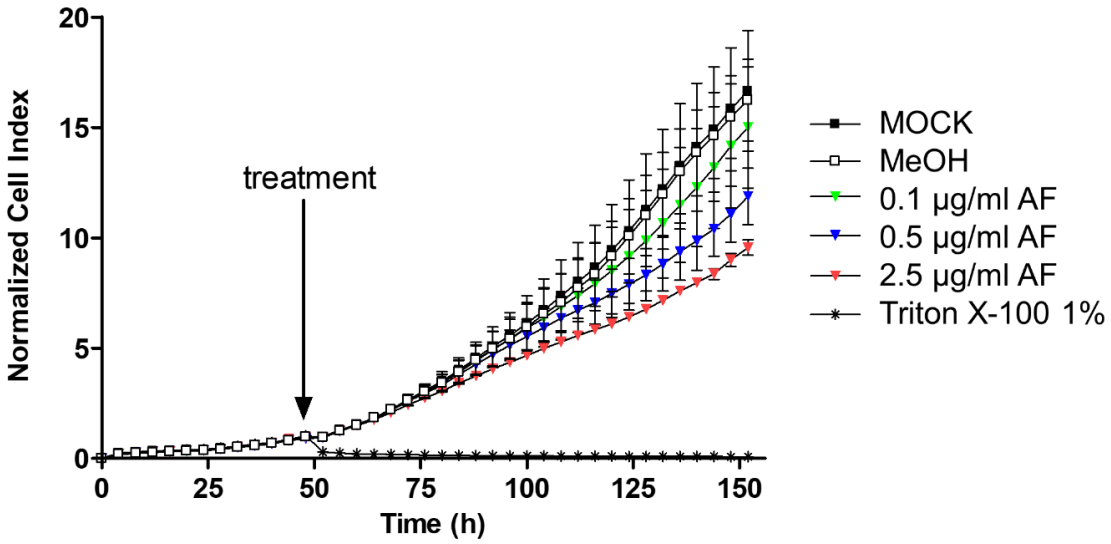

Figure 7: Antiproliferative effects of AF on colorectal carcinoma cells detected by real time cell assay xCELLigence™ system. HCT 116 cells were plated and after 48 hours left untreated (MOCK), treated with vehicle (MeOH), rising concentrations of AF or the detergent Triton X-100. Impedance values were measured for 155 hours. Normalized cell index values (normalized after 48 hours) obtained every four hours are displayed. Values: mean of triplicates. Error bars: SD.

3.2. Virostatic effects of Argyrin F

3.2.1. General proceeding

To investigate potential virostatic effects of a proteasome inhibitor it was necessary to determine a suitable concentration of the proteasome inhibitor and a suitable multiplicity of infection (MOI) of the virus in each cell line. The MOI of the virus had to be in a sector where it showed a measurable oncolytic effect but did not destroy all cells immediately thus allowing to demonstrate a possible cell

protecting effect of the proteasome inhibitor. On the other hand, the concentration of the proteasome inhibitor had to be in a range where it could show a possible virostatic effect but did not destroy all cells by its cytotoxic effect.
Therefore, virus and proteasome inhibitor were tested separately first, using an SRB assay as illustrated in Fig. 8.

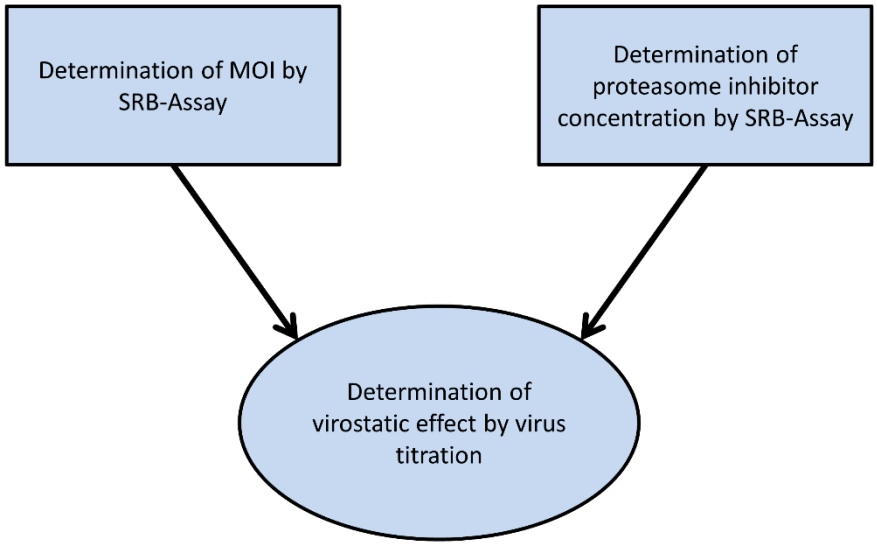

Figure 8: Process of finding suitable concentrations of proteasome inhibitor and virus to detect possible virostatic effects.

3.2.2. Virostatic effects of Argyrin F on MeV-GFP using the cell line HCT 116

Before comparing the virostatic effect between different viruses, cell lines or proteasome inhibitors the above-mentioned general proceeding is demonstrated in the following experiment.
First, HCT 116 cells were treated separately with AF and MeV-GFP. The single treatment with AF exhibiting relevant anti-proliferative activities of AF starting at a concentration of 0.05 µg/ml was already mentioned above (Fig. 6). The single treatment with MeV-GFP is demonstrated in Fig. 9. Colorectal carcinoma cells were infected at rising concentrations of MeV-GFP ranging from MOI 0.5 to 10. The remaining cell mass was determined by SRB assay at 96 hours post infection (hpi). As a result, the oncolytic effect increased at rising MOIs. When using a MOI

of 1 80 % of the cell mass was left at 96 hpi when compared to untreated cells. At a MOI of 10 the remaining cell mass was reduced to only 15 %.

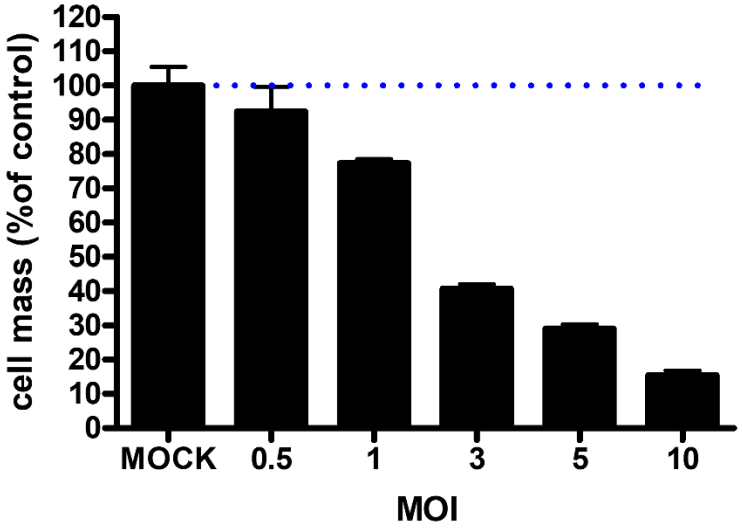

Figure 9: Oncolytic effect of MeV-GFP on the colorectal carcinoma cell line HCT 116. HCT 116 cells were left untreated (MOCK) or infected at rising MOIs with MeV-GFP. At 96 hpi the remaining tumor cell mass was determined by SRB assays. Blue dotted line: mean of untreated cells (100 % cell mass). Values: mean of quadruplicates. Error bars: SD.

Having characterized the monotherapeutic effects of virus and proteasome inhibitor in HCT 116 cells, in the next step cells were treated with a combined therapy. As illustrated in Fig. 10, 24 hours after seeding colorectal carcinoma cells were infected with MeV-GFP. At 3 hpi medium with or without rising concentrations of AF was added. At 96 hpi supernatant and cell lysate were collected and the amount of infective virus particles was quantified by virus titration.

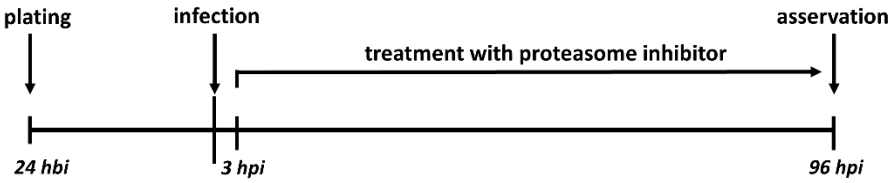

Figure 10: Application scheme for combined treatment with virus and proteasome inhibitor.

For further experiments a MOI of 1 was chosen, where about 80% of the cell mass was left in monotherapy. As even high concentrations of AF did not reduce cell mass under 50 %, concentrations of up to 10 µg/ml were used which were subsequently reduced.

As a result (Fig. 11), in both supernatant and cell lysate, a dose dependent reduction of infective virus particles was detected. At 96 hpi in the absence of AF viral titers reached more than 10^5 pfu/ml in supernatants and more than 10^6 pfu/ml in cell lysates. In contrast in cells treated with 2.5 µg/ml AF at 3 hpi, viral titers were up to 1000-fold lower at 96 hpi (approximately 10^2-10^3 pfu/ml in supernatants and 10^3-10^4 pfu/ml in cell lysates). Reduction of AF concentrations below 2.5 µg/ml resulted in a dose dependent decrease of the antiviral effect. 0.1 µg/ml AF reduced the virus concentrations only less than 10-fold (Fig. 11, upper panels). Higher concentrations of AF of up to 10 µg/ml did not lead to a further reduction of infective virus particles (Fig. 11, lower panels).

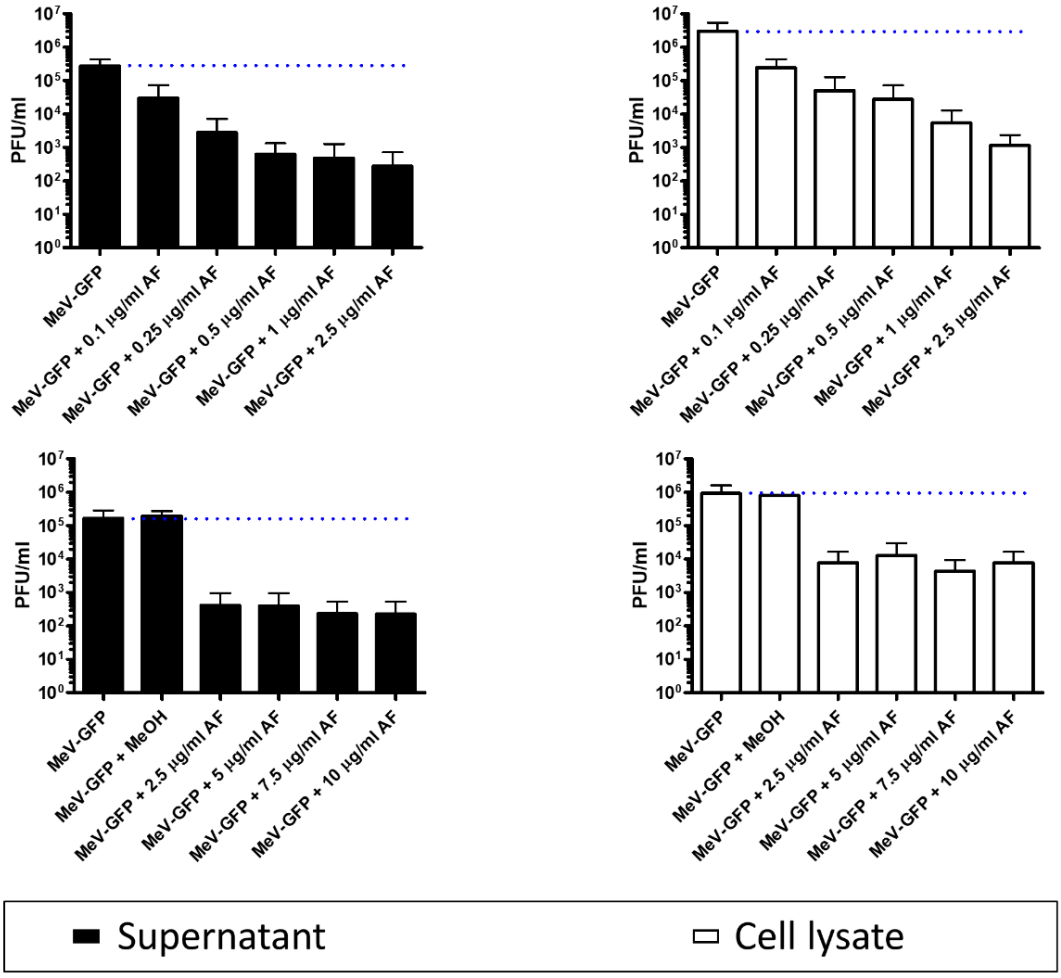

Figure 11: Virostatic effects of AF on MeV-GFP in colorectal carcinoma cells. HCT 116 cells were infected with MeV-GFP at MOI 1. At 3 hpi cells were left untreated or treated with vehicle (MeOH) and rising concentrations of AF, respectively. At 96 hpi supernatant (black columns) and cell lysate (white columns) were collected and virus particles were quantified by titration on Vero cells. PFU = Plaque forming units. Blue dotted line: mean of viral titers without AF or MeOH. Values: low concentrations of AF (upper panel) mean of three independent experiments, high concentrations of AF (lower panel) mean of two independent experiments. Error bars: SD.

3.2.3. Cell line dependent virostatic effects of Argyrin F on MeV-GFP

To characterize the active range of AF other cell lines were tested as well. Therefore, first the human hepatocellular carcinoma cell line Hep3B and the human pancreatic carcinoma cell line MIA PaCa-2 were chosen. Again, initially single treatments with AF and MeV-GFP were performed.

In the single treatment with AF using concentrations ranging from 0.05 to 5 µg/ml, at 96 hpt differences to the colorectal carcinoma cell line were detected by SRB assay analysis (Fig. 12). In the pancreatic carcinoma cell line MIA PaCa-2 a weaker antiproliferative effect was observed. Across all tested concentrations the remaining cell mass was about 80 % compared to untreated cells (Fig. 12, left panel). In contrast only 60 % of HCT 116 cells were left at a concentration of 1 µg/ml (Fig. 6). Since the antiproliferative effect was so weak no lower concentrations were tested. The proliferation of hepatocellular carcinoma cells (Hep3B) was not influenced at all by AF (Fig. 12, right panel). Again, comparable to HCT 116, in both cell lines the vehicle MeOH did not influence proliferation.

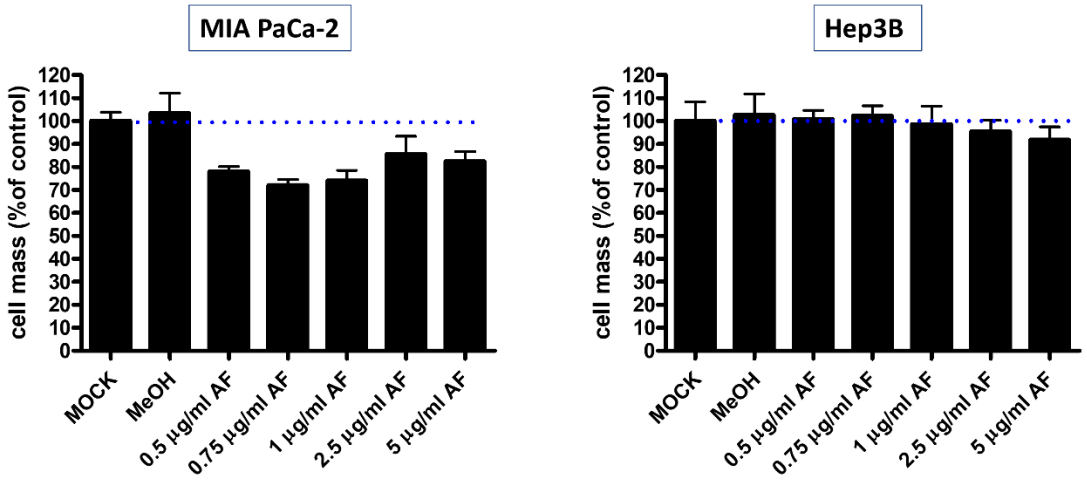

Figure 12: Cell line dependent antiproliferative effects of AF on human pancreatic carcinoma cell line MIA PaCa-2 and human hepatocellular carcinoma cell line Hep3B. Cells were left untreated (MOCK) or treated with vehicle (MeOH) and rising concentrations of AF, respectively. After 96 hours the remaining tumor cell mass was determined by SRB assay. Blue dotted line: mean of untreated cells (100 % cell mass). Values: mean of triplicates. Error bars: SD.

Infection with MeV-GFP also revealed different susceptibilities of these cell lines. The remaining cells mass was determined again by SRB assay at 96 hpi. The oncolytic effect of MeV-GFP on Mia PaCa-2 was comparable to HCT 116 (already demonstrated in Fig. 9). At a MOI of 10 about 20 % of the pancreatic carcinoma cells were left compared to untreated cells, at a MOI of 1 80 % (Fig. 13, left panel) (HCT 116: MOI 10 20 %, MOI 1 80 %). In contrast, Hep3B cells were much more

susceptible to MeV-GFP mediated oncolysis. At 96 hpi at a MOI of 0.5 less than 10 % of the control was left, at a MOI of 0.005 about 90 % (Fig. 13, right panel).

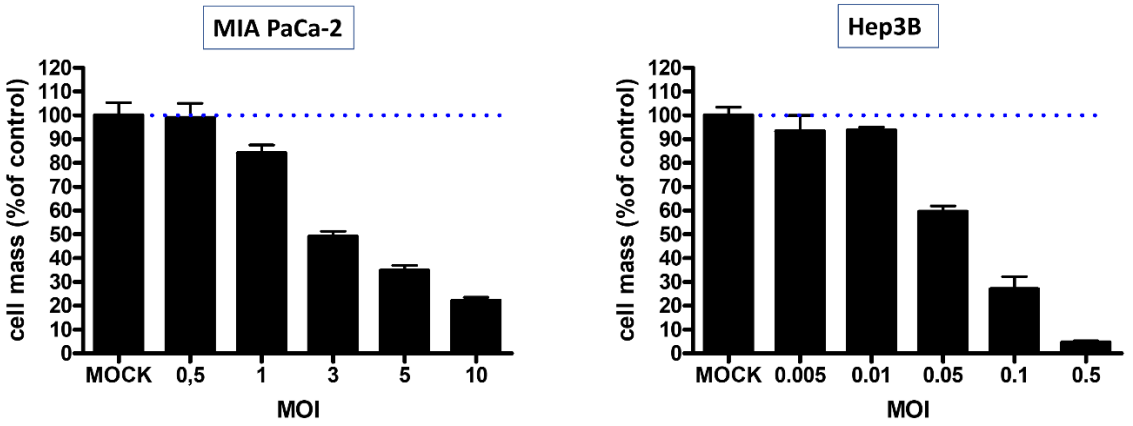

Figure 13: Cell line dependent oncolytic effects of MeV-GFP on human pancreatic carcinoma cell line MIA PaCa-2 and human hepatocellular carcinoma cell line Hep3B. Cells were left untreated (MOCK) or infected at rising MOIs of MeV-GFP. At 96 hpi the remaining tumor cell mass was determined by SRB assays. Blue dotted line: mean of untreated cells (100 % cell mass). Values: mean of quadruplicates. Error bars: SD.

Therefor we decided to choose a lower MOI for Hep3B cells (MOI 0.01) than for Mia PaCa-2 cells (MOI 1) in the combined treatment to achieve comparable oncolytic effects. As AF did not show intense antiproliferative effects, in both settings concentrations ranging from 2.5 to 10 µg/ml were added. As in the combined treatment with HCT 116, cells were treated at 3 hpi with AF and infective virus particles were quantified in supernatant and cell lysate by titration on Vero cells at 96 hpi. As a result (Fig. 14), in MIA PaCa-2 cell lysates virus titers were about 100-fold lower in the setting with AF compared to untreated cells (approximately 10^3 pfu/ml with AF and 10^5 pfu/ml without). In contrast, in the supernatant of MIA PaCa-2 cells no reduced number of infective virus particles was measured (10^3 – 10^5 pfu/ml) (Fig. 14, upper panel). In the supernatant of Hep3B cells under AF treatment only a slight reduction was detected (approximately 10^4 – 10^5 pfu/ml with AF and 10^6 pfu/ml without). In Hep3B cell lysates the virostatic effect of AF was a bit more pronounced (approximately 10^5 pfu/ml with AF and 10^7 pfu/ml in control) (Fig. 14, lower panel). Overall, in HCT 116 cells the virostatic effect with virus titer reductions up to 1000-fold in

supernatant and cell lysate (Fig. 11) was stronger than in Hep3B and MIA PaCa-2, where only in the cell lysate a reduction up to 100-fold was determined.

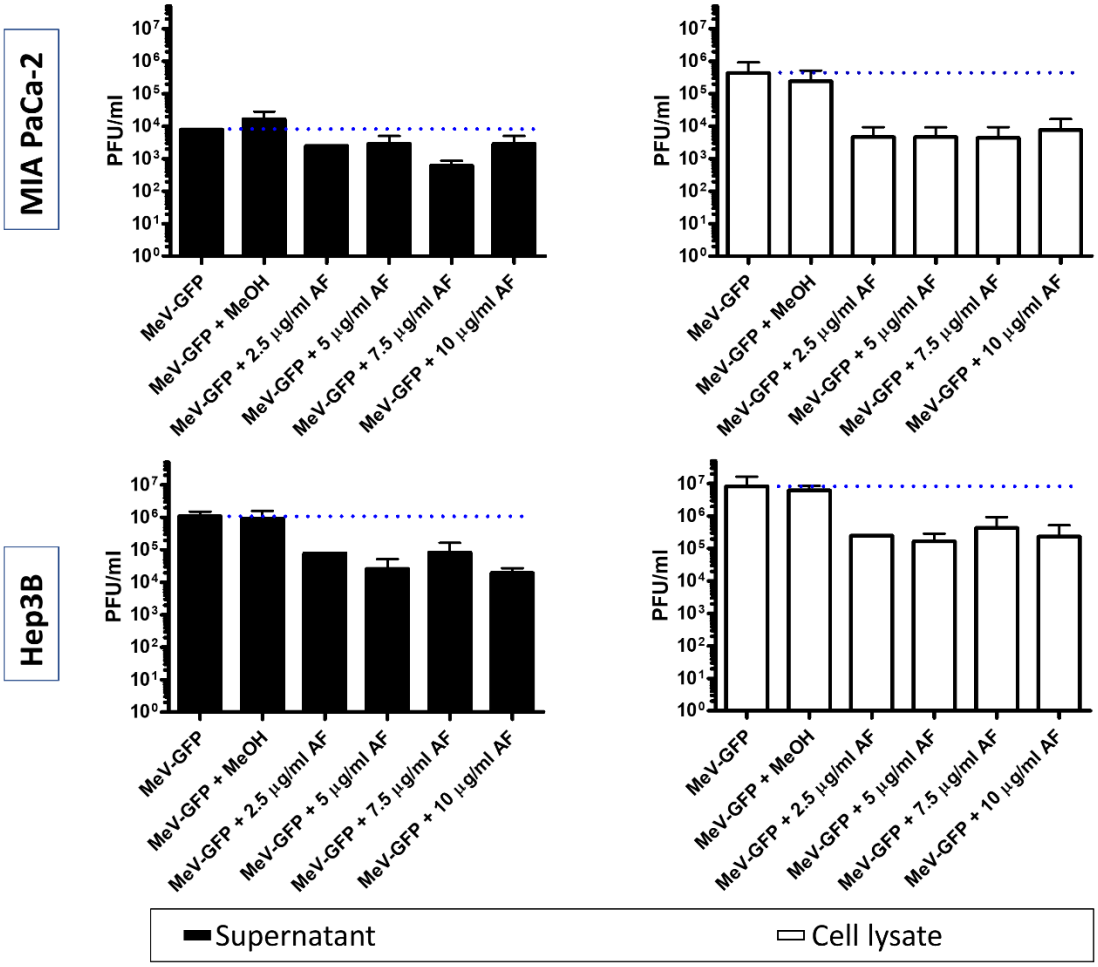

Figure 14: Cell line dependent virostatic effects of AF on MeV-GFP in human pancreatic carcinoma cell line MIA PaCa-2 and human hepatocellular carcinoma cell line Hep3B. Cells were infected with MeV-GFP (Mia PaCa-2: MOI 1, Hep3B: MOI 0.01). At 3 hpi cells were left untreated or treated with vehicle (MeOH) and rising concentrations of AF, respectively. At 96 hpi supernatant (black columns) and cell lysate (white columns) were collected and virus particles were quantified by titration on Vero cells. PFU = Plaque forming units. Blue dotted line: mean of viral titers without AF or MeOH. Values: mean of two independent experiments. Error bars: SD.

3.2.4. Measles vaccine virus strain dependent virostatic effects of Argyrin F

Next, the possible virostatic effect of AF on other measles vaccine virus strains was tested. Therefore, virus strains AIK-C, L-16, Mérieux and Nse-GFP were chosen. Experiments were performed in the colorectal carcinoma cell line HCT 116, where the strongest virostatic effect of AF on MeV-GFP was observed.

First, the oncolytic efficacy of all virus strains was again determined by SRB assay. Thereby striking differences to MeV-GFP were detected (Fig. 15). All tested virus strains showed stronger oncolytic effects than MeV-GFP at 96 hpi (at MOI 10 20 % cell mass was left compared to untreated cells, at MOI 1 80 % as shown in Fig. 9). HCT 116 cells were most susceptible for Nse-GFP, followed by AIK-C, L-16 and Mérieux. Nse-GFP left about 2 % of cell mass compared to untreated cells at 96 hpi at MOI 1, at MOI 0.1 about 10 %. In AIK-C infected samples 3 % compared to the control was left at MOI 1 (at MOI 0.1 35 %) while at 96 hpi with L16 at MOI 1 the cell mass was reduced to 30 % (at MOI 0.1 close to 100 %) and with Mérieux at MOI 1 to about 40 % (at MOI 0.1 close to 100 %).

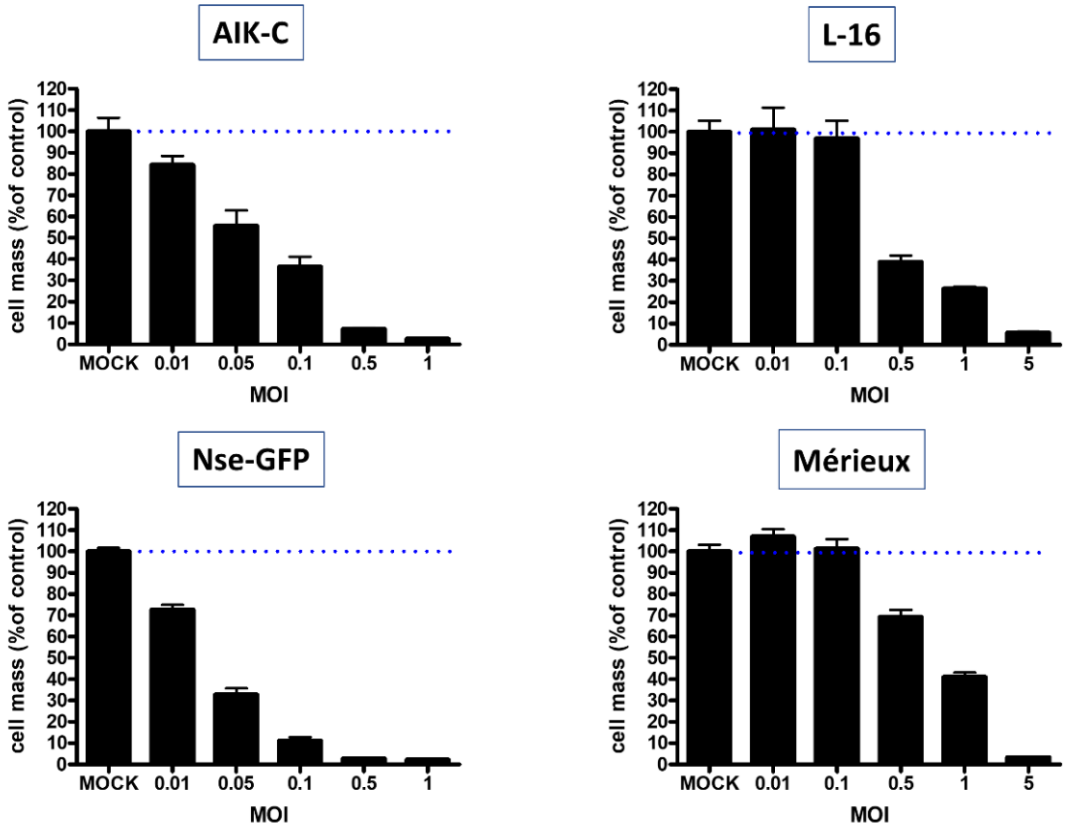

Figure 15: Measles vaccine virus dependent oncolytic effects on the colorectal carcinoma cell line HCT 116. Cells were left untreated (MOCK) or infected at rising MOIs with AIK-C, L-16, Nse-GFP and Mérieux, respectively. At 96 hpi the remaining tumor cell mass was determined by SRB assays. Blue dotted line: mean of untreated cells (100 % cell mass). Values: mean of quadruplicates. Error bars: SD.

In the combined treatment AF concentrations ranging from 2.5 to 10 µg/ml were chosen. To reach comparable oncolytic effects cells were infected with AIK-C at MOI 0.05, with L-16 at MOI 0.25, with Mérieux at MOI 0.5 and with Nse-GFP at MOI 0.025. Again, cells were infected with measles vaccine virus and treated with AF following the same schedule as illustrated in Fig. 10.

As a result (Fig. 16), strong virostatic effects were measured in 3 out of 4 tested measles vaccine virus strains. Only in the supernatant of Nse-GFP infected cells, with already low virus titers without AF (approximately 10^1 pfu/ml), no virostatic effect was detected. In cell lysates infective Nse-GFP virus particles were about 10-fold lower under AF treatment (approximately 10^4 pfu/ml with AF and 10^5 pfu/ml without).

However, compared to MeV-GFP (virus titer reductions up to 1000-fold in supernatant and cell lysate as illustrated in Fig. 11) virostatic effects on AIK-C, L-16 and Mérieux were equal or even stronger:

- In AIK-C infected samples virus titers in supernatant were about 10000-fold lower (approximately 10^1 pfu/ml with AF and 10^5 pfu/ml without) and in cell lysates even 100000-fold lower (approximately 10^1 pfu/ml with AF and 10^6 pfu/ml without).

- Virus titers of L-16 were reduced about 10000-fold in supernatants (approximately 10^2 pfu/ml with AF and 10^6 pfu/ml without) and 100 to 1000-fold in cell lysates (approximately 10^4 -10^5 pfu/ml with AF and 10^7 pfu/ml without).

- For Mérieux viral titers were reduced 10000-fold in supernatant (approximately 10^3 pfu/ml with AF and 10^7 pfu/ml without), in cell lysate 100-fold (approximately 10^5 pfu/ml with AF and 10^7 pfu/ml without).

- On the contrary, in all settings the vehicle MeOH did not reduce viral titers.

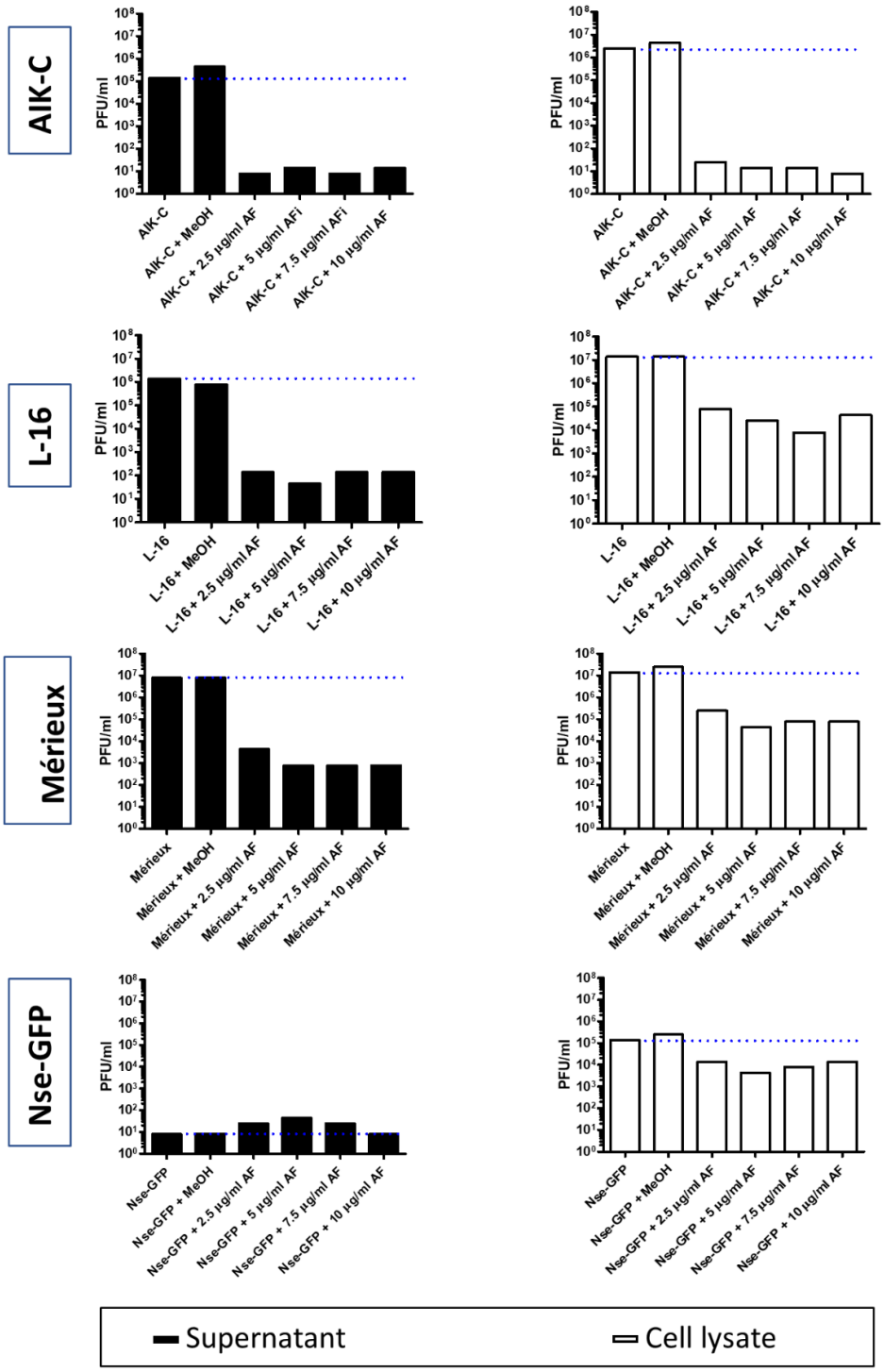

Figure 16: Measles vaccine virus dependent virostatic effects of AF in human colorectal carcinoma cell line HCT 116. Cells were infected with AIK-C (at MOI 0.05), L-16 (at MOI 0.25), Mérieux (at MOI 0.5) or Nse-GFP (at MOI 0.025). At 3 hpi cells were left untreated or treated with vehicle (MeOH) and rising concentrations of AF, respectively. At 96 hpi supernatant (black columns) and cell lysate (white columns) were collected and virus particles were quantified by titration on Vero cells. Blue dotted line: mean of viral titers without AF or MeOH. PFU = Plaque forming units. Values: one experiment.

3.2.5. Application time point dependent virostatic effects of AF

Beside the effective range of AF in relation to dose, vaccine virus strain and infected cell line (shown in chapter 3.2.2 to 3.2.4), for clinical applications the influence of the time interval between infection and treatment is also important. Therefore, in the established setting with the colorectal carcinoma cell line HCT 116, cells were treated at different points in time with AF before and after infection.

As illustrated in Fig. 17 in the pre infection kinetics cells were plated 72 hours before infection (hbi) and treated with 2.5 µg/ml AF at 48 hbi, 24 hbi, 12 hbi or 3 hbi. Before the cells were infected the AF containing medium was removed. Furthermore, the cell density, which was influenced by AF, was determined for each approach to reach a MOI of 1 in all wells. At 96 hpi supernatant and cell lysate were separately collected and the amount of infective virus particles was quantified by virus titration.

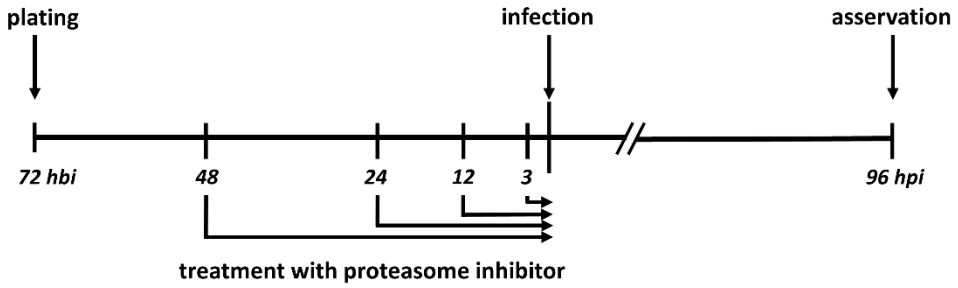

Figure 17: Application scheme of the pre infection kinetics. Cells were plated at 72 hours before infection (hbi) and treated at different points in time before infection with AF. AF containing medium was removed and cells were infected with MeV-GFP at MOI 1. Samples were collected at 96 hpi.

As a result (Fig. 18), a weak reduction of infectious virus particles was measured in supernatant and cell lysate when AF was added at 3 hbi. With 10^4 -10^5 pfu/ml in supernatant and 10^5 -10^6 pfu/ml in cell lysate virus titers were about 10 to 100-fold lower compared to untreated cells. In contrast even weaker or no virostatic effects at all were determined when AF was added earlier than 3 hbi.

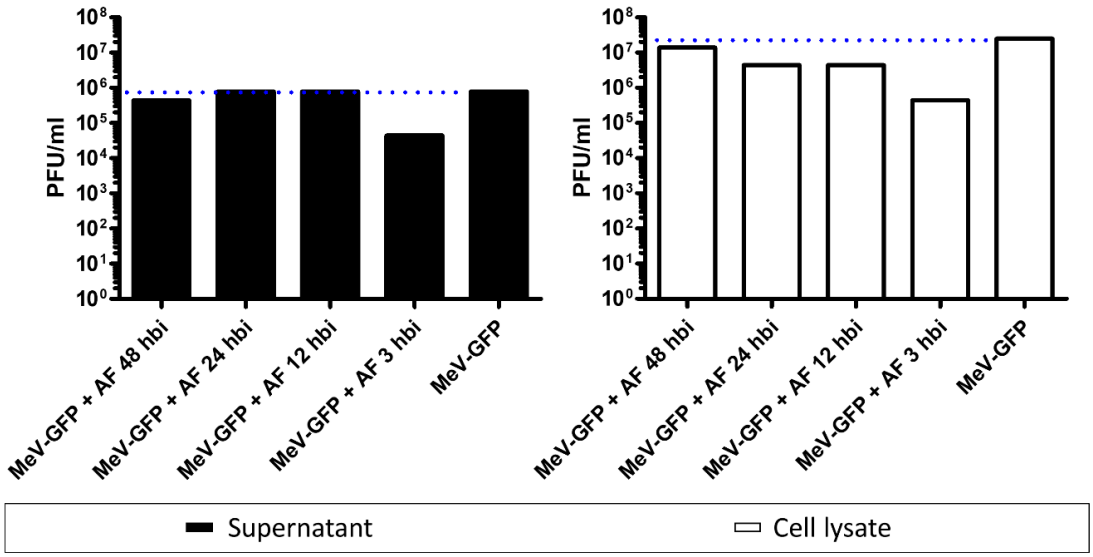

Figure 18: Pre infection kinetics of virostatic effects of AF. HCT 116 cells were plated at 72 hbi and were left untreated or treated with 2.5 µg/ml AF at 48 hours before infection (hbi), 24 hbi, 12 hbi or 3 hbi. AF containing medium was removed and cells were infected with MeV-GFP at MOI 1. At 96 hpi supernatant (black columns) and cell lysate (white columns) were collected and virus particles were quantified by titration on Vero cells. PFU = Plaque forming units. Blue dotted line: virus titer in the absence of AF. Values: single experiment.

In the post infection kinetics (Fig. 19) cells were infected with MeV-GFP at MOI 1 24 hours after seeding and treated with 1 µg/ml AF at 3 hpi, 9 hpi, 12 hpi, 15 hpi, 18 hpi, 21 hpi, 24 hpi, 36 hpi or 48 hpi. Again, supernatant and cell lysate were separately collected at 96 hpi and the amount of infective virus particles was quantified by virus titration.

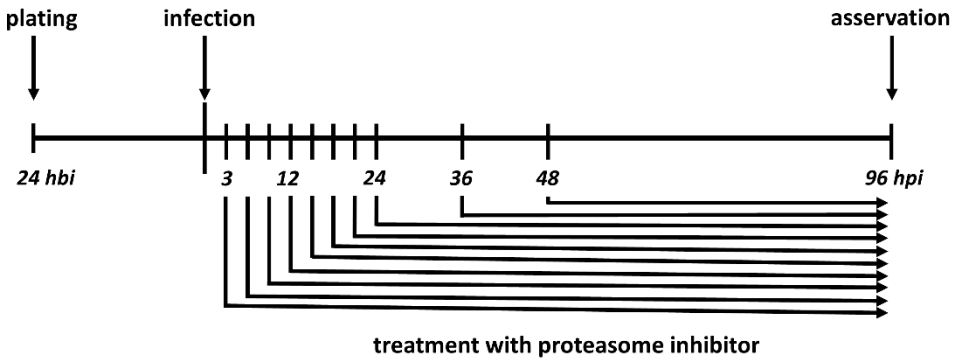

Figure 19: Application scheme of the post infection kinetics. Cells were plated and after 24 hours infected with MeV-GFP at MOI 1. At different points in time after the infection cells were treated with AF. Samples were collected at 96 hpi.

As shown in Fig. 20 an application time point dependent virostatic effect of AF was detected. When AF was added at 3 hpi viral titers were about 10000-fold lower in supernatants (approximately 10^2 pfu/ml with AF and 10^6 pfu/ml without) and 1000-fold lower in cell lysates (approximately 10^4 pfu/ml with AF and 10^7 pfu/ml without) compared to untreated cells. This inhibition decreased the later AF was given. When applying AF at 9 hpi viral titers were already 10-fold higher compared to treatment starting at 3 hpi. However, still virus titers were reduced 1000-fold in supernatant and 100-fold in cell lysate in relation to untreated cells. No reduction of infective virus particles was determined in the supernatant when treatment was more than 24 hours delayed. In cell lysates no virostatic effect could be measured when AF was added after 36 hours.

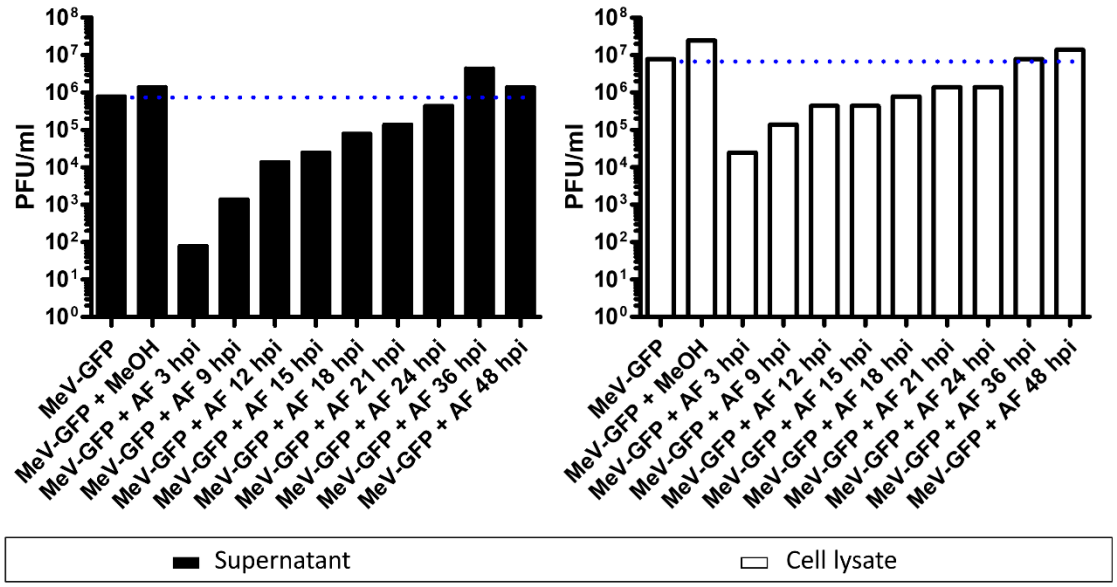

Figure 20: Post infection kinetics of virostatic effects of AF. HCT 116 cells were plated and after 24 hours infected with MeV-GFP at MOI 1. Cells were left untreated or treated with vehicle (MeOH) and 1 µg/ml AF at 3 hpi, 9 hpi, 12 hpi, 15 hpi, 18 hpi, 21 hpi, 24 hpi, 36 hpi or 48 hpi. At 96 hpi supernatant (black columns) and cell lysate (white columns) were collected and virus particles were quantified by titration on Vero cells. PFU = Plaque forming units. Blue dotted line: virus titer in the absence of AF. Values: one experiment.

3.2.6. Analysis of virostatic effects of AF by SRB assay

In addition to the direct quantification of infective virus particles, virostatic effects could also be shown indirectly by measuring a reduced oncolytic effect.

Colorectal carcinoma cells were again MOCK infected or infected with the measles vaccine virus AIK-C. AIK-C was chosen because with this strain the reduction of viral titers was most prominent. At 3 hpi cells were MOCK treated or treated with rising concentrations of AF. At 96 hpi the remaining cell mass was quantified by SRB assay.

As shown in Fig. 21 differences were already visible with the naked eye, after cells were fixed and dyed with SRB. While untreated cells (MOCK) formed a confluent purple cell layer, infection with AIK-C led to a massive destruction of the cell layer as reflected by predominantly white areas. Cells treated with AF only (AF monotherapy) did not differ macroscopically from untreated cells. However, combining virus and proteasome inhibitor (combined therapy) led to a dose-dependent increase in cell mass as reflected by purple stain.

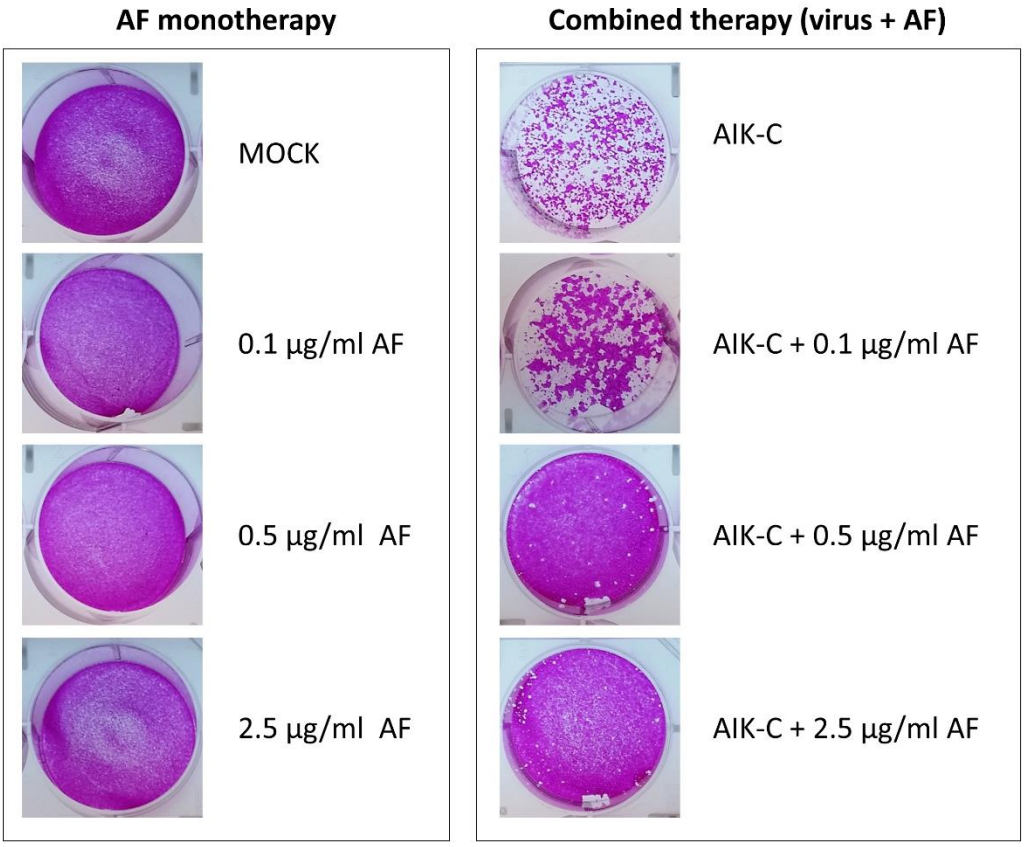

Figure 21: SRB stain reflects virostatic effects of AF on AIK-C in colorectal carcinoma cells. HCT 116 cells were left untreated (MOCK) or infected with AIK-C at MOI 0.05. At 3 hpi medium with or without rising concentrations of AF was added to MOCK infected cells (AF monotherapy, left panel) and to virus infected cells (Combined therapy, right panel). At 96 hpi the remaining tumor cells were fixed and dyed with SRB.

Next the remaining cell mass was exactly determined with a microplate ELISA reader (Fig. 22). In keeping with the macroscopic impression, infection with AIK-C reduced the remaining cell mass to about 40 % when compared to mock infected cells, while under AF monotherapy the cell mass was only reduced to 80 - 85 %. Cells treated with both, AF and virus (combined therapy), showed 45 % (AIK-C + 0.1 µg/ml AF), 85 % (AIK-C + 0.5 µg/ml AF) and 96 % remaining cell mass (AIK-C + 2.5 µg/ml AF) compared to untreated cells.

To summarize, in line with the results of the virus titration there was a dose dependent inhibition of oncolysis by adding AF after infection.

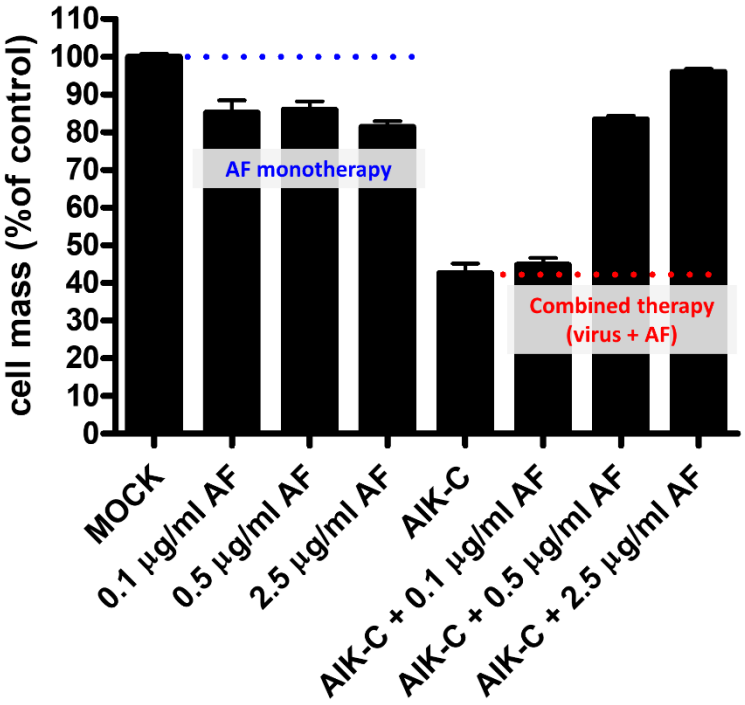

Figure 22: Analysis of virostatic effects of AF on AIK-C in colorectal carcinoma cells **by SRB assay.** HCT 116 cells were left untreated or infected with AIK-C at MOI 0.05. At 3 hpi medium with or without rising concentrations of AF was added to MOCK infected cells (AF monotherapy) and to virus infected cells (Combined therapy). At 96 hpi the remaining tumor cell mass was determined by SRB assay. Blue dotted line: mean of untreated cells (100 % cell mass). Red dotted line: mean of infected cells without AF (43 % cell mass). Values: mean of triplicates. Error bars: SD.

3.2.7. Analysis of virostatic effects of AF by fluorescence microscopy

Besides the determination of infectious virus particles by virus titration, a rough estimate of infected cells could be made by fluorescence microscopy in case of a GFP expressing virus, e.g. MeV-GFP. For this purpose, again colorectal carcinoma cells were infected with MeV-GFP and were left untreated or were treated with rising concentrations of AF. Phase contrast and corresponding fluorescence photos were taken at 96 hpi (Fig. 23).

As a result, cells only infected with MeV-GFP showed green fluorescence, indicating infected cells. Moreover, some virus dependent syncytia formations (large green areas, exemplarily marked with a red arrow) could be recognized. In contrast, under additional AF treatment there was a dose-dependent reduction of the fluorescence signal. At 1 µg/ml AF only a few green glowing cells were left.

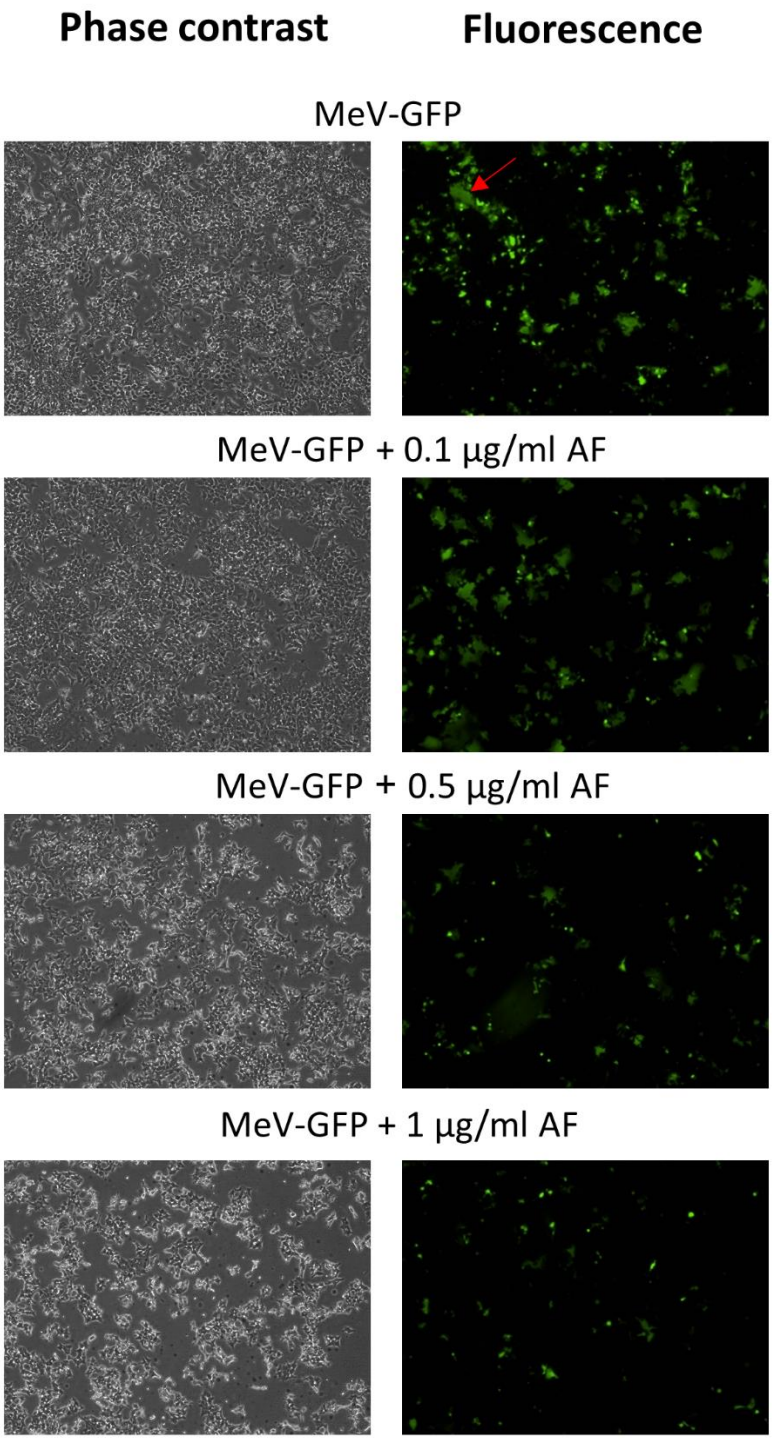

Figure 23: Analysis of virostatic effects of AF on MeV-GFP in colorectal carcinoma cells **by fluorescence microscopy.** HCT 116 cells were infected with MeV-GFP at MOI 1. At 3 hpi cells were left untreated or treated with rising concentrations of AF. At 96 hpi phase contrast and corresponding fluorescence photos were taken at 4x original magnification. Infected cells showed green fluorescence. Red arrow: exemplary virus dependent syncytia formation.

3.3. Determination of potential virostatic effects of further proteasome inhibitors

The next step was to investigate whether other proteasome inhibitors also have virostatic effects. For this purpose, the clinically approved drugs Bortezomib, Carfilzomib and Ixazomib were used. The combination of the colorectal carcinoma cell line HCT 116 and measles vaccine virus MeV-GFP, which was already established for AF, was chosen for this experiment again. First, suitable concentrations for each proteasome inhibitor had to be determined. Therefore, colorectal carcinoma cells were treated with rising concentrations of Bortezomib, Carfilzomib or Ixazomib. The remaining cell mass was determined by SRB assay at 96 hpt (Fig. 24). As a result, a dose-dependent effect was observed with relevant cytotoxic effects of all proteasome inhibitors, starting at a concentration of 2.5 nM of Bortezomib, 2.5 nM of Carfilzomib or 5 nM of Ixazomib. Compared to untreated cells at a concentration of 10 nM a remaining cell mass of about 1 % was determined with Bortezomib, 25 % with Carfilzomib and 80 % with Ixazomib. In contrast to AF, where concentrations higher than 1 µg/ml could not further reduce the cell mass (Fig. 6), almost no adherent cells were left at high concentrations of the other proteasome inhibitors.

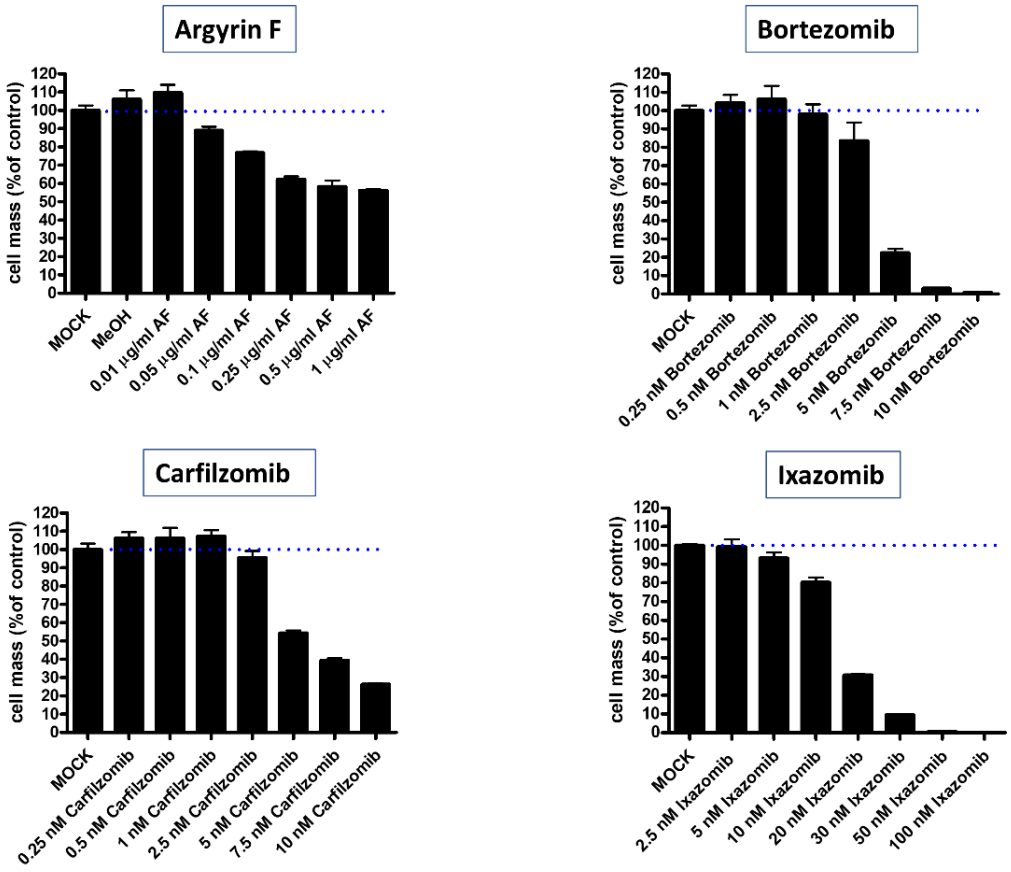

Figure 24: Cytotoxic effects of other proteasome inhibitors on colorectal carcinoma cells. HCT 116 cells were left untreated (MOCK), or treated with rising concentration of Bortezomib, Carfilzomib or Ixazomib. At 96 hpt the remaining tumor cell mass was determined by SRB assay. For direct comparison, the result of AF already described is depicted again. Blue dotted line: mean of untreated cells (100 % cell mass). Values: mean of triplicates. Error bars: SD.

To investigate potential virostatic effects of the proteasome inhibitors, concentrations were chosen which reduced the cell mass up to 25% but did not destroy all cells. Therefore, for Bortezomib we chose concentrations ranging from 1 nM to 3 nM, for Carfilzomib from 1 nM to 10 nM and for Ixazomib from 2.5 nM to 15 nM. Again, HCT 116 cells were infected with MeV-GFP at MOI 1 and treated with rising concentrations of the respective proteasome inhibitor at 3 hpi or were left untreated. At 96 hpi supernatant and cell lysate were collected and the amount of infective virus particles was quantified by virus titration (Fig. 25). In contrast to AF, none of the other proteasome inhibitors was able to lower virus titers in supernatant or cell lysate at any concentration in a relevant manner.

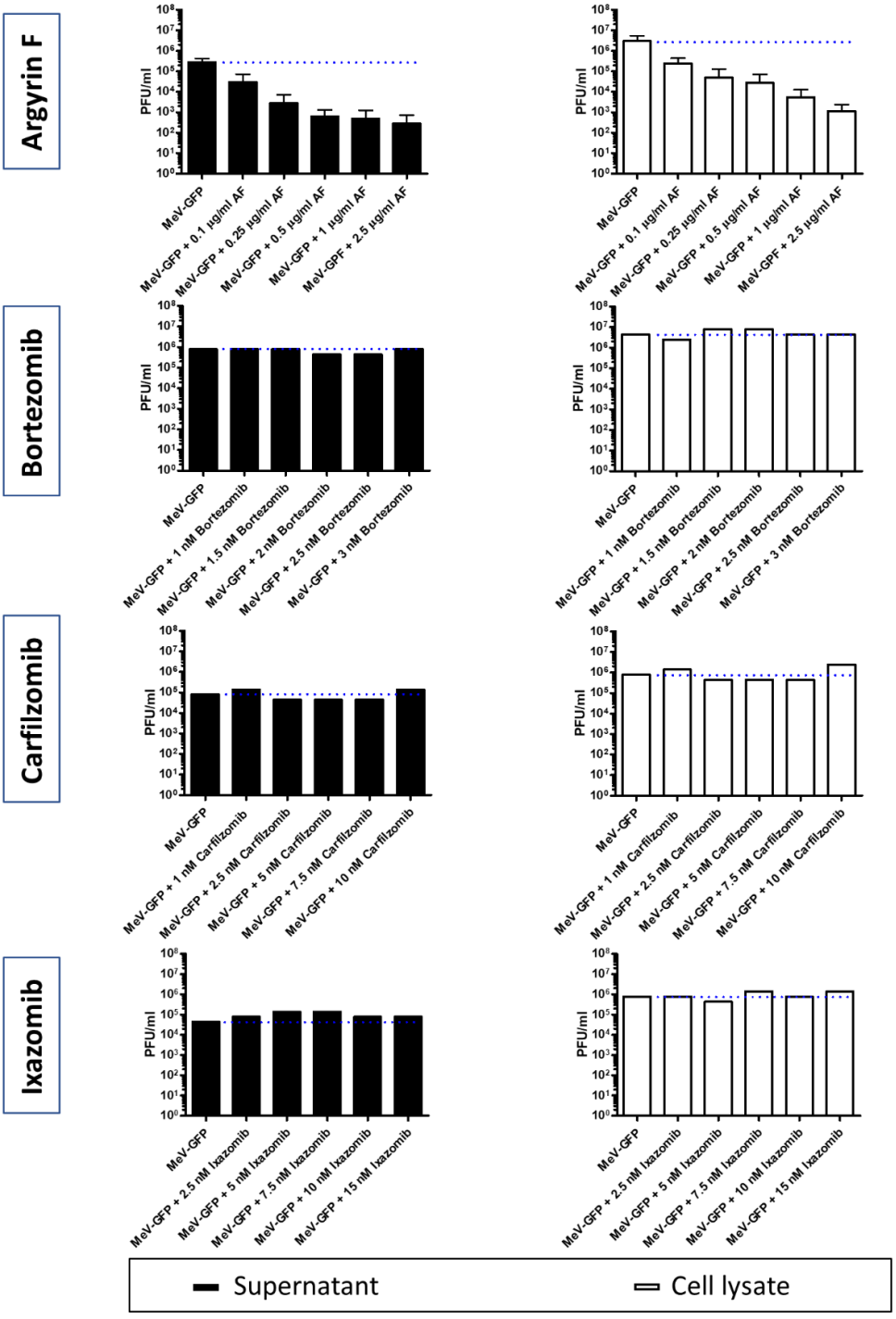

Figure 25: Effects of different proteasome inhibitors on MeV-GFP in colorectal carcinoma cells. HCT 116 cells were plated and infected with MeV-GFP at MOI 1. Cells were left untreated or treated with rising concentrations of Bortezomib, Carfilzomib or Ixazomib at 3 hpi. At 96 hpi supernatants (black columns) and cell lysates (white columns) were collected and virus particles were quantified by titration on Vero cells. For direct comparison, the result obtained with AF is depicted again on top. PFU = Plaque forming units. Blue dotted line: virus titer in the absence of proteasome inhibitor. Values: one representative experiment (AF: mean of three independent experiments. Error bars: SD).

3.4. Virostatic effects of AF on wild-type measles virus

After testing the influence of AF on measles vaccine virus strains, we examined whether AF can also inhibit the replication cycle of wild-type measles virus. However, as described in the introduction, vaccine and wild-type measles virus differ in terms of which receptor protein they can use to enter the cell. It is particularly important here that wild-type other than vaccine measles virus cannot use the CD46 surface marker expressed on most cells. In addition to nectin-4, wild-type virus (as well as vaccine measles virus) can bind via CD150 (SLAMF1), which is only found on activated B and T cells, dendritic cells, monocytes and macrophages. Therefore, we used CD150 expressing cells for the experiments with wild-type measles virus. For infection the cell line B95a, a derivative of the cotton-top marmoset B-lymphoblastoid cell line B95-8 was chosen, which is transformed with EBV. B95a cells were adapted to (semi)-adherent growth.

For virus titration the cell line Vero/hSLAM was used, a derivative of Vero cells transfected with an expression plasmid encoding CD150.

Before experiments with wild-type measles virus were carried out, the CD150 expression of both cell lines was investigated by flow cytometry (Fig. 26). Both cell lines displayed a high amount of CD150 positive cells (99.8 % of B95a cells, 79.3 % of Vero/hSLAM cells).

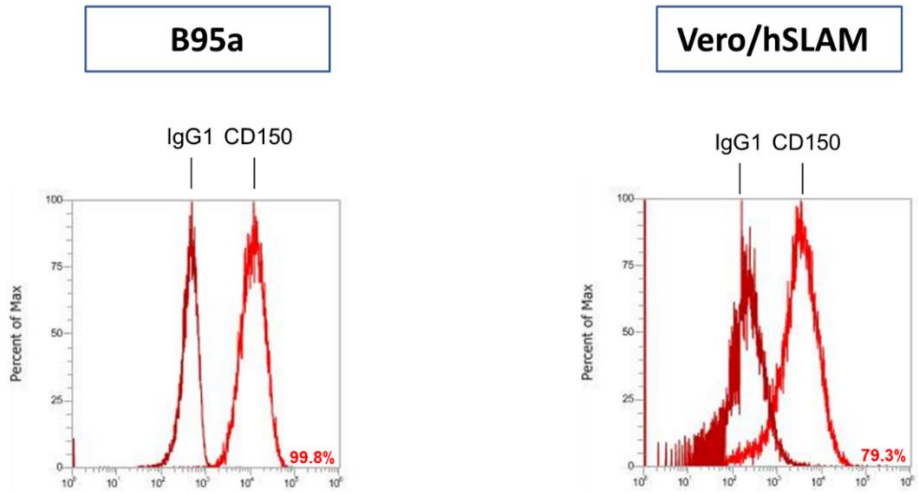

Figure 26: Analysis of CD150 expression by flow cytometry. Cell lines B95a and Vero/hSLAM were stained with PE conjugated anti-CD150 antibody (CD150) and isotype control (IgG1), respectively. The percentage of CD150 expressing cells is indicated. One representative experiment is shown.

Next, the oncolytic efficacy of wild-type measles virus on B95a cells was determined. For this, B95a cells were infected at rising MOIs with wild-type measles virus of genotypes B3, D4 or D8. In addition, one approach was infected with measles vaccine virus MeV-GFP. The remaining cell mass was determined at 96 hpi by SRB assay (Fig. 27). The highest oncolytic efficacy was measured for wild-type measles virus of genotype B3. Compared to untreated cells only 50 % of the cell mass were left at MOI 0.1. When using wild-type measles virus of genotype D8, D4 or MeV-GFP the cell mass was only reduced to 80 % at the same MOI.

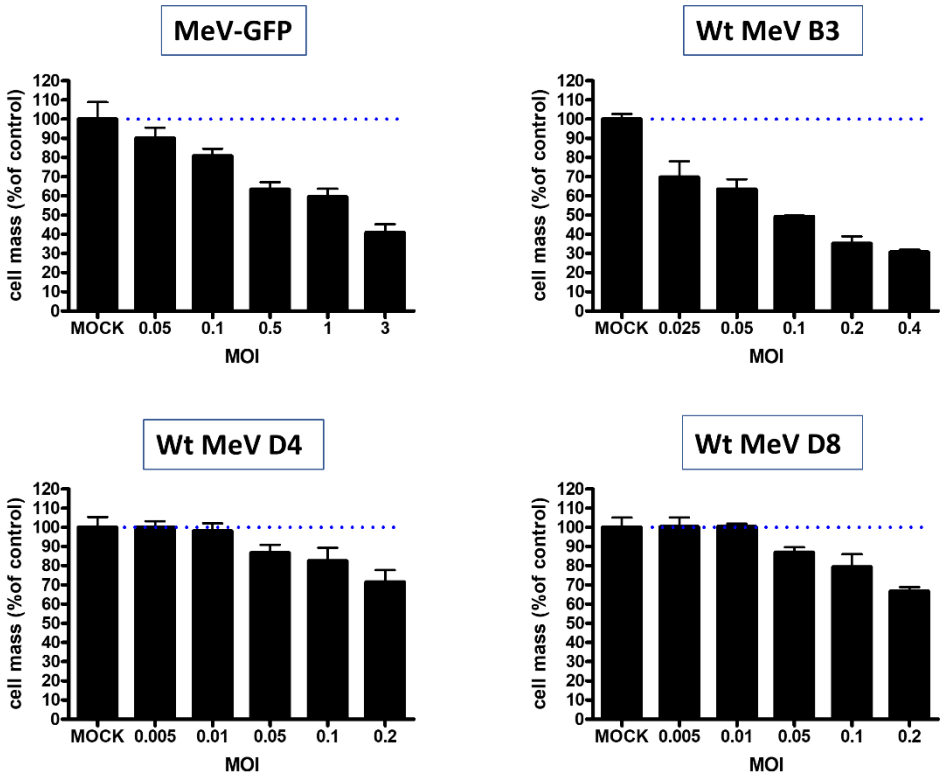

Figure 27: Oncolytic effects of wild-type measles virus on cell line B95a. Cells were left untreated (MOCK) or infected at risings MOIs with wild-type measles virus (Wt MeV) of genotypes B3, D4 or D8 or measles vaccine virus MeV-GFP. At 96 hpi the remaining tumor cell mass was determined by SRB assay. Blue dotted line: mean of untreated cells (100 % cell mass). Values: mean of quadruplicates. Error bars: SD.

Finally, possible virostatic effects of AF on wild-type measles virus were tested. Again, cells were infected with the respective measles virus and treated with AF

at 3 hpi. AF concentrations ranging from 2.5 to 10 µg/ml were chosen. To reach comparable oncolytic effects cells were infected with wild-type measles virus of genotype B3 at MOI 0.025, D4 at MOI 0.2, and D8 at MOI 0.2. Having found, that the virostatic effect on measles vaccine virus strains also depended on the infected cell line (Fig. 14), one approach was also infected with MeV-GFP at MOI 0.1. At 96 hpi supernatant and cell lysate were collected and the amount of infective virus particles was quantified by virus titration.

As shown in Fig. 28, the virostatic effect on wild-type measles virus genotypes B3 and D4 was weak, if any. The virus titers in the supernatant and cell lysate were reduced by a maximum of 10-fold. However, virus titers of wild-type measles virus D8 could be reduced in supernatant by 100-fold (approximately 10^6 pfu/ml without AF and 10^4 pfu/ml with). As with wild-type measles virus D8, MeV-GFP titers in the supernatant were about 100-fold lower in the setting with AF compared to untreated cells (approximately 10^7 pfu/ml without AF and 10^5 pfu/ml with), and about 10 fold lower in the cell lysate (approximately 10^6 pfu/ml with 10 µg/ml AF and 10^7 pfu/ml without).

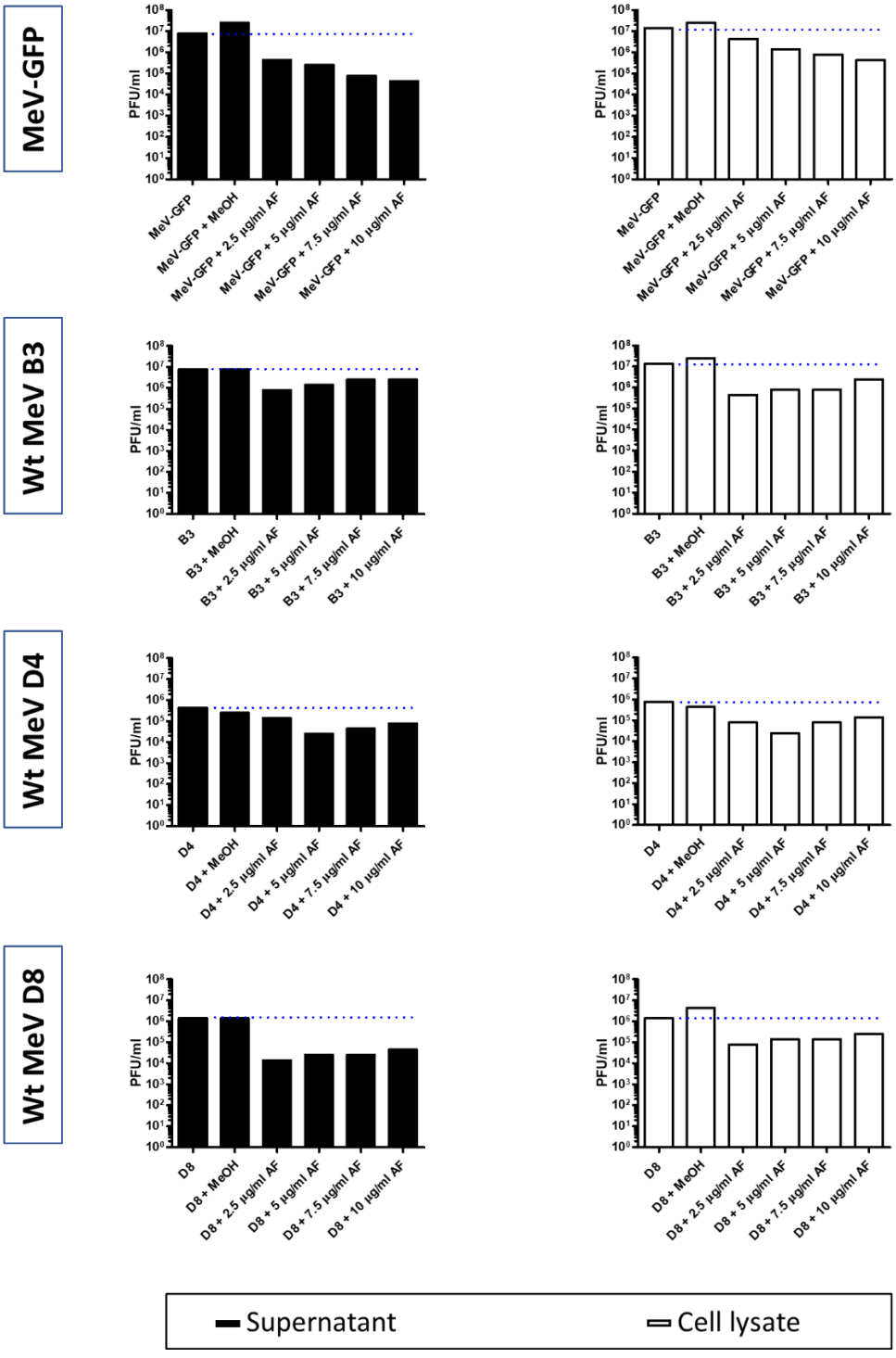

Figure 28: Virostatic effects of AF on wild-type measles virus in cell line B95a. B95a cells were infected with wild-type measles viruses (Wt MeV) of genotypes B3 (MOI 0.025), D4 (MOI 0.2) or D8 (MOI 0.2) and with measles vaccine virus MeV-GFP (MOI 0.1). At 3 hpi cells were left untreated or treated with vehicle (MeOH) and rising concentrations of AF, respectively. At 96 hpi supernatant (black columns) and cell lysate (white columns) were collected and virus particles were quantified by titration on Vero/hSLAM cells. Blue dotted line: viral titer without AF. PFU = Plaque forming units. Values: one representative experiment.

3.5. Virostatic effects of AF on vaccinia vaccine virus GLV-1h68

Having tested the effect of AF on measles virus strains, it was investigated whether AF also shows a virostatic effect on other viruses. Here we focused on the vaccinia vaccine virus GLV-1h68 which has a double stranded DNA genome in contrast to measles virus where the genetic information is stored in the shape of a single stranded negative sense RNA.

As in the previous settings, the oncolytic efficacy was tested first. For this, HCT 116 cells were infected at rising MOIs with GLV-1h68. The remaining cell mass was determined at 96 hpi by SRB assay (Fig. 29). As a result, 45 % of the cell mass was left at MOI 0.5 and 87 % at MOI 0.1.

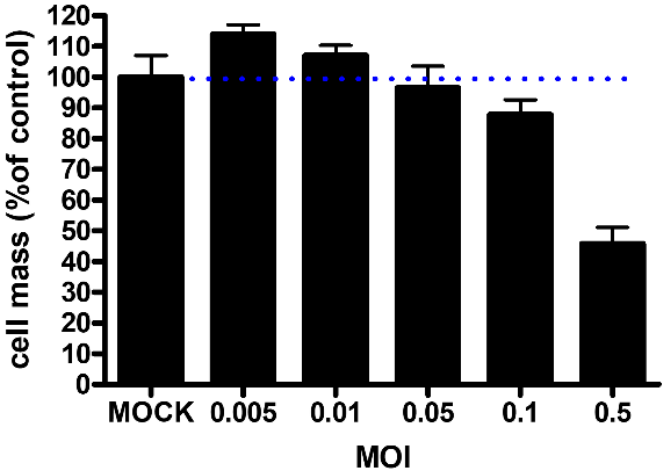

Figure 29: Oncolytic effect of vaccinia virus GLV-1h68 on the colorectal carcinoma cell line HCT 116. Cells were left untreated (MOCK) or infected at risings MOIs with GLV-1h68. At 96 hpi the remaining tumor cell mass was determined by SRB assay. Blue dotted line: mean of untreated cells (100 % cell mass). Values: mean of quadruplicates. Error bars: SD.

In order to achieve an oncolytic effect comparable to measles virus, HCT 116 cells were infected at MOI 0.25 in the combined treatment. As in previous experiments with colorectal carcinoma cells, AF concentrations ranging from 2.5 to 10 µg/ml were added at 3 hpi. Supernatant and cell lysate were collected at 96 hpi and the amount of infective virus particles was quantified by virus titration. The results (Fig. 30) showed that the virus titers of GLV-1h68 were hardly reduced. Compared to untreated cells (supernatant: 1.4 x 10^6 pfu/ml, cell lysate:

3.9 x 10^5 pfu/ml) virus titers were reduced less than 10-fold across all approaches with AF.

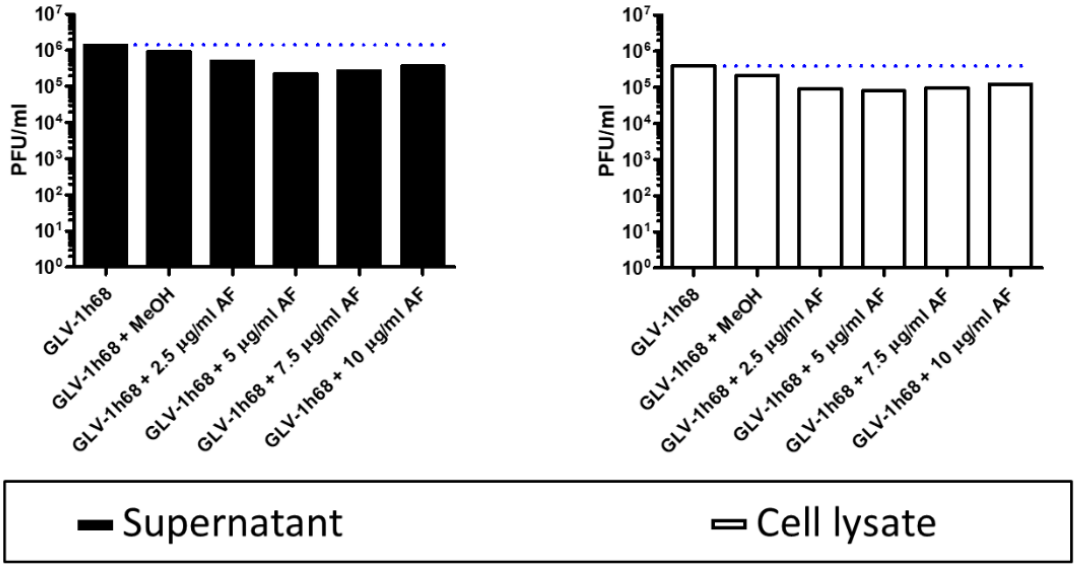

Figure 30: Virostatic effects of AF on GLV-1h68 in colorectal carcinoma cells. HCT 116 cells were infected with GLV-1h68 at MOI 0.25. At 1 hpi cells were left untreated or treated with vehicle (MeOH) and rising concentrations of AF, respectively. At 96 hpi supernatant (black columns) and cell lysate (white columns) were collected and virus particles were quantified by titration on CV-1 cells. PFU = Plaque forming units. Blue dotted line: virus titer in the absence of AF. Values: one representative experiment.

3.6. Studies on the molecular mechanism of action of the virostatic effect of AF

3.6.1. Electron microscopy

In order to elucidate the molecular mechanism of action that caused the virostatic effect of AF electron microscopy was performed. On the one hand, we wanted to find out at the level of cell organelles, to what extent AF treated cells differ from untreated cells. On the other hand, structural differences between cells infected only and those additionally treated with AF or other proteasome inhibitors should be identified.

Therefore HCT 116 cells were left untreated (MOCK) or infected with MeV-GFP at MOI 1. At 3 hpi medium with or without a proteasome inhibitor (AF, Bortezomib,

Carfilzomib, Ixazomib) was added to MOCK infected cells (proteasome inhibitor monotherapy) and to virus infected cells (combined therapy). At 96 hpi cells were fixed in Karnovsky fixative. Electron microscopy investigations were performed by B. Fehrenbacher, Department of Dermatology, University Hospital Tübingen.

In contrast to naïve cells (Fig. 31), cells infected with MeV-GFP exhibited multiple large tumor cell syncytia, indicating imminent MeV-specific oncolysis (Fig. 32). Further, with increasing magnifications large “factory” areas for MeV ribonucleoprotein production (Fig. 33, Fig. 35, Fig. 36) as well as MeV progeny particles in the process of “budding” (Fig. 33) could be identified. MeV particles were distinguished from virus-free plasma offshoots based on the typical spoke-like configuration of MeV-RNPs as well as the presence of MeV-surface proteins (hemagglutinin, fusion protein) as demonstrated in Fig. 34. Increased autophagy (Fig. 36), indicating MeV-induced cellular stress, was found, too.

Cells treated with an AF monotherapy also showed clear differences to untreated cells (Fig. 37). Morphologically altered mitochondria as in cells undergoing apoptosis were noticeable: Instead of a physiological cristae structure, some mitochondria with a swelling without inner structure or vesicular swollen structure were found (Fig. 38).

In the same way as in cells that were only infected with MeV-GFP (Fig. 32), large measles virus induced tumor cell syncytia were observed in the combined treatment with AF and virus (Fig. 39). MeV RNP “factories” were found, too (Fig. 40, Fig. 41). When comparing these between “infection only” and combined treatment (Fig. 42) no distinct significant differences were detected. There were also numerous morphologically altered mitochondria (Fig. 41)

In the combined treatment with MeV-GFP and Bortezomib (Fig. 43), Carfilzomib (Fig. 44) or Ixazomib (Fig. 45) morphologically altered mitochondria and MeV RNP “factories” were found, too.

Summing up, structural differences to naïve cells being characteristic of the virus (RNP “factories”, budding MeV progeny particles) or AF (morphologically altered mitochondria) were found. However, in the combined therapy, no effects of AF on measles virus could be demonstrated neither were there any differences compared to other proteasome inhibitors.

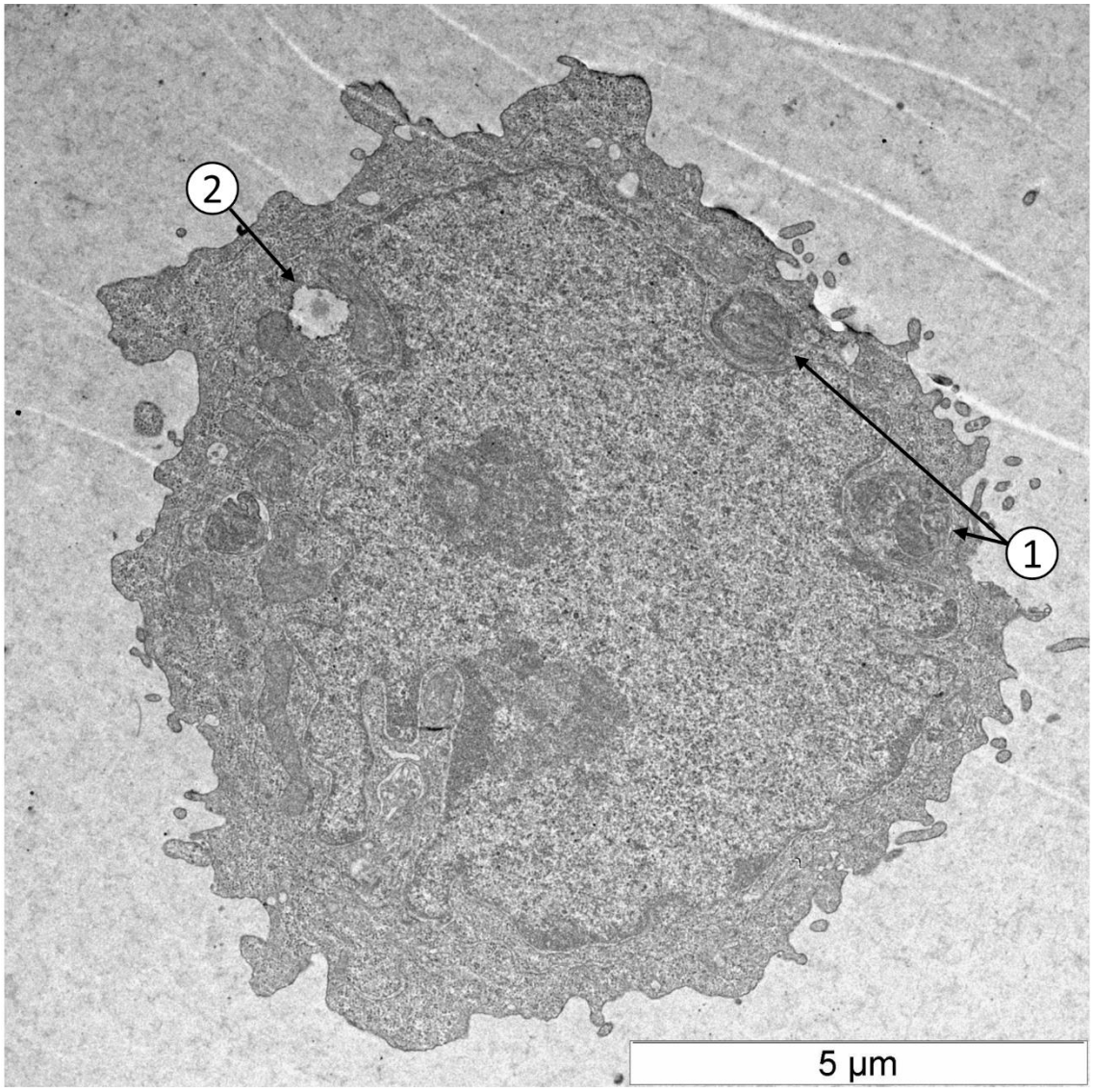

Figure 31: Electron microscopy section of a naïve (uninfected) HCT 116 human colorectal carcinoma cell, presenting with autophagosomes (1) and a fat deposit (2).

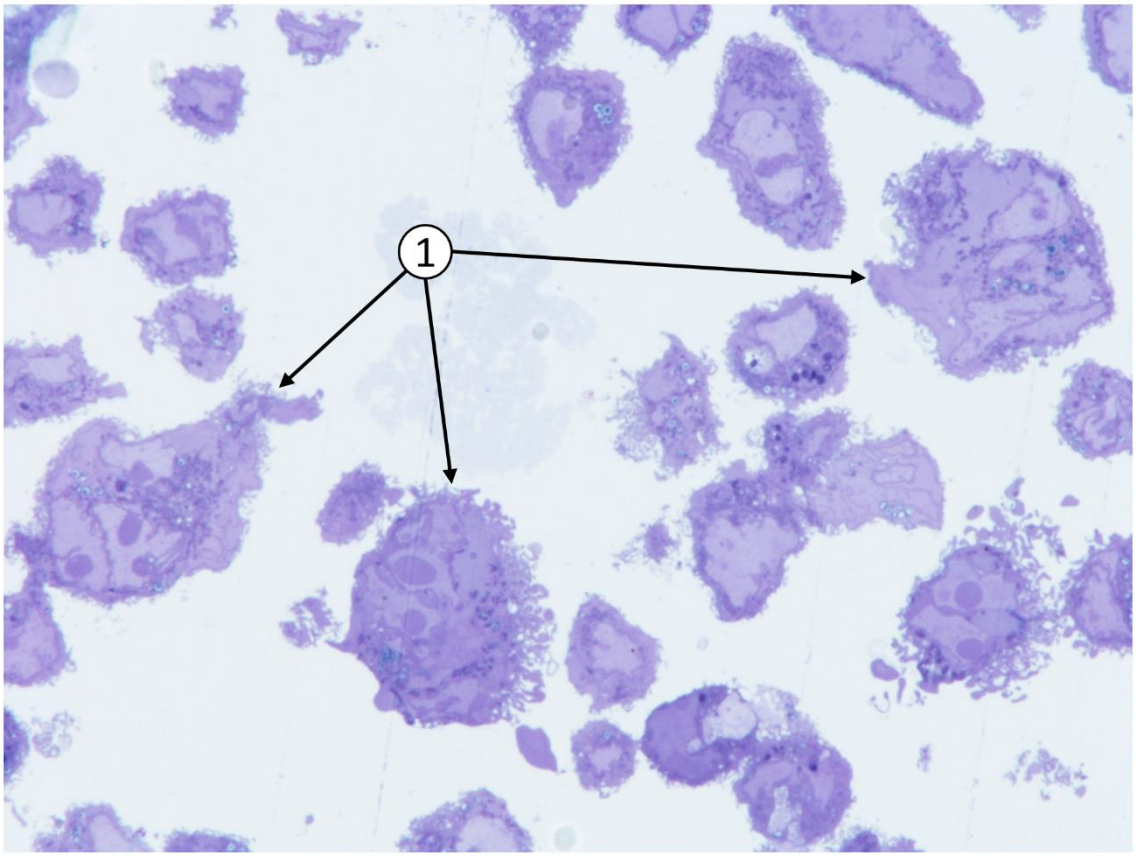

Figure 32: Representative picture of semi thin sections of HCT 116 tumor cells infected with oncolytic measles vaccine virus (MeV-GFP) (MOI 1) taken at 96 hpi, exhibiting multiple large tumor cell syncytia (1) being typical for infected tumor cells with profound replication of MeV; syncytia formation indicates imminent MeV-specific oncolysis.

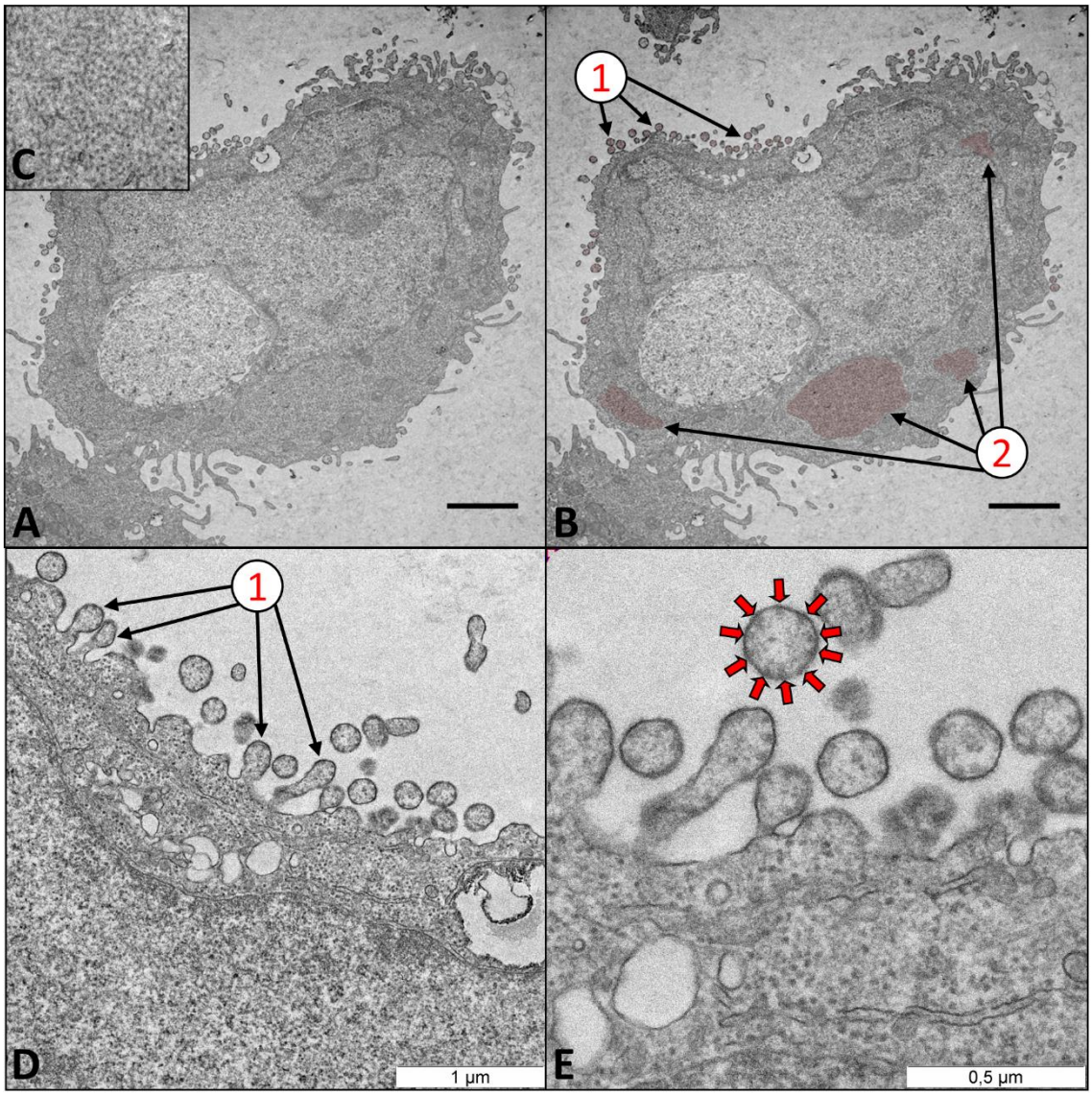

Figure 33: Different magnifications of one and the same HCT 116 tumor cell infected with MeV-GFP (MOI 1) taken at 96 hpi. (A) Overview picture exhibiting basic features of the MeV-infected tumor cell; **(B)** MeV progeny particles in the process of "budding" (1) from the infected tumor cell together with a couple of "factory" areas ((2); highlighted in red) in which progeny MeV ribonucleoproteins (RNPs; i.e., MeV ribonucleic acids in conjunction with RNA-binding MeV proteins) are being produced in huge amounts (scale bar = 2 µm); **(C)** Magnification of a single MeV RNP "factory"; **(D)** multiple budding MeV progeny particles (1), which can be identified **(E)** by a typical "spoke-like" structure of MeV RNPs (indicated by red arrows).

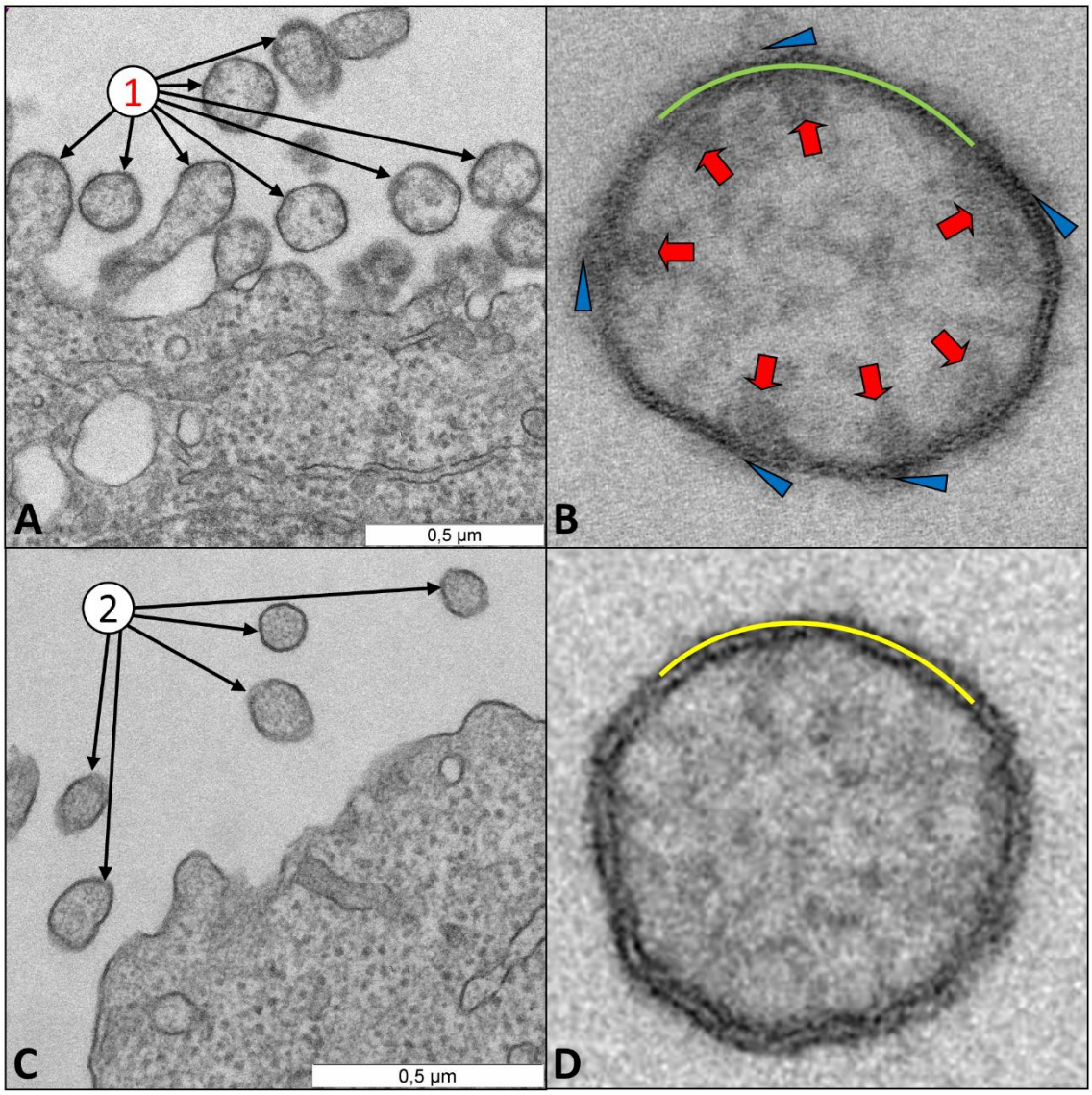

Figure 34: Comparison of budding MeV particles and virus-free/empty plasma offshoots. **(A)** Capture of multiple MeV particles (1) budding from a single HCT 116 tumor cell; **(B)** Magnification of a single budding MeV particle depicting the virus particle membrane (green line), the typical “spoke-like” array of MeV RNPs (red arrows), as well as MeV surface proteins H (hemagglutinin) and F (fusion) (blue triangles); **(C)** Mock infected HCT 116 tumor cell with “empty” (virus-free) plasma offshoots not showing any “spoke-like” configuration (2); **(D)** Magnification of a single empty/virus-free plasma offshoot exhibiting a more even inner structure, surrounded by a lipid double layer (yellow line).

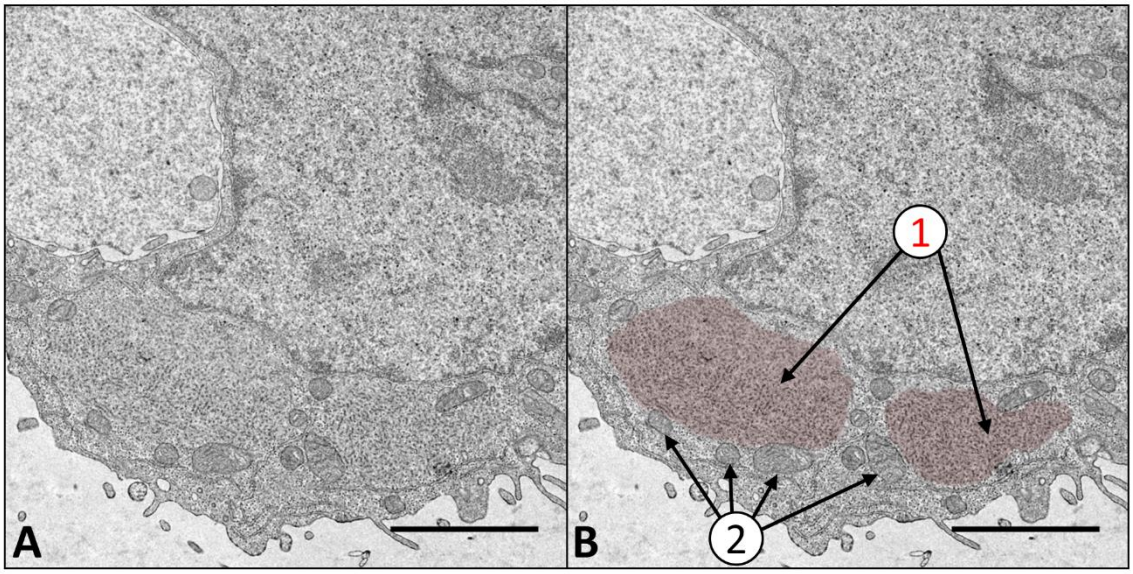

Figure 35: Electron microscopy picture of a HCT 116 tumor cell infected with MeV-GFP (MOI 1) at 96 hpi. (A) Overview picture exhibiting basic features of the MeV-infected tumor cell; **(B)** Two "factory" areas containing progeny MeV RNPs ((1); highlighted in red) are found to be surrounded by numerous mitochondria (2) (scale bar = 2 µm).

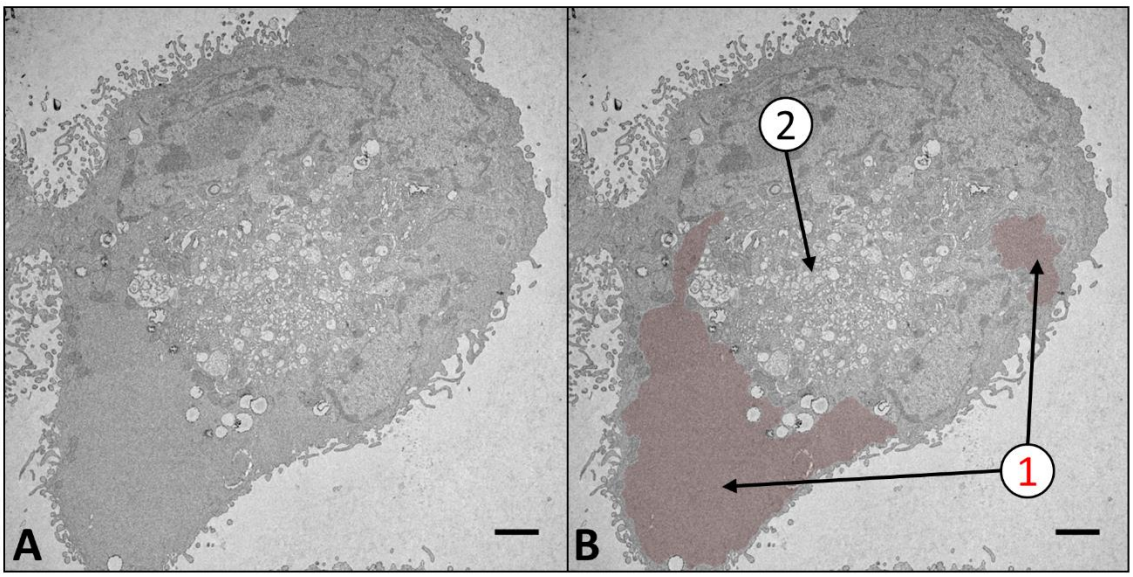

Figure 36: Electron microscopy picture of a HCT 116 tumor cell infected with MeV-GFP (MOI 1) at 96 hpi. (A) Overview picture exhibiting basic features of the MeV-infected tumor cell; **(B)** MeV RNP producing "factory" areas (1) are highlighted again in red; furthermore, MeV induced cellular stress is reflected by increased autophagy (2), which can be identified by intracellular cargo (e.g. cell organelles) inside double-membraned autophagic vesicles [75] (scale bar = 2 µm).

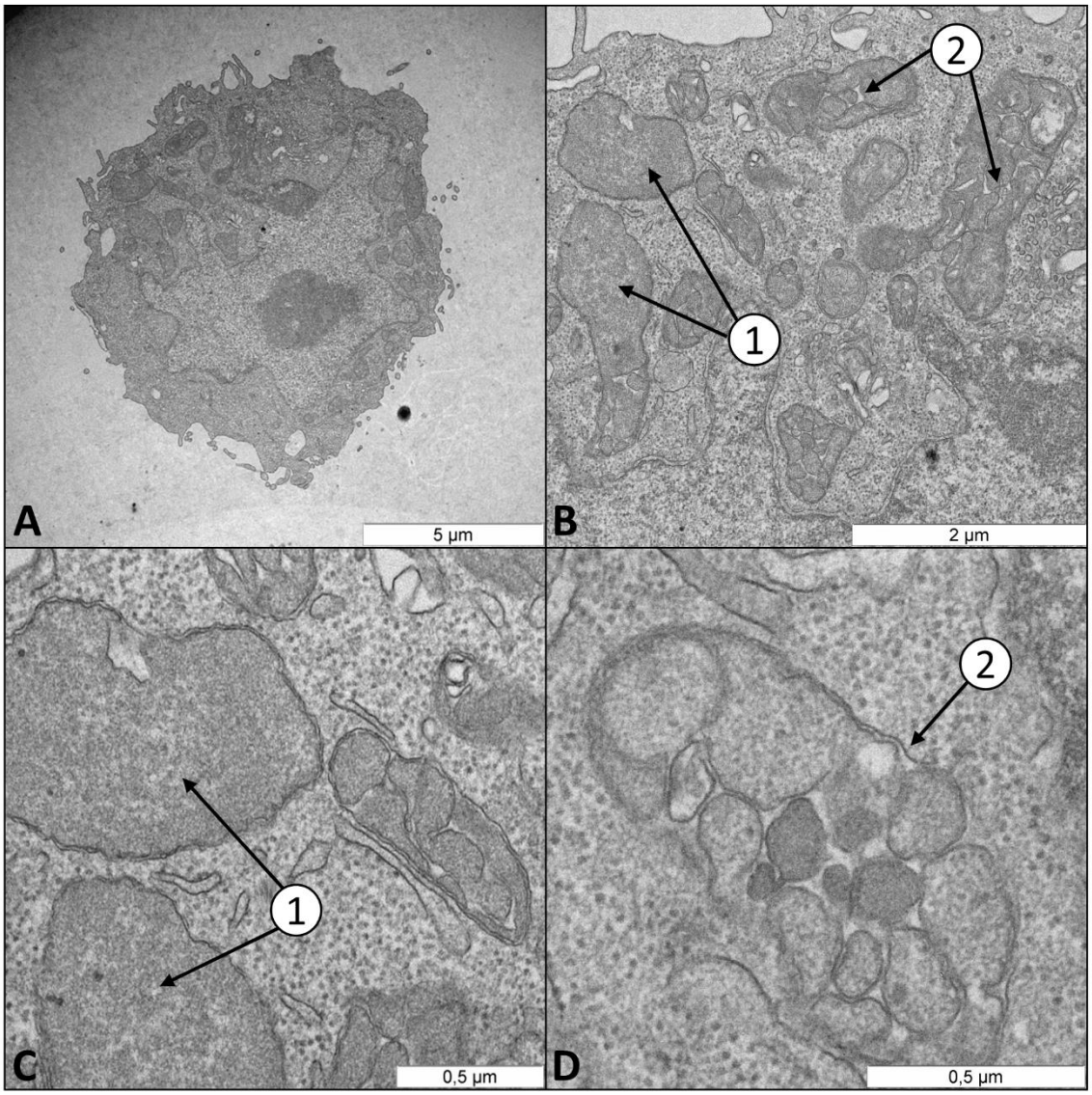

Figure 37: Electron microscopy picture of a HCT 116 tumor cell at 96 h of treatment with the proteasome inhibitor AF. (A) Overview picture; **(B)** AF treatment imposes changes (in comparison to untreated tumor cells) such as mitochondria in cells undergoing apoptosis either exhibiting a “swelling without inner structure” (1), or a “vesicular-swollen structure” (2) [76]; furthermore, typical cristae structures of mitochondria no longer can be identified; **(C)** Magnification of mitochondria exhibiting “swelling without inner structure” (1); **(D)** Magnification of one “vesicular-swollen” mitochondrion (2).

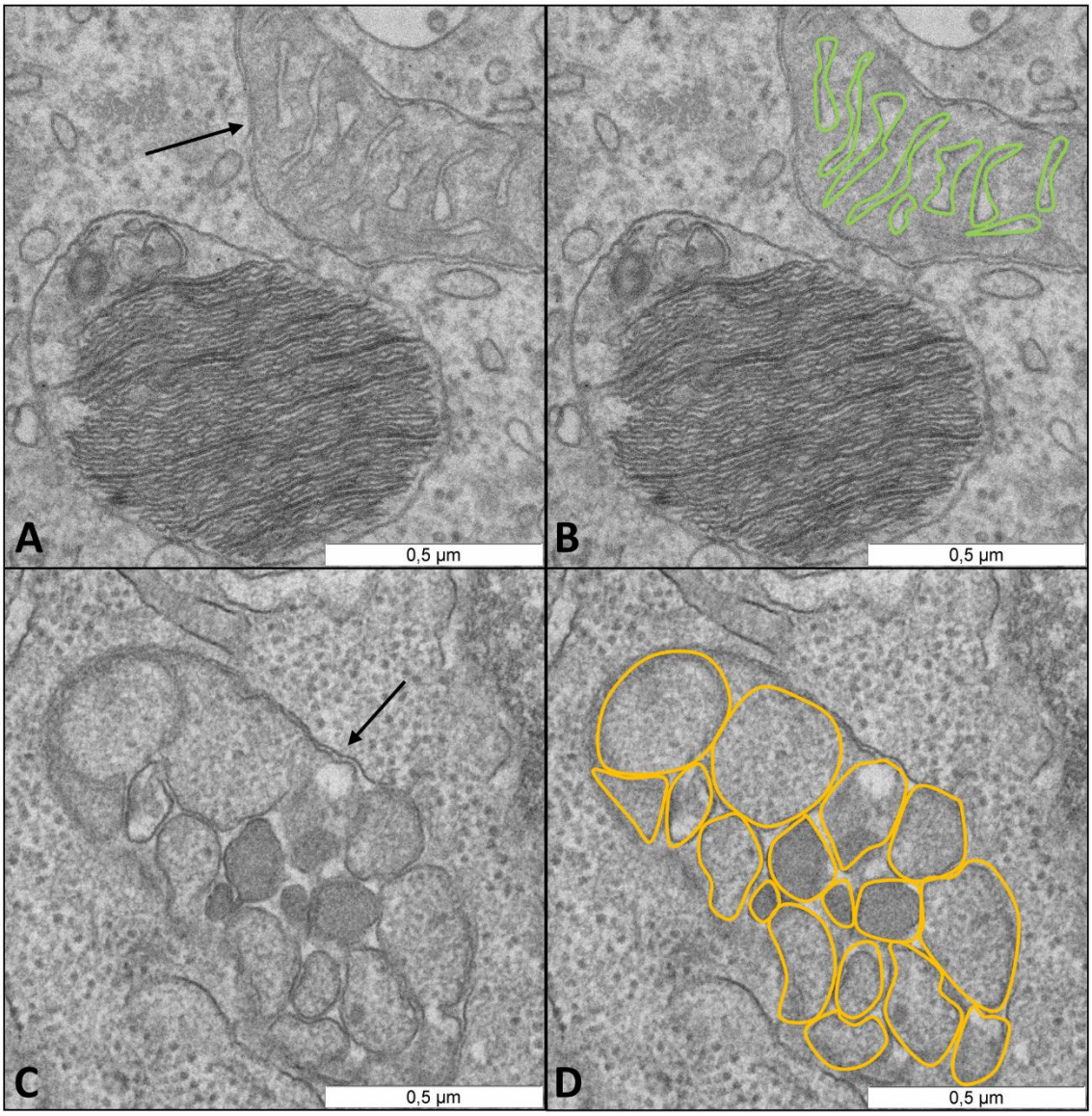

Figure 38: Comparison of mitochondria of naive (A and B) and AF mono-treated (C and D) HCT 116 human colorectal carcinoma cells. While the internal membrane of naive mitochondria shows a physiological cristae structure (green line) under AF mono-treatment the internal membrane is vesicular swollen (orange line).

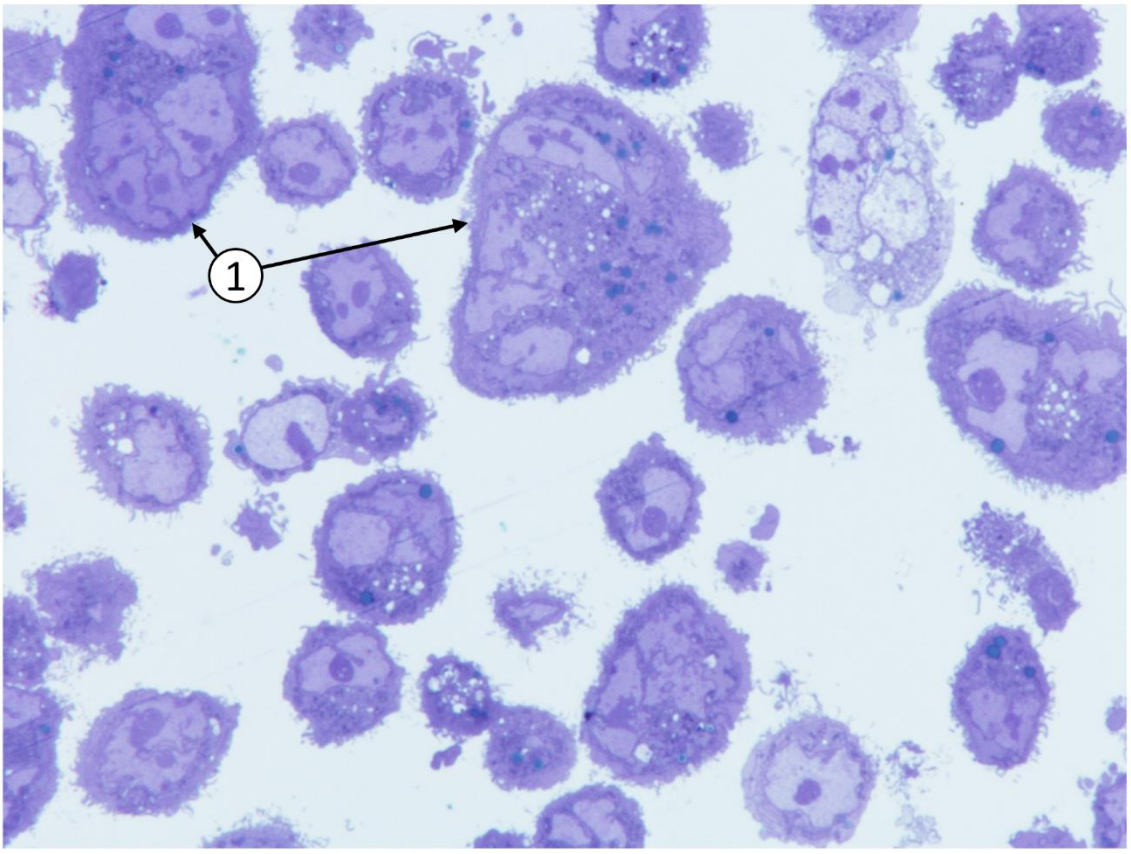

Figure 39: Semi thin section of HCT 116 tumor cells under combined treatment with MeV-GFP and AF. At 96 hpi, large MeV-induced tumor cell syncytia were observed (1), indicating imminent MeV-specific oncolysis.

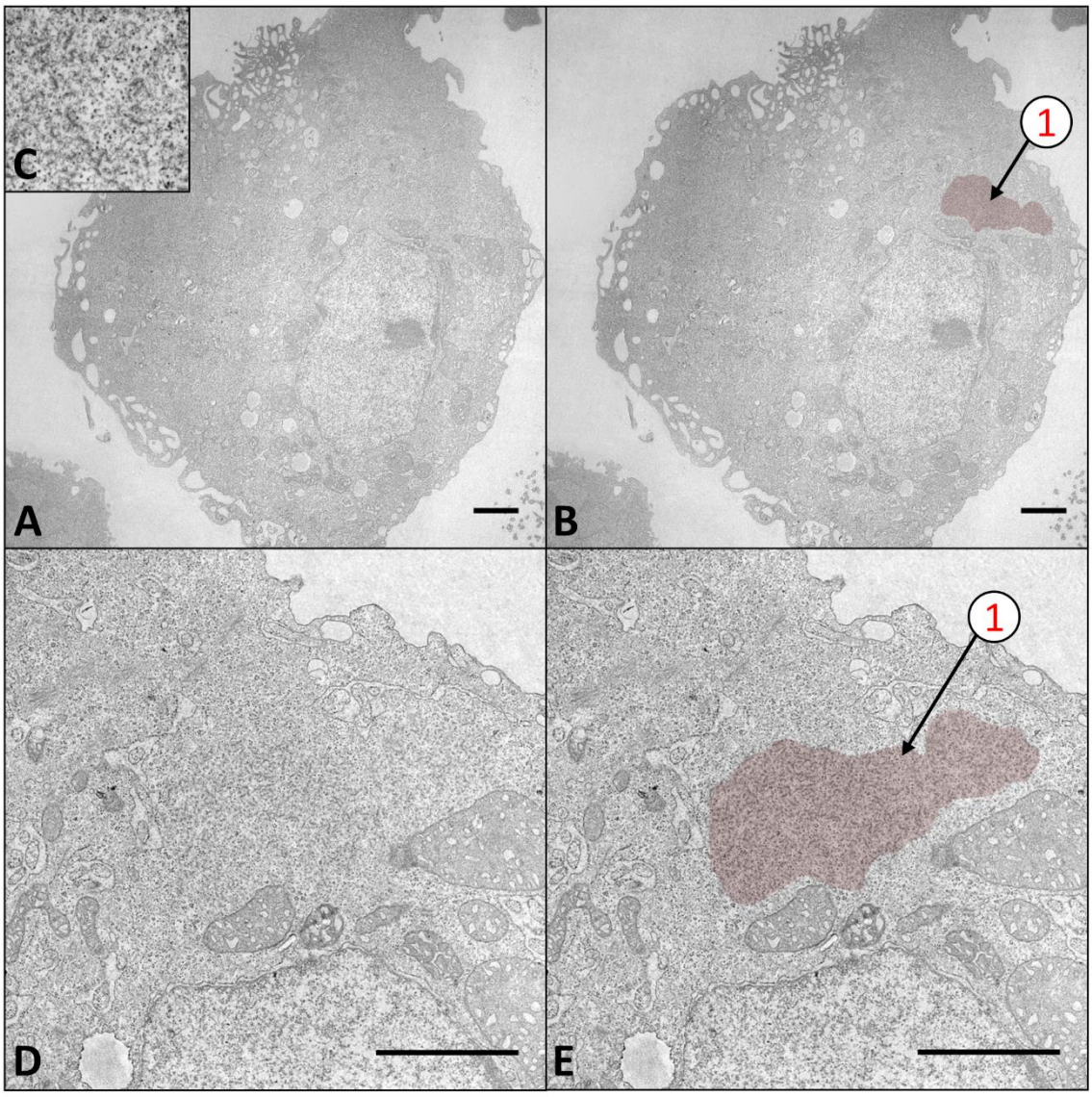

Figure 40: Combined treatment with MeV-GFP and AF. (A) Overview electron microscopy picture exhibiting basic features of a MeV/AF-treated HCT 116 tumor cell; **(B)** A MeV RNP "factory" (highlighted in red) (1); **(C)** Further magnification of this MeV RNP "factory"; **(D)** Magnified MeV RNP "factory", **(E)** which is highlighted in red (scale bar = 2 µm).

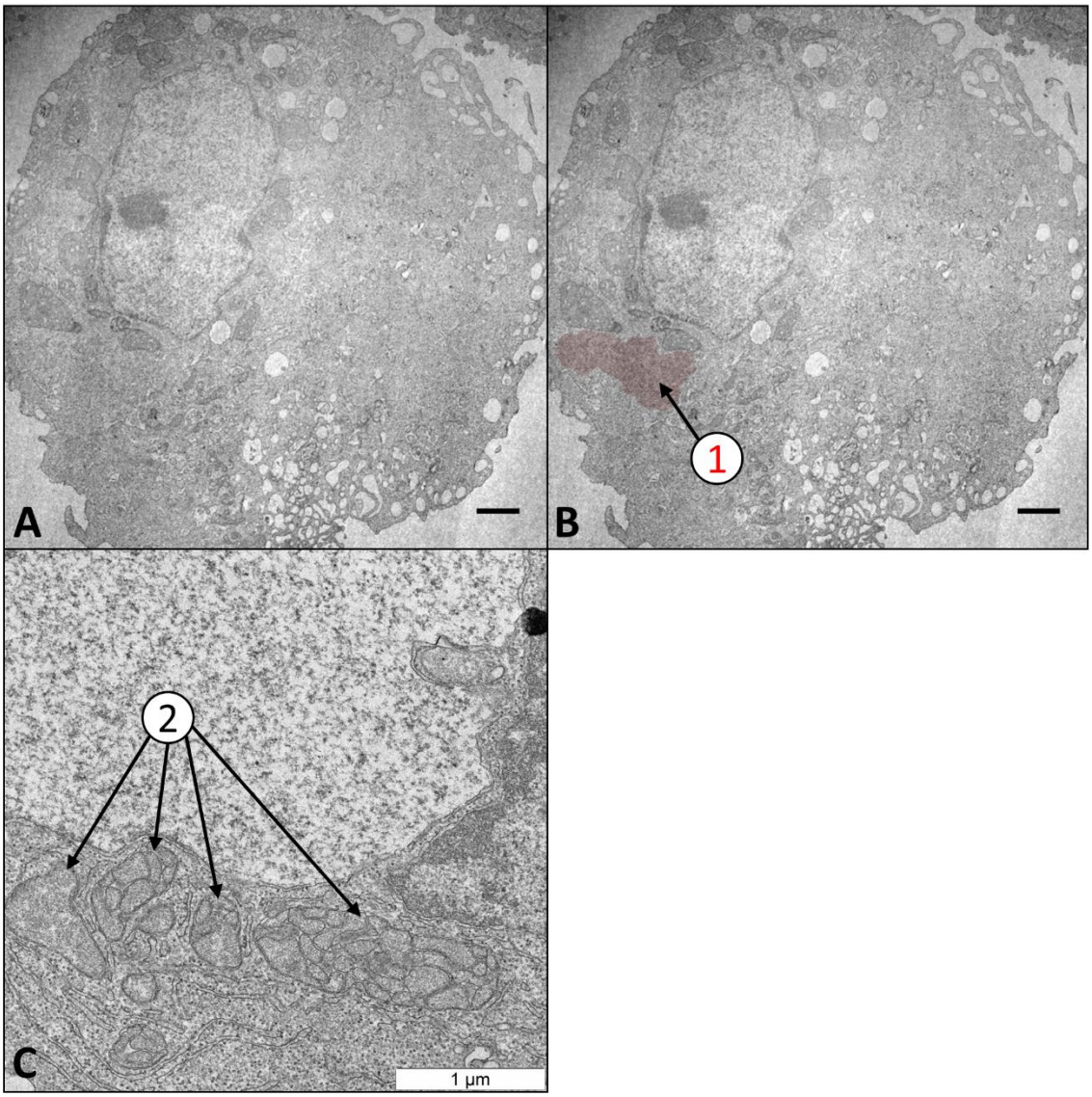

Figure 41: Combined treatment with MeV-GFP and AF. (A) Overview electron microscopy picture exhibiting basic features of a MeV/AF-treated HCT 116 tumor cell; **(B)** Infection by MeV resulted in generation of a MeV RNP "factory" (highlighted in red) (1) (scale bar = 2 µm); **(C)** Treatment with AF resulted in numerous morphologically altered mitochondria (2).

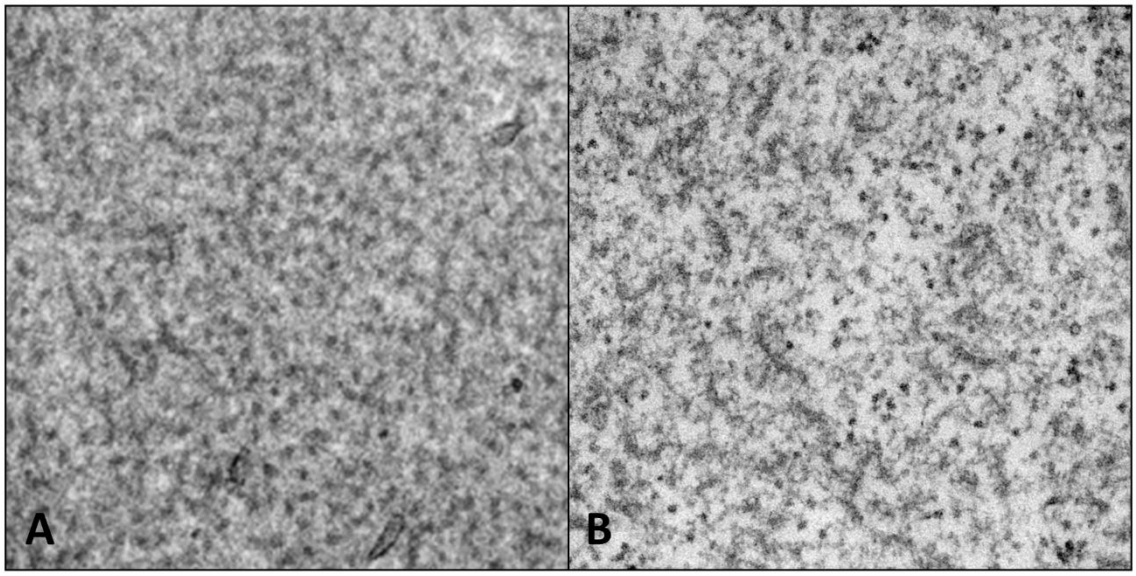

Figure 42: MeV RNP "factories" observed under (A) mono-treatment with MeV-GFP ("infection only") and under (B) combined treatment with MeV-GFP and AF. As a result, no distinct significant differences can be observed.

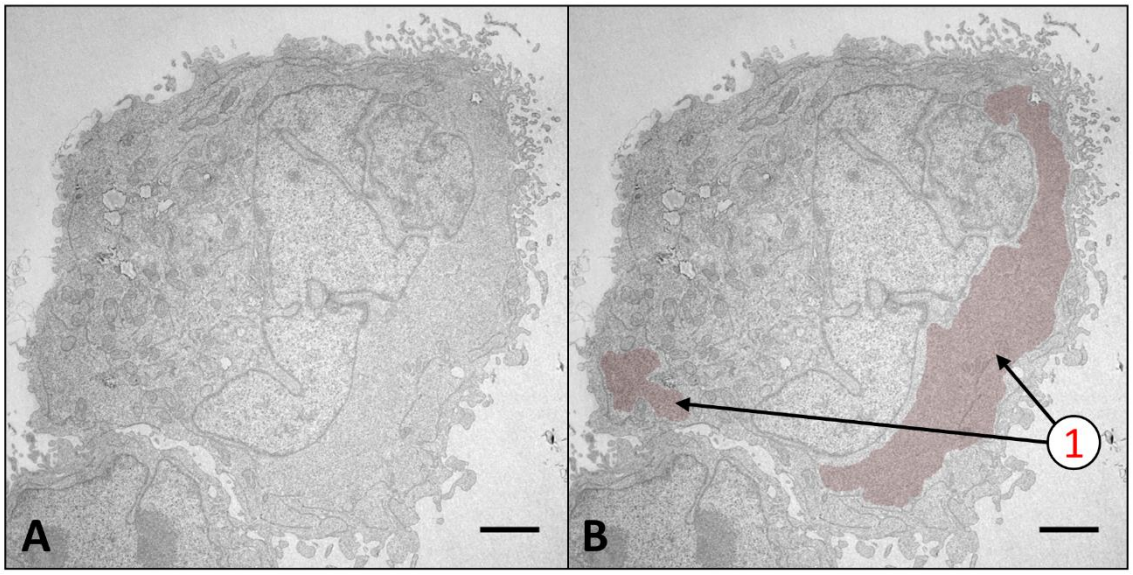

Figure 43: Combined treatment with MeV-GFP and the proteasome inhibitor Bortezomib. (A) Electron microscopy picture exhibiting basic features of a MeV-GFP/Bortezomib-treated HCT 116 tumor cell; **(B)** Infection by MeV-GFP resulted in generation of MeV RNP "factories" (highlighted in red) (1) (scale bar = 2 µm).

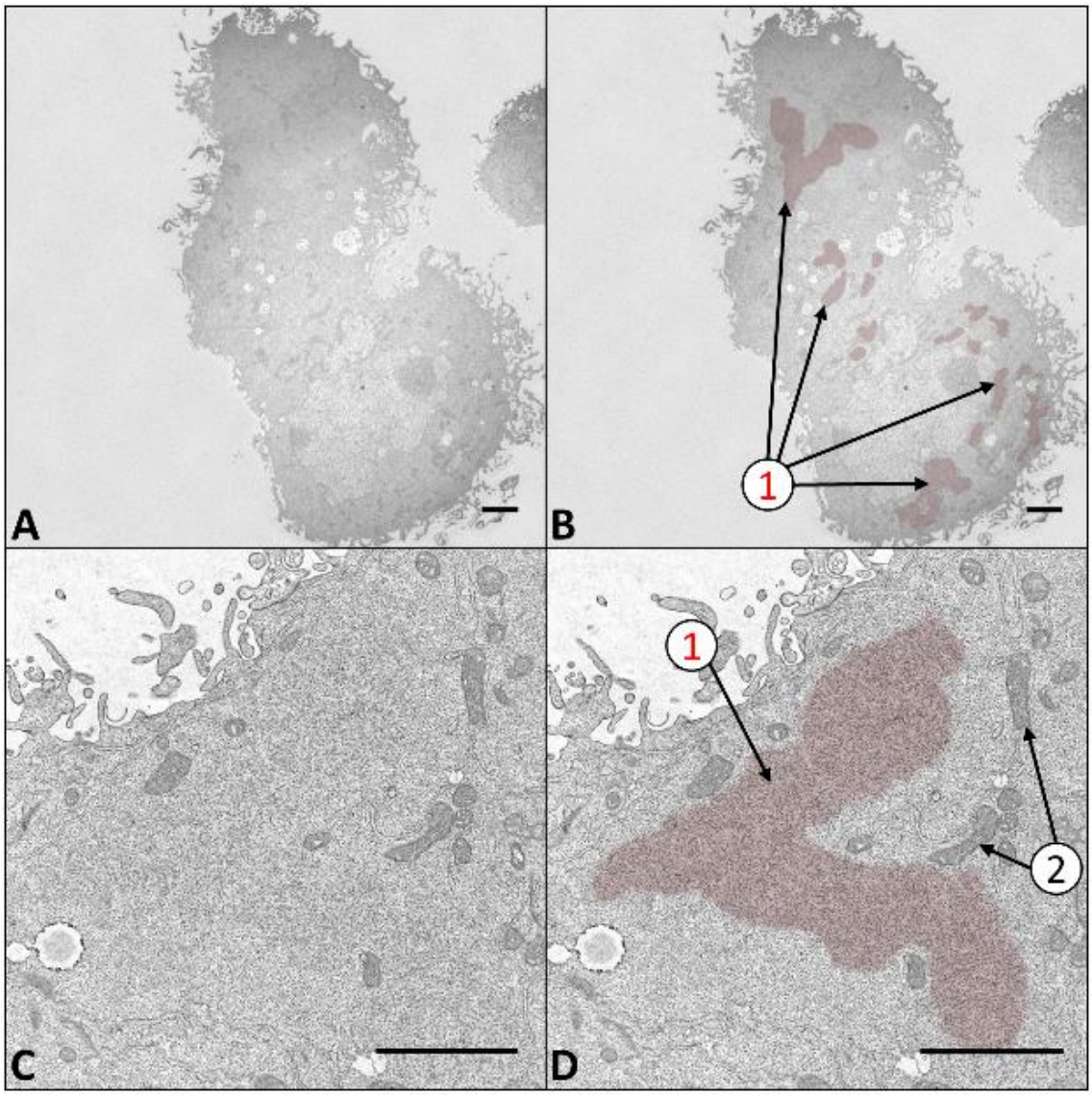

Figure 44: Combined treatment with MeV-GFP and the proteasome inhibitor Carfilzomib. **(A)** Electron microscopy picture exhibiting basic features of a MeV-GFP/Carfilzomib-treated HCT 116 tumor cell; **(B)** Infection by MeV-GFP resulted in generation of MeV RNP "factories" (highlighted in red) (1) (scale bar = 2 µm); **(C)** MeV RNP "factories" are magnified and **(D)** highlighted in red (1); furthermore, treatment with Carfilzomib resulted in numerous morphologically altered mitochondria (2) (scale bar = 2 µm).

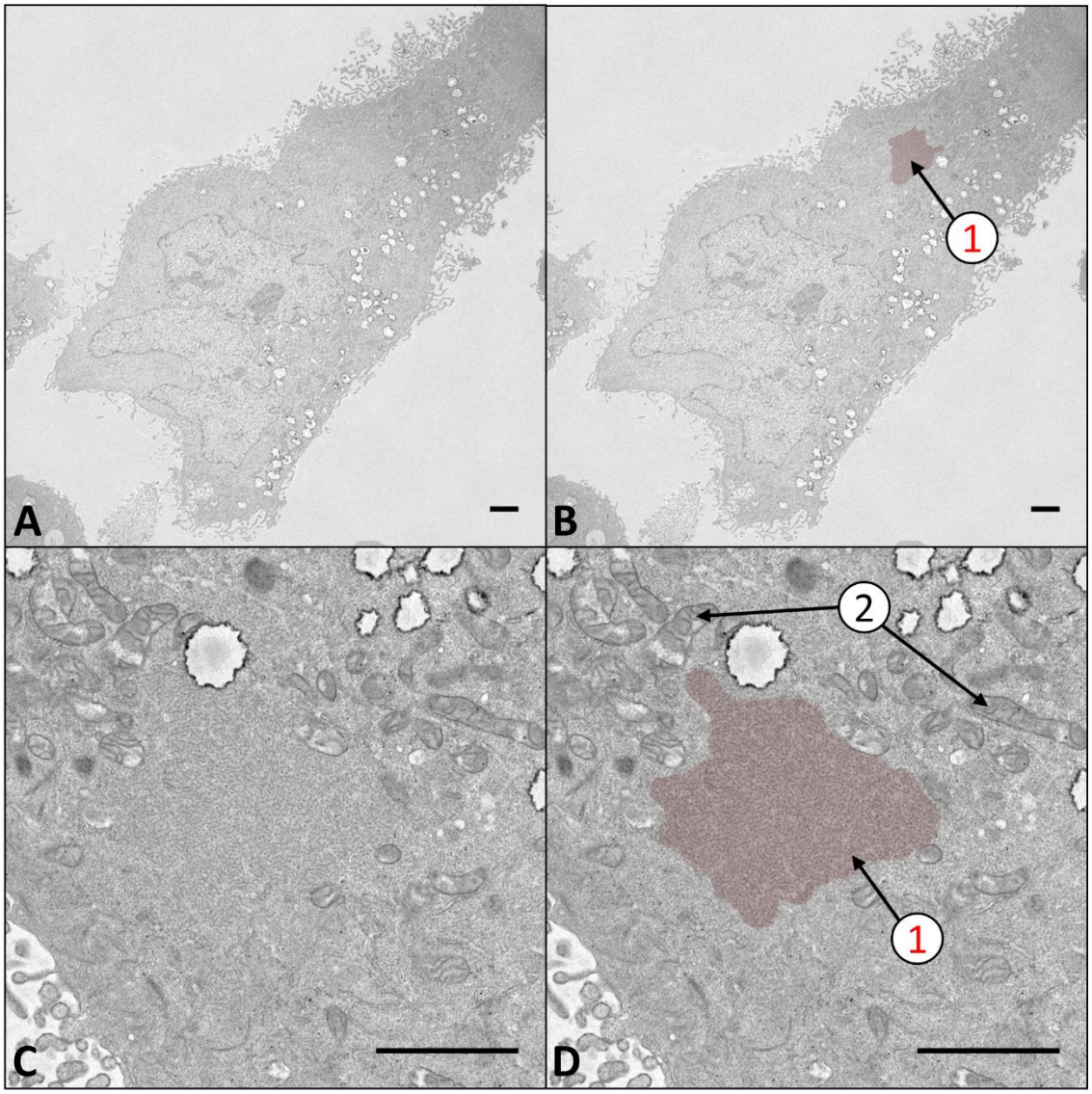

Figure 45: Combined treatment with MeV and the proteasome inhibitor Ixazomib. (A) Electron microscopy picture exhibiting basic features of a MeV/Ixazomib-treated HCT 116 tumor cell; **(B)** MeV RNP-"virus factories" (1) are highlighted in red; **(C)** MeV RNP-"virus factories" are magnified and **(D)** highlighted in red (1); furthermore, treatment with Ixazomib resulted in numerous morphologically altered mitochondria (2) (scale bar = 2 µm).

3.6.2. Experiments with Argyrin derivatives

In order to further research the molecular mechanism of action of the virostatic effect of AF, experiments were performed with argyrin derivatives that do not have proteasome activity. Especially since the other tested proteasome inhibitors did not show any virostatic effect (Fig. 25), we wanted to determine, whether there is possibly a second active region in the molecule being independent of its function as a proteasome inhibitor which causes the virostatic effect.

First, suitable concentrations for each argyrin derivate had to be determined. Therefore, colorectal carcinoma cells were treated with rising concentrations of KD-022-2, KD-046-1 and KD-158-3. The remaining cell mass was determined by SRB assay at 96 hpt (Fig. 46). As a result, even with the highest concentration (10 µg/ml), no argyrin derivative was able to reduce the cell mass considerably (KD-022-2: 97 %, KD-046-1: 85 %, KD-158-3: 107 %). This corresponded to the lack of proteasome inhibition, which would have affected cell growth. In contrast, 10 µg/ml AF reduced the cell mass to 59 %.

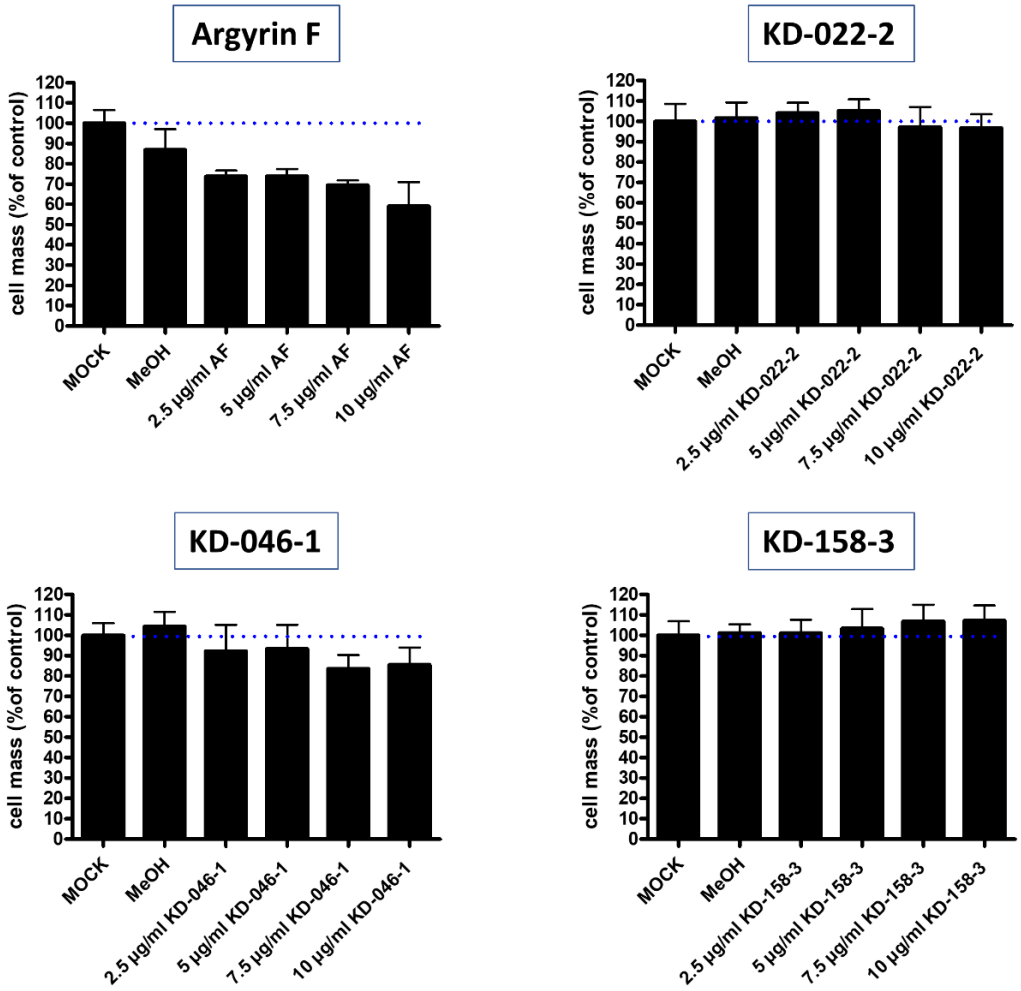

Figure 46: Antiproliferative effects of argyrin derivatives on colorectal carcinoma cells. HCT 116 cells were left untreated (MOCK) or treated with rising concentrations of AF or argyrin derivatives KD-022-2, KD-046-1 or KD-158-3. After 96 hours the remaining tumor cell mass was determined by SRB assay. Blue dotted line: mean of untreated cells (100 % cell mass). Values: mean of two experiments performed in quadruplicates. Error bars: SD.

Finally, in the already established experimental setting with the colorectal carcinoma cell line HCT 116 and measles vaccine virus MeV-GFP, argyrin derivatives were tested for possible virostatic effects. HCT 116 cells were infected with MeV-GFP at MOI 1 and treated with AF or an argyrin derivative at 3 hpi. Concentrations ranging from 2.5 to 10 µg/ml were chosen. At 96 hpi supernatant and cell lysate were collected and the amount of infective virus particles was quantified by virus titration (Fig. 47). It turned out that in contrast to AF none of the argyrin derivates could lower the virus titers in supernatant or cell lysate in a relevant manner.

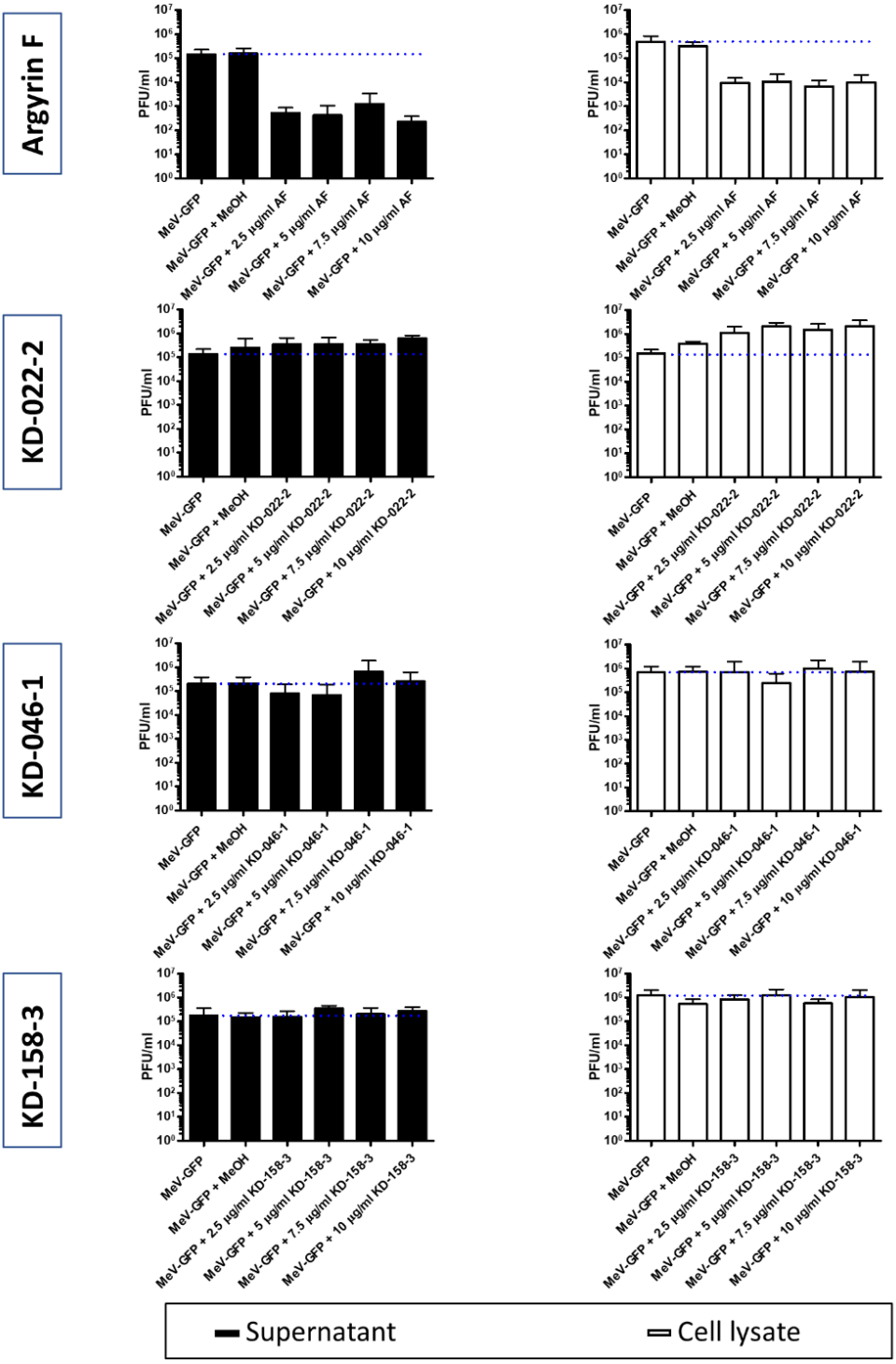

Figure 47: Effects of argyrin derivates on MeV-GFP in colorectal carcinoma cells. HCT 116 cells were infected with MeV-GFP at MOI 1. Cells were left untreated or treated with rising concentrations of AF or argyrin derivates KD-022-2, KD-046-1 or KD-158-3 at 3 hpi. At 96 hpi supernatants (black columns) and cell lysates (white columns) were collected and virus particles were quantified by titration on Vero cells. PFU = Plaque forming units. Blue line: mean of viral titers without argyrin derivatives. Values: mean of four independent experiments. Error bars: SD

4. Discussion

Even though safe and effective vaccines are available, measles still have a tremendous impact on public health. Therefor it seems desirable to have in addition to the vaccination a specific antiviral drug. But no measles specific drug has yet been clinically approved [19]. In the present study we examined *in vitro* whether AF is suitable as a lead compound for this purpose. In the following, the necessary precise characterization of the virostatic effect of AF on measles is first summarized in order to subsequently evaluate it with regard to a possible clinical application.

The following results on the objectives mentioned in the introduction were achieved in this dissertation:

I) Which dosage is necessary to achieve a significant antiviral effect when using Argyrin F (AF) in combination with MeV-GFP?

   In infected human colorectal carcinoma cells concentrations of 0.1 µg/ml AF were required to achieve a virostatic effect.

II) To which extent can titers of MeV-GFP be reduced when using AF in combination with MeV-GFP?

   Virus titers were up to 1,000-fold lower in supernatants and cell lysates when treating MeV-GFP infected human colorectal carcinoma cells with AF at 3 hpi.

III) In which time period before and after infection with MeV-GFP inhibition of measles virus replication was achieved by application of AF?

   AF reduced MeV-GFP virus titers when added in a time period between 3 hours before and 24 hours post infection.

IV) Does the virostatic effect of AF also depend on the used cell lines?

The virostatic effect of AF depends on the used cell lines. While MeV-GFP virus titers were reduced strongly in the human colorectal carcinoma cell line HCT 116, a weaker virostatic effect was found in infected human pancreatic carcinoma (MIA PaCa-2) and human hepatocellular carcinoma cells (Hep3B).

V) Does AF also inhibit measles vaccine virus strains other than MeV-GFP?

In addition to MeV-GFP, AF showed a strong virostatic effect on 3 out of 4 tested measles vaccine virus strains (AIK-C, L-16, Mérieux).

VI) Does AF also inhibit measles wild-type virus strains?

AF reduced measles wild-type virus titers, but to a lesser extent compared to measles vaccine virus strains. The effect also varied between the genotypes of the tested measles wild-type viruses. While virus titers of wild-type measles virus strain D8 were reduced in supernatant up to 100-fold, the virostatic effect of AF on wild-type measles virus genotypes B3 and D4 was much weaker, if any.

VII) What is the molecular mechanism of the virostatic effect of AF?

As with the cytotoxic effect of AF, the most obvious mechanism would be an action via the proteasome. Supporting this hypothesis, the proteasome also interacts with the replication cycle of different viruses at different points (as summarized by Gao in 2006 [77]):

Amongst others, the Epstein Barr virus nuclear antigen 1 (EBNA1) aims at immune evasion by inhibiting viral protein degradation by the proteasome and thus presentation of epitopes on major histocompatibility complex I [78].

Retroviruses depend on proteins which are processed by the proteasome for the process of budding [79]. The human papillomavirus E6 protein suppresses apoptosis by inhibiting the proteasomal degradation of the anti-apoptotic protein p53 thus fostering virus replication [80].

Therefore, it is not surprising that virostatic effects already have been demonstrated with other proteasome inhibitors. Schneider et al. published in 2019 [81], that Bortezomib inhibits the early steps in Herpes Simplex virus infection by perturbing two distinct proteasome-dependent steps: “the transport of incoming viral nucleocapsids to the nucleus and the virus-induced disruption of host nuclear domain 10 structures”.

However, no inhibition by a proteasome inhibitor has been published so far for the measles virus.

In our experiments, none of the clinically approved proteasome inhibitors (Bortezomib, Carfilzomib, Ixazomib) could lower measles virus titers either. Compared to these, however, AF has different active moieties as described in the introduction. A mechanism of action via the proteasome is supported by the fact that in our experiments AF derivates without proteasome inhibitor activity showed no virostatic effect. The strong discrepancy of the amount of reduction between the individual virus strains and the fact that AF did not show any virostatic effect on other viruses such as the DNA-based vaccinia vaccine virus argue against a general non-specific virostatic effect. The difference between the strong inhibition of most measles vaccine viruses and the comparably weak inhibition of wild-type viruses could for example relate to the different receptor affinity to enter a cell. While both enter the cell via the surface markers CD150 (SLAMF1) and nectin-4, only vaccine virus strains can use CD46 as an additional receptor. An effect of AF on CD46 would therefore be a theoretical consideration that could explain the difference in inhibition. Summing up, further approaches are necessary to elucidate the molecular mechanism of the virostatic effect of AF.

For effective clinical use as a drug, in addition to the central medical effect, other properties are of almost equal importance. These core requirements, which were listed recently by Plemper [3] and which go beyond the appropriate reduction of the virus titers, can be assessed as follows for AF:

I) Cost effective manufacture

The fact that the drug is affordable is a basic requirement for effective use, especially in African countries with weak health systems. AF can be produced synthetically, as published by Bülow et al. in 2010 [54]. Therefore, it should be possible to produce the drug in large quantities and, due to the associated economic scalability, at relatively low costs.

II) Shelf stability at ambient temperature

AF was stored in the refrigerator at a temperature of 5-7 °C. No loss of function was found over several months of storage. Whether AF is stable at ambient temperature has not been published yet.

III) Orally bioavailable

No data concerning the oral bioavailability of AF have been published yet. In general, orally bioavailable cyclic peptides such as, for example, the immunosuppressant Cyclosporin A [82], are possible to generate. Bioavailability depends on various factors such as hydrogen bonds, lipophilicity, size, flexibility and structure [83].

IV) Safe for prophylactic use in children

So far, AF is in the preclinical phase of cell culture and animal experiments. Due to the cytotoxic effects of AF, which are still present to some extent at therapeutic doses for reduction of virus titers, side effects seem likely.

Is Argyrin F a suitable candidate as a drug against measles?

Summing up, the results of this dissertation demonstrate both directly by reduced virus titers and indirectly by reduced oncolysis that measles viruses are affected by AF. AF achieves a reduction in virus titers when applied up to 24 hours post infection (hpi). This makes it possible to use it as a post-exposure prophylaxis, at least in terms of time. This time period is comparable to the recommended start of treatment in other viral infections (compare the influenza approved

neuraminidase inhibitor Oseltamivir, which has to be applied within 2 days after infection to prevent symptoms and shorten the duration of illness [84, 85]).

Furthermore, AF could potentially be manufactured inexpensively and is stable at least at refrigerator temperature.

However, the following points show that AF cannot be considered as the final drug:

First, as a proteasome inhibitor, AF also exhibits cytotoxic effects. These are only present in a reduced form in the dosages required for the virostatic effect, but serious side effects still must be suspected. For example, when treating human colorectal carcinoma cells with the low dose of 0.1 µg/ml AF, the remaining cell mass of tumor cells was reduced to 80%. In addition, the cytotoxic effect also varied between the individual cell lines, which makes a prediction of possible side effects even more difficult. On top regarding side effects, there are particularly high demands in the preferred approach as a post-exposure prophylaxis. Finally, only a weak virostatic effect was measured for wild-type measles viruses and only in certain wild-type measles virus genotypes raising the question whether AF could effectively fight a wild-type measles infection or weaken the course of the disease.

In summary AF is considered as a lead compound, which must be further adapted by medicinal chemistry to optimize pharmacodynamics and pharmacokinetics.

Even if AF could not be used against wild-type measles viruses, it still shows promise in oncolytic virotherapy. Based on a positive phase 3 clinical trial [86] the US Food and Drug Administration (FDA) [87] as well as the European Medicines Agency (EMA) [88] approved a first virotherapeutic compound (IMLYGIC®) in 2015. Henceforth, patients with advanced skin cancer (melanoma) can be treated with this first-in-market virotherapeutic compound produced by the company AMGEN. It is expected that further virotherapeutics will become clinically licensed in the next years [89, 90]. To optimize their oncolytic and immunogenic potential, virotherapeutics (in particular of the second and third generation) will be genetically modified in order to alleviate the antiviral immune response against

virus particles used in virotherapy. Thus, on the one hand e.g. reapplications could be enabled which are currently ineffective because of the humoral immune response induced through the primal application. On the other hand, these modifications carry the danger that in case of a too efficient virus replication in the tumor cells the state of an unlimited, uncontrollable secondary virus replication can occur at worst leading to lethal consequences as an uncontrollable cytokine storm or tumor lysis syndrome. Therefore, it is necessary to determine for each virotherapeutic before any virotherapy trial or standard application which medical interventions can be taken in case of such a dangerous overshooting replication. In contrast to wild-type viruses, a strong virostatic effect of AF as well as a reduced oncolysis was already demonstrated for measles vaccine viruses in this dissertation. Therefore, AF could be this medical intervention for measles virus based virotherapeutics in terms of a potential rescue medication.

5. Summary

In contrast to the pathogen causing smallpox (Variola virus), the measles virus has not yet been eradicated, despite the availability of effective vaccines. On the contrary, in recent years there has been a significant increase of reported cases, reaching its worldwide peak with more than 850,000 cases in 2019. Most fatal cases occur in children under the age of 5. Therefore, further measures in dealing with the virus are urgently needed.

One of these is the expansion of therapeutic options to generate and license a first-in-class measles-specific antiviral drug. So far in addition to prevention through vaccination, only supportive therapies have been available such as rehydration, vitamin A substitution or the treatment of secondary bacterial infections.

By searching for antitumorigenic synergisms between small molecule agents and recombinant measles vaccine virus virotherapeutics, our working group surprisingly found, when using the proteasome inhibitor Argyrin F in combination with measles vaccine virus, in contrast to the assumed increased anti-tumor effect, a reduced oncolysis. Follow-up experiments showed a clear reduction of measles virus titers when applying this combined therapy. We hypothesized that Argyrin F could represent a completely unknown potent novel antiviral drug against measles.

The aim of this dissertation was to better evaluate the possible clinical application of argyrin F as an antiviral agent in measles. In this context, it was necessary to confirm the antiviral effect and to characterize it precisely.

In this dissertation it was found that Argyrin F strongly inhibited replication of the measles vaccine virus MeV-GFP. The virostatic effect was dose-dependent up to a minimum effective dose of 0.1 µg/ml Argyrin F. Furthermore, it was dependent on the time point of application before/after infection with measles viruses. We found that Argyrin F can inhibit measles vaccine virus replication when given up to 24 hours after infection. The potent virostatic effect could also be demonstrated in another 3 out of 4 measles vaccine virus strains tested. In contrast, depending on the genotype, measles wild-type viruses could only be inhibited weakly or not

at all. Further approaches are necessary to elucidate the molecular mechanism of the virostatic effect of Argyrin F.

Summing up Argyrin F in its current form cannot yet be considered for clinical application against wildtype measles viruses. At the required therapeutic dosage, a cytotoxic effect still occurs making the occurrence of serious side effects possible. In addition, depending on the genotype of wild-type measles viruses, virus titers were reduced only weakly or not at all. Further adaptations of the molecule by medicinal chemistry are therefore necessary.

In contrast, use of Argyrin F in virotherapy, employing only measles vaccine viruses, as a medical intervention for excessively replicating measles virus based virotherapeutics seems to be promising.

6. Zusammenfassung

Anders als der Erreger der Pocken (Variola Virus), konnte das Masernvirus trotz einer effektiven Impfung noch nicht ausgerottet werden. Ganz im Gegenteil zeigte sich in den letzten Jahren sogar eine deutliche Zunahme der berichteten Fälle auf weltweit über 850.000 im Jahr 2019. Ein Großteil der tödlich verlaufenden Fälle findet sich in Entwicklungsländern als Ausdruck unzureichender Impfkampagnen bei Kindern unter 5 Jahren. Dies verdeutlicht, dass weitere Maßnahmen gegen das Virus dringend erforderlich sind.

Eine davon stellt die Erweiterung der therapeutischen Möglichkeiten um ein Masern-spezifisches, antivirales Medikament dar, mit dem insbesondere die Mortalität der Masern, aber auch die Weiterverbreitung des Masernvirus signifikant abgesenkt werden könnten. Bisher sind über die Prävention durch Impfen hinaus lediglich supportive Maßnahmen wie Rehydrierung, Vitamin A Substitution oder Behandlung sekundärer bakterieller Infektionen möglich.

Unsere Arbeitsgruppe stellte auf der Suche nach antitumoralen Synergismen zwischen *small molecule* Wirkstoffen und rekombinanten Masern-Impfvirus Virotherapeutika bei Verwendung des Proteasom-Inhibitors Argyrin F in Kombination mit Masern-Impfvirus entgegen der eigentlich erwarteten gesteigerten Onkolyse eine signifikant reduzierte Onkolyse fest. Im Rahmen von Folgeversuchen zeigte sich, dass die Anzahl an Masernviren in der kombinierten Therapie immer deutlich erniedrigt war. Wir stellten die Hypothese auf, dass der verwendete Proteasom-Inhibitor Argyrin F ein bisher völlig unbekanntes, gegenüber Masern antiviral wirkendes Medikament darstellt.

Ziel dieser Arbeit war es, einen möglichen klinischen Einsatz von Argyrin F als Virostatikum bei Masern besser beurteilen zu können. Dazu galt es, den nachgewiesenen antiviralen Effekt erneut zu bestätigen und davon ausgehend genauer zu charakterisieren.

Im Rahmen dieser Promotionsarbeit konnte erneut eine deutliche Reduktion der Titer des Masern Impfvirus MeV-GFP unter Zugabe von Argyrin F gezeigt werden. Der virostatische Effekt verhielt sich dosisabhängig bis zu einer minimalen Wirkdosis von 0.1 µg/ml. Ebenfalls beeinflusste der Zeitpunkt der

Behandlung die Stärke der Reduktion. Argyrin F konnte bei einer Gabe bis zu 24 Stunden nach Infektion das Masernimpfvirus hemmen. Ferner ließ sich der potente virostatische Effekt auch bei weiteren 3 von 4 getesteten Masern Impfvirusstämmen nachweisen. Masern Wildtypviren hingegen ließen sich abhängig vom Genotyp nur schwach, beziehungsweise nicht, hemmen. Diese letztere Beobachtung bietet Anlass, ausgehend von der *lead* Substanz Argyrin F, auch weitere Argyrin Derivate in die Testreihen einzubeziehen bzw. neuartige Derivate zu generieren und dann ebenfalls mit zu testen.

Weitere Versuche sind insbesondere dahingehend notwendig, um den bisher noch nicht identifizierten molekularen Wirkmechanismus des virostatischen Effekts aufzuklären.

Zusammenfassend lässt sich sagen, dass Argyrin F in seiner jetzigen Form noch nicht für den klinischen Einsatz gegen Masern Wildtypviren geeignet ist. Bei der benötigten therapeutischen Dosierung tritt weiterhin ein zytotoxischer Effekt auf, was das Auftreten von schweren Nebenwirkungen wahrscheinlich macht. Daneben konnte je nach Genotyp der eingesetzten Masern Wildtypviren keine, beziehungsweise nur eine schwache Reduktion der Virustiter festgestellt werden. Wie bereits oben ausgeführt, sind daher weitere Anpassungen des Moleküls im Rahmen der Medizinalchemie nötig.

Demgegenüber stellt der Einsatz von Argyrin F in der Virotherapie, bei der ausnahmslos Masern-Impfviren eingesetzt werden, eine erfolgsversprechende Alternative als Intervention bei einer etwaig überschießenden Vermehrung von Masernvirus Virotherapeutika dar.

7. References

1. World Health Organization. *Measles*. 2020 25.08.2020]; Available from: https://www.who.int/immunization/diseases/measles/en/. [Access Date 25.08.2020]
2. World Health Organization. *More than 140,000 die from measles as cases surge worldwide*. 2019; Available from: https://www.who.int/news-room/detail/05-12-2019-more-than-140-000-die-from-measles-as-cases-surge-worldwide. [Access Date 25.08.2020]
3. Plemper, R.K., *Measles Resurgence and Drug Development.* Curr Opin Virol, 2020. **41**: p. 8-17.
4. World Health Organization, *Reported Cases of Selected Vaccine Preventable Diseases (VPDs), Update 2020-7-10*.
5. Roberts, L., *Why measles deaths are surging - and coronavirus could make it worse.* Nature, 2020. **580**(7804): p. 446-447.
6. Salmon, D.A., et al., *Vaccine hesitancy: Causes, consequences, and a call to action.* Vaccine, 2015. **33 Suppl 4**: p. D66-71.
7. The Lancet Child Adolescent, H., *Vaccine hesitancy: a generation at risk.* Lancet Child Adolesc Health, 2019. **3**(5): p. 281.
8. World Health Organization. *Ten threats to global health in 2019*. 2019; Available from: https://www.who.int/vietnam/news/feature-stories/detail/ten-threats-to-global-health-in-2019. [Access Date 29.08.2020]
9. World Health Organization. *Measles - Key facts*. 2019; Available from: https://www.who.int/news-room/fact-sheets/detail/measles. [Access Date 25.08.2020]
10. World Health Organization, *Global measles and rubella strategic plan : 2012-2020.* 2012. [Access Date 25.08.2020]
11. Anderson, R.M. and R.M. May, *Directly transmitted infections diseases: control by vaccination.* Science, 1982. **215**(4536): p. 1053-60.
12. Moss, W.J., *Measles.* The Lancet, 2017. **390**(10111): p. 2490-2502.
13. Lessler, J., et al., *Incubation periods of acute respiratory viral infections: a systematic review.* Lancet Infect Dis, 2009. **9**(5): p. 291-300.
14. Di Pietrantonj, C., et al., *Vaccines for measles, mumps, rubella, and varicella in children.* Cochrane Database Syst Rev, 2020. **4**: p. CD004407.
15. Griffin, D.E., *Measles virus and the nervous system.* Handb Clin Neurol, 2014. **123**: p. 577-90.
16. Mina, M.J., et al., *Long-term measles-induced immunomodulation increases overall childhood infectious disease mortality.* Science, 2015. **348**(6235): p. 694-9.
17. Pirquet, C.v., *Das Verhalten der kutanen Tuberkulinreaktion während der Masern.* Dtsch Med Wochenschr, 1908. **34**(30): p. 1297-1300.
18. de Vries, R.D. and R.L. de Swart, *Measles immune suppression: functional impairment or numbers game?* PLoS Pathog, 2014. **10**(12): p. e1004482.
19. RKI. *Masern, RKI Ratgeber*. 2020; Available from: https://www.rki.de/DE/Content/Infekt/EpidBull/Merkblaetter/Ratgeber_Masern.html. [Access Date 06.09.2020]

20. World Health Organization, *Measles vaccines: WHO position paper – April 2017.* Wkly Epidemiol Rec, 2017. **92**(17): p. 205-27.
21. Huiming, Y., W. Chaomin, and M. Meng, *Vitamin A for treating measles in children.* Cochrane Database Syst Rev, 2005. **2005**(4): p. Cd001479.
22. STIKO, *Stellungnahme der Ständigen Impfkommission (STIKO) am RKI; Fachliche Anwendungshinweise zur Masern-Postexpositionsprophylaxe bei Risikopersonen.* Epidemiologisches Bulletin, 2017.
23. Young, M.K., et al., *Post-exposure passive immunisation for preventing measles.* Cochrane Database Syst Rev, 2014(4): p. Cd010056.
24. Nelson, A.N., et al., *Evolution of T Cell Responses during Measles Virus Infection and RNA Clearance.* Sci Rep, 2017. **7**(1): p. 11474.
25. Cox, R.M. and R.K. Plemper, *Structure and organization of paramyxovirus particles.* Curr Opin Virol, 2017. **24**: p. 105-114.
26. Noyce, R.S. and C.D. Richardson, *Nectin 4 is the epithelial cell receptor for measles virus.* Trends Microbiol, 2012. **20**(9): p. 429-39.
27. Dörig, R.E., et al., *The human CD46 molecule is a receptor for measles virus (Edmonston strain).* Cell, 1993. **75**(2): p. 295-305.
28. Tatsuo, H., et al., *SLAM (CDw150) is a cellular receptor for measles virus.* Nature, 2000. **406**(6798): p. 893-7.
29. Noyce, R.S., et al., *Tumor cell marker PVRL4 (nectin 4) is an epithelial cell receptor for measles virus.* PLoS Pathog, 2011. **7**(8): p. e1002240.
30. Ader-Ebert, N., et al., *Sequential conformational changes in the morbillivirus attachment protein initiate the membrane fusion process.* PLoS Pathog, 2015. **11**(5): p. e1004880.
31. Jardetzky, T.S. and R.A. Lamb, *Activation of paramyxovirus membrane fusion and virus entry.* Curr Opin Virol, 2014. **5**: p. 24-33.
32. Jiang, Y., Y. Qin, and M. Chen, *Host-Pathogen Interactions in Measles Virus Replication and Anti-Viral Immunity.* Viruses, 2016. **8**(11).
33. Cox, R. and R.K. Plemper, *The paramyxovirus polymerase complex as a target for next-generation anti-paramyxovirus therapeutics.* Front Microbiol, 2015. **6**: p. 459.
34. Salditt, A., et al., *Measles virus M protein-driven particle production does not involve the endosomal sorting complex required for transport (ESCRT) system.* J Gen Virol, 2010. **91**(Pt 6): p. 1464-72.
35. El Najjar, F., A.P. Schmitt, and R.E. Dutch, *Paramyxovirus glycoprotein incorporation, assembly and budding: a three way dance for infectious particle production.* Viruses, 2014. **6**(8): p. 3019-54.
36. Christoph Springfeld, A.F., Kah-Whye Peng, Evanthia Galanis, Stephen J Russell, Roberto Cattaneo, *Measles virus: Improving natural oncolytic properties by genetic engineering*, in *Viral Therapy of Human Cancers*. 2004: CRC Press. p. 459-480.
37. Bichon, A., et al., *Case report: Ribavirin and vitamin A in a severe case of measles.* Medicine (Baltimore), 2017. **96**(50): p. e9154.
38. Pal, G., *Effects of ribavirin on measles.* J Indian Med Assoc, 2011. **109**(9): p. 666-7.
39. Uylangco, C.V., et al., *A double-blind, placebo-controlled evaluation of ribavirin in the treatment of acute measles.* Clin Ther, 1981. **3**(5): p. 389-96.

40. Roy Moulik, N., et al., *Measles outbreak in a pediatric oncology unit and the role of ribavirin in prevention of complications and containment of the outbreak.* Pediatr Blood Cancer, 2013. **60**(10): p. E122-4.
41. Hara, S., et al., *Combination therapy with intraventricular interferon-alpha and ribavirin for subacute sclerosing panencephalitis and monitoring measles virus RNA by quantitative PCR assay.* Brain Dev, 2003. **25**(5): p. 367-9.
42. Tomoda, A., et al., *Combined treatment with interferon-alpha and ribavirin for subacute sclerosing panencephalitis.* Pediatr Neurol, 2001. **24**(1): p. 54-9.
43. Kwak, M., et al., *A long-term subacute sclerosing panencephalitis survivor treated with intraventricular interferon-alpha for 13 years.* Korean J Pediatr, 2019. **62**(3): p. 108-112.
44. Plemper, R.K. and A.L. Hammond, *Synergizing vaccinations with therapeutics for measles eradication.* Expert Opin Drug Discov, 2014. **9**(2): p. 201-14.
45. Plemper, R.K., et al., *Design of a small-molecule entry inhibitor with activity against primary measles virus strains.* Antimicrob Agents Chemother, 2005. **49**(9): p. 3755-61.
46. Plemper, R.K., et al., *A target site for template-based design of measles virus entry inhibitors.* Proc Natl Acad Sci U S A, 2004. **101**(15): p. 5628-33.
47. Krumm, S.A., et al., *An orally available, small-molecule polymerase inhibitor shows efficacy against a lethal morbillivirus infection in a large animal model.* Sci Transl Med, 2014. **6**(232): p. 232ra52.
48. White, L.K., et al., *Nonnucleoside inhibitor of measles virus RNA-dependent RNA polymerase complex activity.* Antimicrob Agents Chemother, 2007. **51**(7): p. 2293-303.
49. Ndungu, J.M., et al., *Non-nucleoside inhibitors of the measles virus RNA-dependent RNA polymerase: synthesis, structure-activity relationships, and pharmacokinetics.* J Med Chem, 2012. **55**(9): p. 4220-30.
50. Sasse, F., et al., *Argyrins, immunosuppressive cyclic peptides from myxobacteria. I. Production, isolation, physico-chemical and biological properties.* J Antibiot (Tokyo), 2002. **55**(6): p. 543-51.
51. Ferrari, P., et al., *Antibiotics A21459 A and B, new inhibitors of bacterial protein synthesis. II. Structure elucidation.* J Antibiot (Tokyo), 1996. **49**(2): p. 150-4.
52. Nyfeler, B., et al., *Identification of elongation factor G as the conserved cellular target of argyrin B.* PLoS One, 2012. **7**(9): p. e42657.
53. Nickeleit, I., et al., *Argyrin a reveals a critical role for the tumor suppressor protein p27(kip1) in mediating antitumor activities in response to proteasome inhibition.* Cancer Cell, 2008. **14**(1): p. 23-35.
54. Bülow, L., et al., *Synthesis and biological characterization of argyrin F.* ChemMedChem, 2010. **5**(6): p. 832-6.
55. Loizidou, E.Z. and C.D. Zeinalipour-Yazdi, *Computational inhibition studies of the human proteasome by argyrin-based analogues with subunit specificity.* Chem Biol Drug Des, 2014. **84**(1): p. 99-107.

56. Chen, X., et al., *Therapeutic effects of Argyrin F in pancreatic adenocarcinoma.* Cancer Lett, 2017. **399**: p. 20-28.
57. Yong, K., et al., *The start of a new wave: Developments in proteasome inhibition in multiple myeloma.* Eur J Haematol, 2018.
58. Bard, J.A.M., et al., *Structure and Function of the 26S Proteasome.* Annu Rev Biochem, 2018. **87**: p. 697-724.
59. Stauch, B., et al., *Elucidation of the structure and intermolecular interactions of a reversible cyclic-peptide inhibitor of the proteasome by NMR spectroscopy and molecular modeling.* Angew Chem Int Ed Engl, 2010. **49**(23): p. 3934-8.
60. National Center for Biotechnology Information. *PubChem Compound Summary for CID 387447, Bortezomib*. 2020; Available from: https://pubchem.ncbi.nlm.nih.gov/compound/Bortezomib. [Access Date 05.09.2020]
61. National Center for Biotechnology Information, *PubChem Compound Summary for CID 11556711, Carfilzomib.* 2020. https://pubchem.ncbi.nlm.nih.gov/compound/Carfilzomib. [Access Date 05.09.2020]
62. National Center for Biotechnology Information, *PubChem Compound Summary for CID 25183872, Ixazomib.* 2020. https://pubchem.ncbi.nlm.nih.gov/compound/Ixazomib. [Access Date 05.09.2020]
63. Chauhan, D., et al., *A novel orally active proteasome inhibitor induces apoptosis in multiple myeloma cells with mechanisms distinct from Bortezomib.* Cancer Cell, 2005. **8**(5): p. 407-19.
64. Demo, S.D., et al., *Antitumor activity of PR-171, a novel irreversible inhibitor of the proteasome.* Cancer Res, 2007. **67**(13): p. 6383-91.
65. Kupperman, E., et al., *Evaluation of the proteasome inhibitor MLN9708 in preclinical models of human cancer.* Cancer Res, 2010. **70**(5): p. 1970-80.
66. FDA. *Highlights of prescribing information VELCADE® (bortezomib)*. 2019; Available from: https://www.accessdata.fda.gov/drugsatfda_docs/label/2019/021602s044lbl.pdf. [Access Date 03.09.2020]
67. FDA. *Highlights of prescribing information KYPROLIS® (carfilzomib)*. 2020; Available from: https://www.accessdata.fda.gov/drugsatfda_docs/label/2020/202714s030lbl.pdf. [Access Date 05.09.2020]
68. FDA. *Highlights of prescribing information NINLARO® (ixazomib)*. 2015; Available from: https://www.accessdata.fda.gov/drugsatfda_docs/label/2015/208462lbl.pdf. [Access Date 05.09.2020]
69. Condit, *Principles of Virology*, in *Fields Virology, 4th edition (Lippincott Williams & Wilkins, Philadelphia, PA)*. 2001. p. 25 - 58.
70. Spearman, C., *The method of 'right and wrong cases' ('constant stimuli') without Gauss's formulae.* British Journal of Psychology, 1904-1920, 1908. **2**(3): p. 227-242.

71. Kärber, G., *Beitrag zur kollektiven Behandlung pharmakologischer Reihenversuche **162**.* Naunyn-Schmiedeberg's Archives of Pharmacology, 1931: p. 480 - 483.
72. Skehan, P., et al., *New colorimetric cytotoxicity assay for anticancer-drug screening.* J Natl Cancer Inst, 1990. **82**(13): p. 1107-12.
73. Agilent. *Cellular Impedance*. 2020; Available from: https://www.agilent.com/en/technology/cellular-impedance. [Access Date 21.12.2020]
74. Agilent. *xCELLigence RTCA SP - Single Plate*. 2020; Available from: https://www.agilent.com/en/product/cell-analysis/real-time-cell-analysis/rtca-analyzers/xcelligence-rtca-sp-single-plate-741232. [Access Date 22.12.2020]
75. Barth, S., D. Glick, and K.F. Macleod, *Autophagy: assays and artifacts.* J Pathol, 2010. **221**(2): p. 117-24.
76. Sun, M.G., et al., *Correlated three-dimensional light and electron microscopy reveals transformation of mitochondria during apoptosis.* Nat Cell Biol, 2007. **9**(9): p. 1057-65.
77. Gao, G. and H. Luo, *The ubiquitin-proteasome pathway in viral infections.* Can J Physiol Pharmacol, 2006. **84**(1): p. 5-14.
78. Levitskaya, J., et al., *Inhibition of ubiquitin/proteasome-dependent protein degradation by the Gly-Ala repeat domain of the Epstein-Barr virus nuclear antigen 1.* Proc Natl Acad Sci U S A, 1997. **94**(23): p. 12616-21.
79. Strack, B., et al., *A role for ubiquitin ligase recruitment in retrovirus release.* Proc Natl Acad Sci U S A, 2000. **97**(24): p. 13063-8.
80. Scheffner, M., et al., *The HPV-16 E6 and E6-AP complex functions as a ubiquitin-protein ligase in the ubiquitination of p53.* Cell, 1993. **75**(3): p. 495-505.
81. Schneider, S.M., et al., *Early Steps in Herpes Simplex Virus Infection Blocked by a Proteasome Inhibitor.* mBio, 2019. **10**(3).
82. Fachinformationsverzeichnis Deutschland, *Fachinformation für Ciclosporin dura Weichkapseln.* 2020.
83. Wang, C.K. and D.J. Craik, *Cyclic peptide oral bioavailability: Lessons from the past.* Peptide Science, 2016. **106**(6): p. 901-909.
84. Fachinformationsverzeichnis Deutschland, *Fachinformation für Tamiflu® 30 mg/45 mg/75 mg Hartkapseln.* 2020.
85. Jefferson, T., et al., *Neuraminidase inhibitors for preventing and treating influenza in healthy adults: systematic review and meta-analysis.* Bmj, 2009. **339**: p. b5106.
86. Andtbacka, R.H., et al., *Talimogene Laherparepvec Improves Durable Response Rate in Patients With Advanced Melanoma.* J Clin Oncol, 2015. **33**(25): p. 2780-8.
87. FDA. *Highlights of prescribing information - Imlygic* 2015; Available from: https://www.fda.gov/media/94129/download. [Access Date 15.12.2020]
88. European Medicines Agency. *Imlygic*. 2020; Available from: https://www.ema.europa.eu/en/medicines/human/EPAR/imlygic. [Access Date 15.12.2020]
89. Lawler, S.E., et al., *Oncolytic Viruses in Cancer Treatment: A Review.* JAMA Oncol, 2017. **3**(6): p. 841-849.

90. Harrington, K., et al., *Optimizing oncolytic virotherapy in cancer treatment.* Nat Rev Drug Discov, 2019. **18**(9): p. 689-706.

8. Erklärung zum Eigenanteil der Dissertationsschrift

Die Arbeit wurde in der Medizinischen Universitätsklinik Tübingen in der Abteilung VIII für Medizinische Onkologie und Pneumologie (Ärztlicher Direktor: Prof. Dr. med. Lars Zender), in der Arbeitsgruppe Virotherapie unter Betreuung von Professor Dr. med. Ulrich M. Lauer durchgeführt.

Die Konzeption der Studie erfolgte in Zusammenarbeit mit Professor Dr. med. Ulrich M. Lauer und Dr. med. Susanne Berchtold (Laborleiterin und wiss. Mitarbeiterin).

Sämtliche Versuche (mit Ausnahme der Erstellung der Elektronenmikroskopie-Bilder) wurden nach Einarbeitung durch die Labormitglieder Frau Dr. med. Susanne Berchtold und Frau Irina Smirnow (MTA) von mir eigenständig durchgeführt.

Ich versichere, das Manuskript selbstständig (nach Anleitung durch Frau Dr. Susanne Berchtold und Professor Dr. med. Ulrich M. Lauer) verfasst zu haben und keine weiteren als die von mir angegebenen Quellen verwendet zu haben.

Tübingen, den 29.04.2021

[Unterschrift]

Paul-Philipp Armin Warth

9. Danksagung

Ein ausgesprochen großer Dank gilt der Dr. K. H. Eberle Stiftung für die Unterstützung des Forschungsprojektes „Neuartige Masern-Virostatika als Schlüssel für die globale Eradikation von Masern Viren".

Ein ebenso großer Dank gilt dem IZKF-Promotionskolleg für die Förderung der Doktorarbeit.

Herzlich bedanken möchte ich mich bei Professor Malek und Dr. Bozko für die Bereitstellung von Argyrin F, bei Professor Kalesse für die Bereitstellung der Argyrin F Derivate bei sowie bei dem Robert Koch Institut für die Bereitstellung der Wildtypmasernviren.

Mein ganz besonderer Dank gilt dem Team der Arbeitsgruppe Virotherapie um meinen Doktorvater Professor Dr. med. Ulrich M. Lauer sowie meine Betreuerin Dr. med. Susanne Berchtold für die hervorragende wissenschaftliche Ausbildung und Unterstützung.